

https://dspace.org/

A design-oriented analytical approach to simplify the computational aspects of low pass planar multi EMI filters

Botes, Nicholus James

2016
http://hdl.handle.net/10539/20046

Downloaded from a DSpace repository. https://dspace.org/

A Design-Oriented Analytical Approach to Simplify the Computational Aspects of Low Pass Planar Multipath EMI Filters

Nicholas James Botes

A dissertation submitted to the Faculty of Engineering and the Built Environment, University of the Witwatersrand, Johannesburg, in fulfilment of the requirements for the degree of Master of Science.

Johannesburg, 2015

Declaration

I declare that this dissertation is my own, unaided work, other than where specifically acknowledged. It is being submitted for the degree of Master of Science at the University of the Witwatersrand, Johannesburg. It has not been submitted before for any degree or examination at any other university.

Signed at _____on _____ , 2015.

_____

Nicholas James Botes

Abstract

Industry pressures of fabricating smaller components coupled with Electromagnetic Compliance (EMC) regulations are driving the development of alternative solutions in the EMI space. A possible solution to EMC lies in distributed frequency-selective filters, such as multipath conductors. The involved complexity in the field, however, hinders interest and capabilities for potential researchers and engineers working in this domain. The ability to design multipath conductors is identified as a restrictive aspect to advancing in the field of low pass filter design using these conductors. This work aims to develop a design-oriented analytical approximation approach, using established methods, for a given desired resistance-frequency plot. The method aims to provide designers with an initial design that can be refined subsequently using more involved techniques. This stands to broaden the scope of this field from experts to non-experts by allowing easier analysis and design processes. The approach develops from a low frequency method of modelling multipath conductors as separate structures that are valid over different frequency bands. A method is developed to model multipath structures as theoretical single layer conductors composed of effective material property values. This approach forms the basis on which the design-oriented equations are developed solving for the material properties of the required structure. The approaches developed are against the exact full frequency analytical equations. Practical aspects to the design of multipath conductors in this manner are discussed with main goal of feasible, stable design.

Acknowledgements

Although this dissertation marks my first academic contribution, I genuinely believe that without the guidance and support available to me, I would not have enjoyed the experience as much as I did.

I am sincerely grateful to my supervisor, Prof Ivan Hofsajer, for the numerous early morning discussions that have consequently shaped me as a person, an engineer, and now, a researcher. Your enthusiasm in the field and approach to problems is inspiring. Thank you for taking the time to transfer a part of your knowledge to me.

To my family and friends, your continued interest in my progress with this work (at the risk of initiating a conversation on the matter), leave me feeling truly blessed. I appreciate the hours you spent proof reading and helping me prepare my final documentation.

Thank you.

1. Introduction 3
1.1 Current Landscape of EMI Solutions 4
1.1.1 Passive and active solutions to EMI 4
1.1.2 Multipath conductor solutions to EMI 5
1.2 Body of Work 8
1.3 Scope of work 8
2. Outline of Work 11
2.1 Simplified Structural Model 11
2.2 Structural Averaging 17
2.3 Design Ability 19
2.4 Summary 20
3. Modelling a Simpler Understanding of Multipath Theory 21
3.1 Generalised Model 21
3.1.1 Behavioural equivalency of similar single layer conductors 22
3.1.2 Behavioural equivalency within partitions of single layer conductors 25
3.1.1 Behavioural equivalency in multipath conductors 28
3.2 The Peel Off Method 31
4. Mathematically Modelling the *n*-structure Method 34
4.1 Low Frequency Impedance of Structural Scenarios Using Material Properties 35
4.1.1 Development of resistance equations 36
4.1.2 Development of internal inductance equations 36
4.2 Aggregation of Material Properties in Structural Scenarios 40
4.2.1 Resistance using effective material properties 42
4.2.2 Internal inductance using effective material properties 44
4.2.3 Averaged Structural Analysis Concept Development 45
4.3 Skin Depth Using Effective Material Properties 46
4.3.1 Salient Point Analysis Concept Development 47
4.4 Significance of DC modelling and Effective Material Properties 48
5. Analysis Capabilities 51
5.1 Demonstration of Methods 51
5.1.1 Peel Off Method 52
5.1.2 Averaged Structural Analysis 53
5.1.3 Low Frequency Salient Point Analysis Method 55
6. Mathematical Design Methodology 60
6.1 Development of Design Equations 61
6.2 Practical Design Considerations 63
7. Design Capabilities 66

7.1 Conceptual design and trade-off considerations 67
7.2 Validation and Error Cases 69
7.3 Working design 70
8. Conclusion 73
8.1 Summary of findings 73
8.2 Aspects for Further Research 74
9. References 77

1. Introduction

Electromagnetic Interference (EMI) is a well-established concept when considering the electromagnetic environment of electronic equipment [1]. Natural sources of EMI include cosmic activity, lightning, and electrostatic discharge [1]. Electronic equipment, and more specifically switching power converters, can be a major source of EMI when ineffective measures are in place to mitigate these effects [1]. Power Electronics is a field where EMI is an on-going challenge. Power conversion, in boost or buck converters, is often achieved through high frequency switching of power using a square wave. The sharp rising and falling edges of the square wave are composed of high frequencies. EMI emission is a common and undesirable side effect of the high frequency switching – further exacerbated by a direct connection to a transmission line. These sources of EMI can potentially permeate electronic equipment by coupling with- or being conducted by transmission lines, and may result in the electronic application to malfunction [1].

Electromagnetic Compliance (EMC) regulations are in place to manage EMI and standardise an application's intended electromagnetic environment [1] [2]. Chapter 13 of [1] summarises the various EMC standards that applications in different environments are required to adhere to, both geographically – e.g. European Standards, FCC Regulation in U.S.A – and by specification, e.g. MIL-STD. With the proliferation of electronic applications, and trade within and across borders, EMC is placing more pressure on industry to the extent that magazine articles are published aimed at the layman [3]. The work of [3] provides an accessible understanding of EMC, specific to the European Union (EU) Directive. The EU Directive established regulations when the internal market borders of the EU were done away with in 1992. The EU Directive is similar to other EMC regulations in that it specifies compatibility in terms of [3]:

- Emissions – to not further pollute the electromagnetic environment [2]
- Susceptibility (immunity) – to safeguard against natural sources, malfunctioning electronics and unregulated applications.
- The intended environment of the application – for example, household, medical or industrial.

Adhering to EMC regulation is difficult [2] especially with the progression to smaller electronic modules. This is emphatically expressed by [3] in the following:

> *"EMC is a real problem and finding solutions which are technically suitable and economically competitive is today's challenge for design engineers."*

This work focuses on power electronics and the mitigation of conducted EMI along transmission lines in the frequency range below 30 MHz as specified by CISPR 11. Conceptually, a Low Pass Filter (LPF) is a sound approach to removing undesired

higher frequency propagation (as in the case of EMI) and is fundamental to achieving compliance. Implementation of a LPF must cater for the transmission of low frequency nominal power and elimination of small signal high frequency noise.

1.1 Current Landscape of EMI Solutions

This section details relevant solutions in the EMI space. The shortfalls of well-established solutions are presented here. The main limitation lies in achieving a practical power-to-volume ratio whilst being electromagnetically compliant. The field of multipath conductors potentially holds a solution to this problem. This section provides an introduction to multipath conductors. An analysis of the difficulties in multipath technology is presented with reference to the current body of knowledge in this domain. The applicable difficulties are acknowledged by incorporating them as constraints to this work.

1.1.1 Passive and active solutions to EMI

Low pass filter design and implementation, with the specific purpose of electromagnetic compatibility, has been a concern for many years [2]. The concerns with passive filter solutions for conducted EMI lie in [2] [4]:

1. Impedance matching of the filter to the application – limiting effective operation due to unavoidable mismatch and potential amplification of EMI [5].
2. The impractical size of the filter in order to accommodate the rated power.

Various methods are proposed in [2] in order to confront these concerns. Active reduction of EMI is discussed as a solution to combat the prohibitive size issues by not requiring the nominal power to flow through the filter. Active reduction uses an opposing signal, equal in magnitude to the interference, in order to achieve cancellation of EMI. Active reduction is proposed in [2], as an unconventional method at the time – stating that the solution does not lie in conventional approaches – yet was not able to provide conclusive evidence regarding the spatial efficacy of the filter, but did conclude that if successful results were achieved, the bulk size issue would have been addressed. However, the technology available at the time of [2] was far more limited than today. Forty-three years later, active reduction methods are still being investigated [6]. By making better use of the topology of the power converter, [6] aims to remove conducted common mode EMI to solve the bulk filter size issue. Difficulties were experienced in successfully opposing the EMI with further work suggesting improving the control system that governs the opposing currents. No actual size improvements were reported on, but rather assumed [6].

Another proposed solution is to consider EMI in the design of the system with regard to high frequency components and physical layout of the circuitry in order to reduce coupling [2]. Slower rising edges result in fewer high frequency components present in the system. This is a feasible solution yet may hamper performance in certain

applications. Faster switching times and higher performance are becoming increasingly relevant in today's applications, thereby limiting the scope of this approach.

The issues with LPF identified in [2] [3] are still relevant. Both sources, [2] [3], are in agreement that EMC is difficult and will require design engineers to use unconventional methods to find effective solutions.

1.1.2 Multipath conductor solutions to EMI

The overarching problem of eliminating EMI in order to adhere to EMC standards remains. This is furthered by the two prohibitive constraints encountered in passive filter solutions. The field of dissipative transmission line filters, and more specifically, multipath conductors shows potential in solving these issues [7].

A multipath conductor is illustrated in Figure 1 and is described as an n-layered composite structure where each layer has arbitrary material properties of conductivity (σ), permeability (μ), and thickness in the vertical direction (w). The terminal current enters these layers on the *send* transmission line and flows back through the *return* line – symmetrically structured.

It is important to note that the magnitude of impedance is frequency dependent. Skin- and proximity effects cause current to migrate towards the inner layers of the conductor in differential mode, and to the outer layers in common mode – see Figure 1. The migration of current results in different materials conducting the current at different frequencies, thus resulting in a potentially enhanced frequency dependent impedance value, depending on the material.

Early solutions of dissipative transmission lines were developed for coaxial cables using experimental findings of ferrite that showed lossy characteristics at high frequency [8]. The application was specific to the elimination of high power radio frequency interference causing unintentional detonations of explosives [8]. In this sort of application, a positive result using experimental data is a successful solution and the research is usually complete. In this case, it was experimental observations that concluded a positive result rather than the ability to understand the internal workings of the solution. Research in subsequent years into the behavioural understanding of such solutions, however, suggests that the electric and magnetic fields within the conductor can be controlled through better use of the transmission line's material properties by the nature of skin- and proximity effects [7].

The behavioural understanding is that currents across the frequency range are spatially distributed according the material properties of the conductor layers and the frequency. It is possible that undesirable frequencies be conducted in lossy layers with the desired frequencies being conducted by materials that do not hinder it [7]. This

action is aligned with LPF principles with its unconventional implementation showing potential to dissipate the energy in the signal considered to be undesirable [7] [9]:

- At frequencies higher than that of the nominal power.
- While not requiring series filters to be specified at the base power rating – addressing the size constraint.
- By being independent of load.

With such benefits, multipath conductors are becoming a popular solution for addressing EMC.

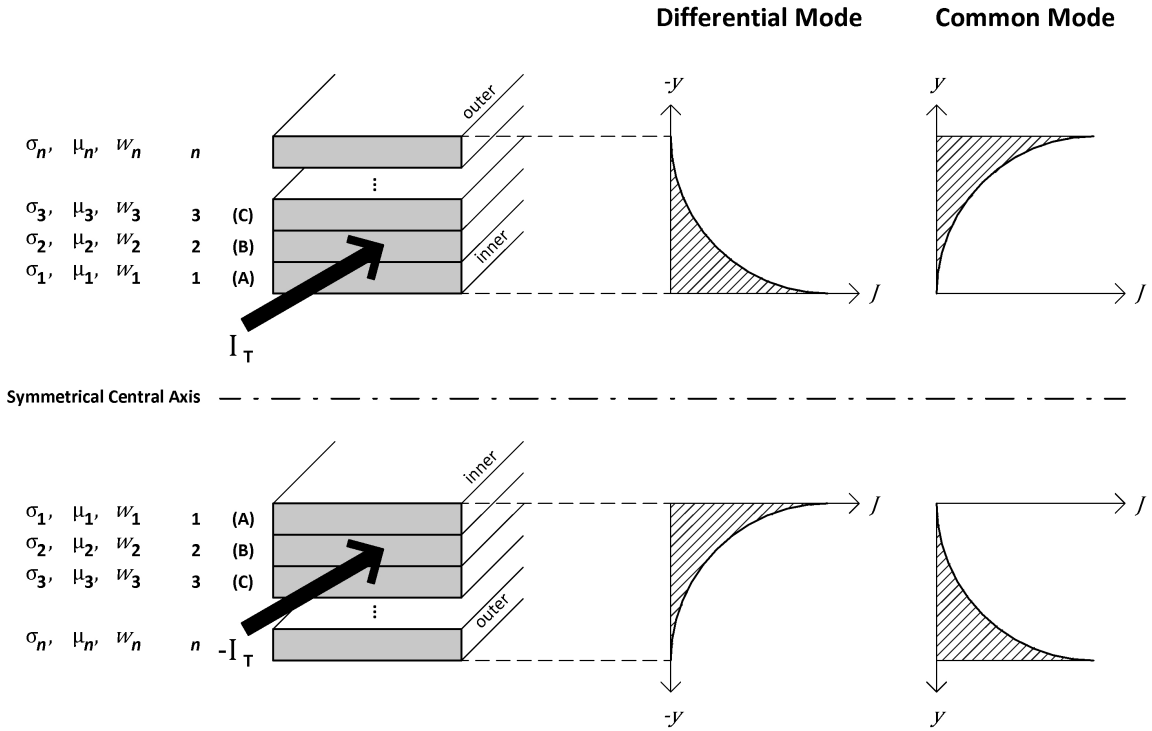

Figure 1: Schematic of a planar multipath conductor for which the terminal current is defined as flowing into the top conductor and returning in the bottom conductor. There can be n layers of different material properties that the terminal current distributes itself across the frequency range. Generic curves show the general migration of current to either side of the conductor for differential- and common modes of operation (current densities are arbitrary).

Although very promising in addressing major compliance and feasibility problems outlined previously, multipath conductor solutions have their own challenges as their behaviour strays from the established literature and understanding. There is no commonly accepted body of knowledge currently stating the exact behaviour of multipath conductors. Without such a basis, various modelling approaches are evolving throughout the research community to better represent the conductor action.

Limited insights into multipath conductor behaviour make for a tough field of study with regard to discovery, analysis and design.

The most relevant purpose of multipath conductor solutions is in EMI filter design across a multitude of applications. From a technical perspective, the goal is to establish a means to design multipath conductors such that the extent of their efficacy in EMI reduction can be determined upfront. Proposed methods of finding viable multipath solutions often suffer from a lack of design ability, presenting narrowly scoped solutions rather than generic methodologies.

A common simulation and discovery tool for geometrical structures is Finite Element Method (FEM). Simulations in this context involve changing material properties and viewing the results. As a validation tool, FEM is incredibly powerful as the results are tightly bound to the inputs. Using FEM as a design tool, however, is difficult as there are no insights into the relationships of the inputs. Physical implementation of the FEM simulation may produce vastly different results due to practical difficulties in parameter value variance. An analytical approach has an advantage over FEM by being able to contextualise designs in terms of stability, to account for variance in parameter value specification.

Categorising the effects of parameter changes in physical structures, through parametric design approach, allows for a look-up style design approach that may leave the designer relying on intuition. A parametric design approach carried out in [10] is validated through using physical structures as an improvement to using FEM. The approach has difficulties in experimental repeatability and measurement of exact parameters used with analysis and design inefficiencies.

Another attempt at designing a multipath solution was through a hybrid approach, which was explored by [11] in the application of a motor drive system. The approach made use of a multipath conductor and an additional choke to achieve the desired attenuation. The approach adds flexibility to the parametric designs in [10] and does improve filter performance. However, a series passive filter is made use of in the solution, making it infeasible considering the constraints of this work. The additional choke can be seen to act as a tuning circuit to the multipath conductor component – illustrating that there is still an inability to design a standalone, well-specified multipath conductor filter. The work does however contribute to the lumped parameter transmission line model described in [7].

The lumped parameter transmission line model that many works either contribute to or use in their applications has gained much popularity and has improved filter performance over the years [10] [12] [13] [14] [15] [16] [17] [18] [19]. The lumped parameter model has its roots in a transmission line model and is referred to by the authors as a lumped parameter transmission line model. The transmission line aspects of the model fall away as [7] reduces the model to a one-dimensional, RL (Resistance

and Inductor) based system, without travelling wave effects modelled – a key concept in transmission line theory. The relevance of the transmission line roots in [7] is questioned by [9] where the capacitive component is considered negligible from its foundations. The lumped parameter values, however, are often resolved using FEM analysis or circuit simulations, and whilst successful findings are obtained, this signifies that the mathematical model requires further development to be used as an efficient analysis and design tool [20]. [9] provides an excellent review of the various other modelling approaches to date.

Multipath conductors are modelled in [9] at a fundamental level by obtaining the electric and magnetic field distributions using Maxwell's equations. The lack of abstraction in the model to rather work with material properties of conductivity (σ), permeability (μ), and thickness (w), rather than Resistance (R) and inductance (L) bridges the gap between the mathematics and the physical structure. The benefits here overcome the need for FEM analysis as seen in [7]. The approach of [9] provides a closed form solution for n-layered conductors with the ability to later calculate R and L – capacitance is negligible by the structural and modelling assumptions. The analytical method from [9] elucidates the internal workings of multipath conductors where other methodologies fell short. This is, however, difficult to understand and an inaccessible solution for many researchers due to its high level of complexity. The analytical solution provides an excellent means of simulation, yet limited design capabilities. This solution requires the full frequency domain to be simulated over and is therefore termed the Full Frequency Analytical Methodology in this work.

1.2 Body of Work

In all approaches identified, either the lack of insights or the complexity of the solution obstructs the identification of an analytical design methodology for multipath conductors at a material property level. This work uses [9], as an enabling analytical methodology to validate simpler modelling approaches. The simpler models can be used to mathematically design multipath conductors to an approximate specification.

The primary goal of this work is to develop a simple mathematical approach to designing multipath conductors through a simplified understanding of their behaviour.

A secondary advantage to a simpler approach is in broadening the access, to multipath research or use, from experts to non-experts by simplifying the understanding of the impedance behaviour.

1.3 Scope of work

This work is scoped under the constraints of:

- Planar multipath conductors.
- Treated as one-dimensional, through physical specifications of the conductor being much wider than it is thick.
- Differential mode operation, although common mode operation is explored where possible.

A first approximation design approach is identified here to quickly establish starting point material property values. The designed material properties can then be simulated in more detail if necessary. This work focuses on a means of multipath conductor design. This work does not focus on how effective multipath conductors are, or can potentially be, in mitigating EMI. This work merely provides an understanding and design ability for a desired impedance characteristic – and not a feasibility study of multipath solutions.

To begin understanding multipath conductor behaviour, [9]'s analytical methodology is implemented as a software tool. This software tool allows for improved discovery and exploration as the results represent the truth across the appropriate frequency domain – illustrating [9] as a key enabler to this work. Further details regarding the implementation and validation of the software against FEM can be found in the following progression.

- Appendix A - A basic guide to implementing the analytical approach as software, specifically using *Mathematica*. Here, the analytical methodology of [9] is recapped with the in-depth mathematics explored. The implementation is validated against the work of [9] to provide a reliable software implementation. Repeatable and less error prone coding practices are elaborated on in order to gain confidence in the software and allow for faster adoption of future work in this domain. This is shown for up to three layers only. The equations for four- and five-layer multipath conductors are not displayed here, as they cannot be made sense of in this medium. There are an overwhelmingly large number of terms in these functions, taking up to 76 pages to describe the coefficients, making it inappropriate to house in the written appendix.
- Appendix B – A comparison of the analytical method of [9] through the use of the implemented software against a FEM analysis to verify that [9]'s solution is, in fact, accurate.

A high level outline of the work is presented in Section 2. This outline presents the argument in a procedural manner to guide the reader through the document. A simple analytical model is developed in Section 3. The model encapsulates the behavioural understanding in a simple manner such that it can be used later for design purposes. Section 4 develops a mathematical model based on the simpler understanding. Section 5 applies the developed analytical model to examples in order to better explain the analysis capabilities and behaviour of multipath conductors. Section 6 uses the

concepts of the analytical approach to solve for required layer material properties in mathematical design equations. A demonstration of the design ability created in this work can be found in Section 7. The design equations acts to satisfy the aims of this work and the shortcomings identified in the literature review. Improvements to the body of knowledge that could not be explored in this work are noted in the concluding section of this work, Section 8.

2. Outline of Work

This section outlines the flow through the document to better contextualise the concepts presented. This outline is a detailed summary of the work presented. All the concepts presented here will be treated more formally later on in the work. The reader should therefore expect to see these concepts again. The methodologies presented in this work depend on the established theories of resistance, internal inductance, skin-depth and skin- and proximity effects. An unconventional perspective on these properties is explored, with its validity demonstrated in later sections. This perspective arises due to the unfamiliar territory associated with multipath conductors and may be strange to the reader at first. The sections of work presented follow on from this outline in order to justify, explain or demonstrate the principles of the methodologies.

2.1 Simplified Structural Model

As mentioned previously, the Full Frequency Analytical Methodology [9] suffers from being extremely complex and has no direct design ability – however, iterative simulation design methods are theoretically possible. The Full Frequency Analytical Methodology provides the magnitude of the impedance for all values of frequency – or for as many as are specified, see Figure 2. These (continuous) characteristic impedance profiles (resistance and internal inductance) for the multipath conductor show the behaviour of the structure across all frequencies, however, the mathematical insights are obscured by complex mathematics spanning a large number of terms for structures composed of more than one layer. On the path to simplifying the multipath mathematics, it is necessary to understand the behavioural mechanics of the multipath system, thus allowing for more basic modelling methods.

This work is dual purpose:

- Provide the design ability to identify multipath conductor material properties that will allow for an approximation of the desired outcome.
- Simplify the mathematical overhead/complexity when analysing multipath conductors.

Considering the designer and the representation a designer would typically make use of, the methodology is based on a log-log scale representation of the approximate frequency-resistance profile – the resistance profile, see Figure 2. This typical representation provides the designer with relevant loss-oriented (using resistance) information across the frequency range. The nature of a log-log scale is that it expands graphical resolution in low frequencies and compresses resolution in the higher frequencies. The benefit of this approach over linear scales is that initial designs focus on the high-level aspects even though they may be less accurate. Resistance, the quantity on the vertical axis, is chosen as it can easily be found from the material

properties themselves. Further abstraction of the real losses to power losses in decibels introduces extra complexity and is not seen as necessary for the theoretical development of this work. There are two key concepts that arise from this representation:

- The magnitude of resistance and internal inductance
- At given frequency values.

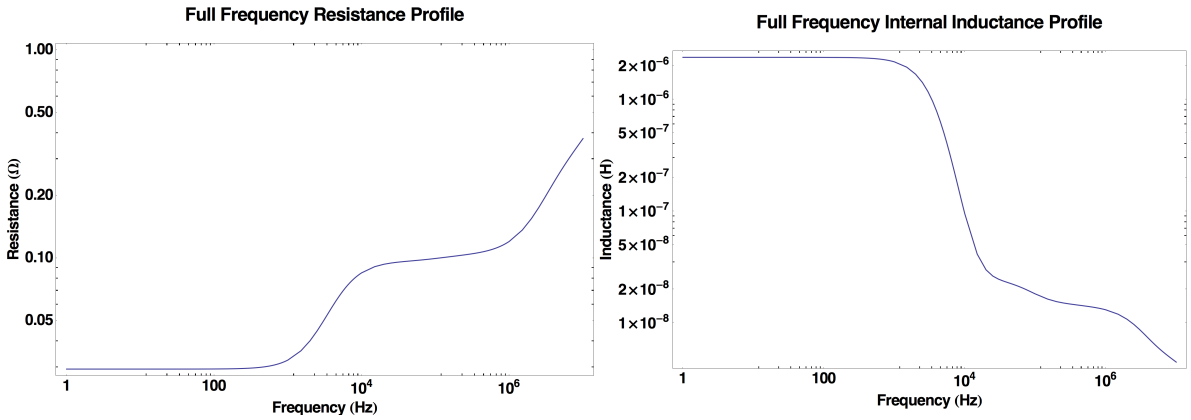

Figure 2: Typical example of general full frequency impedance plots showing resistance vs frequency (left) and inductance vs frequency (right). The log-log scale is illustrated and is a typical representation to describe impedance profiles.

In the search for identifying a simpler understanding of multipath conductors and thus, a simpler approach to modelling them, the general direction of current migration is explored. Section 3 investigates skin- and proximity effects with the specific aim to identify possible simplifications to the system. This is achieved by simplifying the behavioural understanding of the current migration. The method focuses on finding a relationship in the changes in impedance behaviour due to the current migrations within the underlying conducting structure. The development of a general approach is summarised by the steps that follow –Figure 3 also captures this, for clarity purposes. This approach is termed here as the *n-structure method* and is represented graphically in Figure 4.

- Combinations of layers describe the impedance profile of certain frequencies
    - For multiple layers of the **same** material properties
        - All layer properties (as if one layer, since they are the same) contribute to the low frequency profile
        - After some frequency value, all layers less one (e.g. the outer layer when operating in differential mode) contribute to the impedance value of the next frequency range.
        - In the highest frequency range only the remaining one layer contributes to the impedance value

- By the same approach, even this last layer can be partitioned into many layers of the same material properties to gain resolution into which components of the layer contribute to the impedance profile.

- For multiple layers of **differing** material properties (described from highest frequency range to lowest)
  - In the highest frequency domain, only one layer describes the impedance profile and acts as a single layer over that region.
  - At one frequency region lower, some combination (to be identified later) of the material properties of the remaining two layers can be used to describe the impedance profile.
  - This continues until a certain combination of the frequency band's active material properties compose the impedance profile.

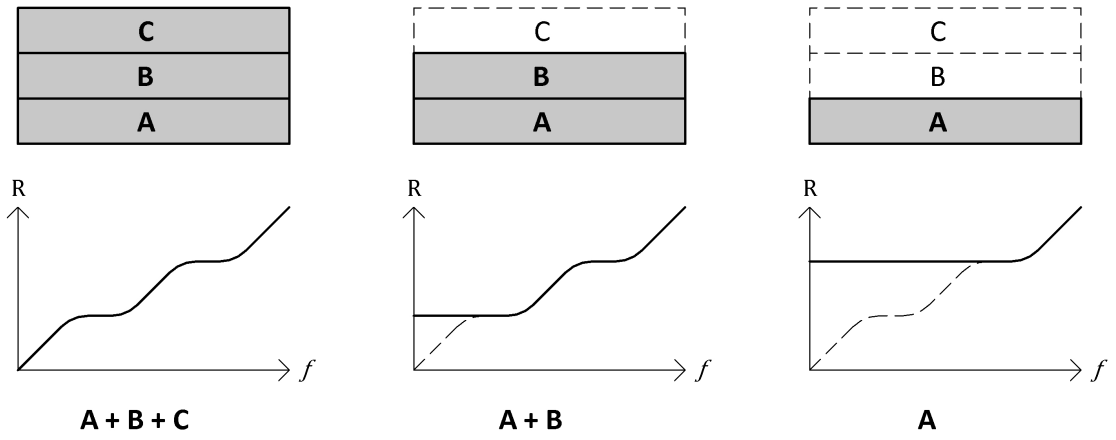

Figure 3: Theoretical progression through current migrations in the two types of conductors showing related resistance profiles (axes are scaled logarithmically and the origin does not denote zero).

- The terminology here is that the scenario that has all layers active is the *n-layer scenario*. With one layer less it is termed the *n-1 layer scenario*, and so on, resulting in *n* number of structural scenarios that are analysed over *n* frequency bands – see Figure 4.

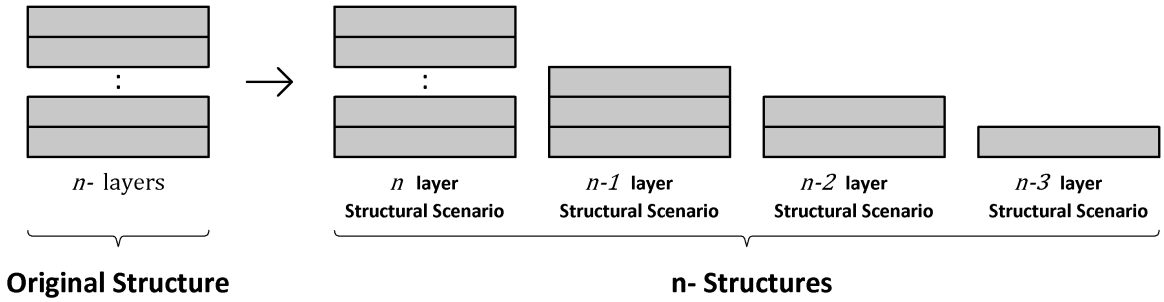

Figure 4: Visual representation of the n-structure terminology.

- Unknowns at this point are the following:
    - The frequency values that bound the frequency bands and how they can be found.
    - The relationship in which the material properties contribute to the calculated impedance profile.
- The salient frequency-impedance values occur at the scenario's transition points. The impedance value changes due to a new combination of the active material properties under consideration. This is when the next layer has been removed.
    - This approach lends itself to a piecewise linear interpolation of points on the log-log scale set of axes - Figure 5.

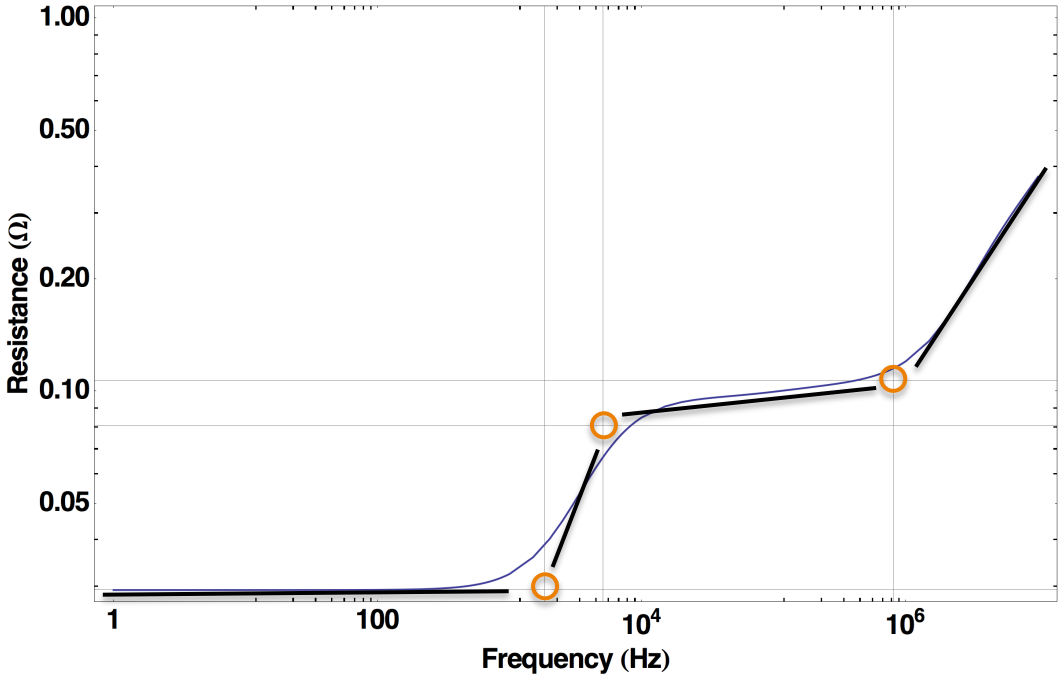

Figure 5: Piecewise linear conceptual interpolation of resistance profile illustrating the end goal of the analytics capabilities of the simplified approach.

This method provides only a simplified understanding of the *n* number of scenarios that arise from the whole structure. It shows that for each increase in frequency band, the scenario is composed of one layer less than the previous frequency band's scenario. Layers that are no longer considered in the scenario are termed *inactive*. The generalised principles behind the *n-structure method* provide the necessary simpler behavioural mechanics of multipath systems. The next aspect of this model that needs to be identified is how to obtain the frequency bounds.

Section 3.2 on the *peel off method* is a validation of the *n-structure method* and provides practical insights to enhance the method. The *peel off method* is a full frequency

analysis, using the Full Frequency Analytical Methodology, over the *n* scenarios that result from disregarding inactive layers (the *n-structure method*).

With reference to Figure 6, the three-layer structural scenario is simulated over the full frequency range, as are the two- and one-layer structural scenarios. The three-, two- and one-layer scenarios are labelled in Figure 6 with reference to the layers that are active in the scenario i.e. three layer scenario is represented by A+B+C and the two-layer scenario is just A+B, as C is inactive in this case – see Figure 3. Although all the dynamics of the profile do not fully agree with the complete simulation of all the layers, the two-layer scenario does show good agreement over a frequency band. In this way the *peel off method* validates the *n-structure method*. The discrepancy is due to the fact that the other layers still contribute to the impedance profile, yet the simplification is to disregard these dynamics in light of a simpler working estimate.

The simplification disregards inactive layers because it is more desirable to have a clear and simple means to identify the partitions – provided by the physical layer separations. However, if it were desirable for the Peel Off Method to agree closer to the complete three-layer simulation then partial contributions from the other inactive layers needs to be introduced. Knowing that the inactive layers do contribute some value of impedance at different frequencies, it is possible to add back in a *portion* of the inactive layers such that their presence, when simulated, improves the agreement as desired. There is a large amount of complexity in finding what *portion* of the inactive layers is required to be added back in. In order to find the correct portion one would need to solve the complex equations of the Full Frequency Analytical Method – avoiding this is the purpose of this simplified method. It is for this reason that the layer boundaries are the preferred distinctions between which materials compose the structural scenarios. This is at the cost of the error introduced by the method.

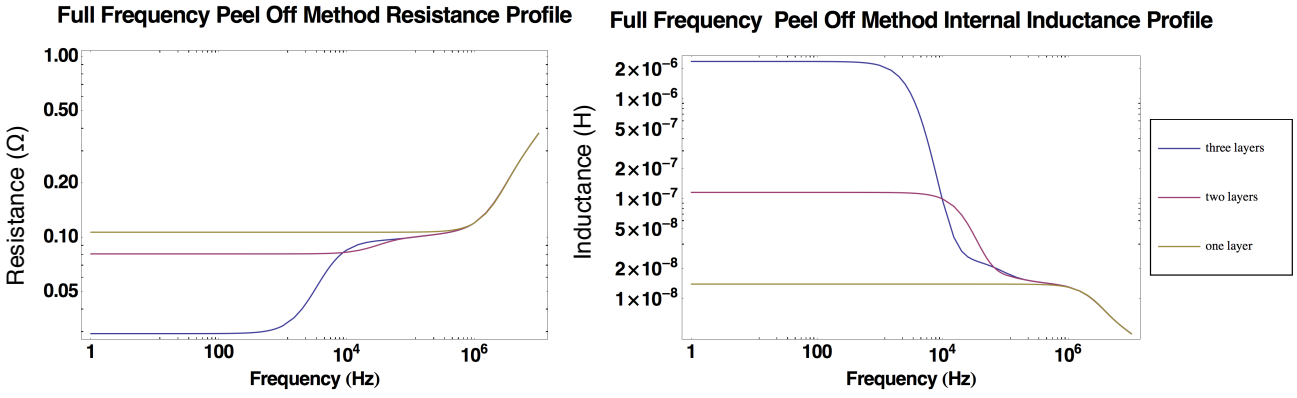

Figure 6: Peel off method reference impedance profiles. Agreement is with the three layers profile.

Another convenient point in the simplification where access to easier calculations is preferred over accuracy is in using the skin depth frequency as the frequency band boundaries. The total thickness of the active layers is used as the skin depth to find a skin depth frequency for the scenario. Consider a two-layer single material property case shown by Figure 7. The one-layered structural scenario, composed only of A, can be considered to estimate the total resistance for frequencies greater than A's skin depth frequency. It is known, however, that this is not accurate, yet the convenience of A's skin depth frequency is more valuable in this work than eliminating the introduced error.

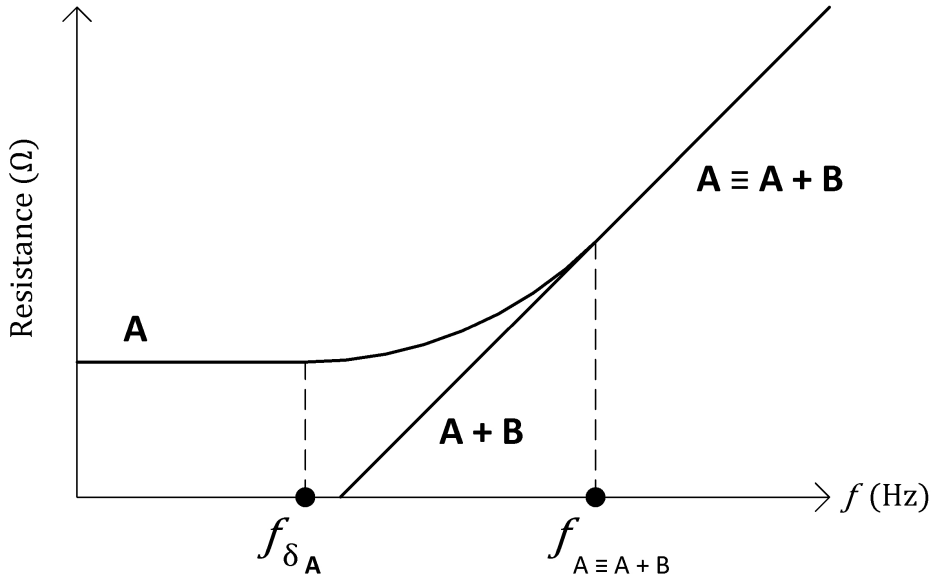

Figure 7: Skin depth approximations of frequency boundaries whereby the structural scenarios can approximately represent the full impedance profile.

Skin depth is a concept that is relevant to single layer structures. Applying the skin depth frequency concept to multiple different layers does not make sense. However, should a multi-layered conductor be represented as a single layer then a method to understanding the frequency bounds for layers with differing material properties could be based on skin depth frequency concepts. An approach of this nature is necessary and is explored in this work.

The combined findings from the *n-structure method* and the *peel off method* are that:

- The layers become inactive one-by-one, in order, with increasing frequency.
- It is not necessary to make use of all frequency points but rather to identify the magnitude of the resistance and internal inductance values for specific frequency points.
- The impedance values can be found by some combination of the active material properties

- The skin depth frequency is a significant value for finding scenario impedance values.
- The low frequency (near DC) value is fairly constant until it reaches the significant frequency value and can be used as the corresponding impedance value.

The approach does not describe:

- How to combine the material properties to obtain the impedance value
- How to identify the frequency at which the impedance value should be taken.

2.2 Structural Averaging

The n-structure method results in many layers in each of the structural scenarios. The low frequency (near DC) value of resistance and internal inductance for each scenario can be found using established methods. Section 4 contains a general solution for resistance and is shown in Equation (1) and for internal inductance by Equations (2)-(3). The internal inductance equation is shown here to illustrate the complexity of it. This equation is solved for any number of layers required. Appendix C simplifies the equation by presenting a five-layer tutorial style progression through the necessary integrals.

The summation terms in the denominator of Equation (1) can be parameterised out to be of the form of Equation (4). The mathematical encapsulation can be viewed as structurally averaging the layers contained within a structural scenario to reduce it to an effective single layer structure – the subscript *e* indicates that it is an *effective* property. Only the effective conductivity and effective thickness can be found using this *resistance* approach. The general structure of the *internal inductance* can theoretically be used to identify, with better accuracy, the effective permeability through the same action of parameterising the summations in the terms. This method was not pursued due to the difficulty of the approach. Rather, the structural scenario is viewed as a magnetic circuit and the properties are solved for in the same way the resistance was used, instead using the analogous properties in the reluctance formula. This simpler method further simplifies away the detail that could be achieved using Equations (2)-(3) and narrows the scope of application for the method. High contrasts in material properties present greater error margins due to this effect. Improvement to the approach at this point is noted as future enhancements to this work and will provide improved accuracy in the design equations.

$$r_n = \frac{l}{width \sum_{i=1}^{n} w_i \sigma_i} \tag{1}$$

$$L = \frac{2}{I_T^2}\sum_{j=n}^{1}\left(\frac{1}{2}length\ width\ \mu_j \int_{\sum_{z=n}^{j+1} w_z}^{\sum_{z=n}^{j} w_z}\left(\left[\frac{1}{width}\sum_{z=n}^{j+1} i_z\right] - \left[\frac{i_j}{width\ w_j}\sum_{z=n}^{j+1} w_z\right] + \left[\frac{i_j}{width\ w_j} y\right]\right)^2 dy\right) \tag{2}$$

Where

$$i_j = \frac{w_j \sigma_j}{\sum_{z=1}^{n} w_z \sigma_z} I_T \tag{3}$$

$$r_n = \frac{l}{width\ w_{e_n} \sigma_{e_n}} \tag{4}$$

Structural averaging provides the basis of multipath conductors by hiding complexity and allowing many layers to be represented as a single layer. The immediate benefit here is that each single layer in the *n* structural scenarios can be simulated – using established methods – over the whole frequency domain. The *n* impedance plots can then be interpolated by tracing the lowest value per frequency point across all the plots, transitioning between knee point (skin depth) frequencies, Figure 8. This is termed the Full Frequency *Average Structural Analysis* method. The method illustrates the use of intrinsic skin depth frequencies as interpolation points. As expected, from the equations in this section, the resistance values agree with those from the Peel Off Method. This approach validates the *n-structure method* and suggests that:

- The average structure material properties can be used to find the resistance value
- A skin depth frequency can be identified using the effective single layers

The ability to find this frequency point is highly significant in the analysis of each *n-layer* scenario, and therefore the structure as a whole.

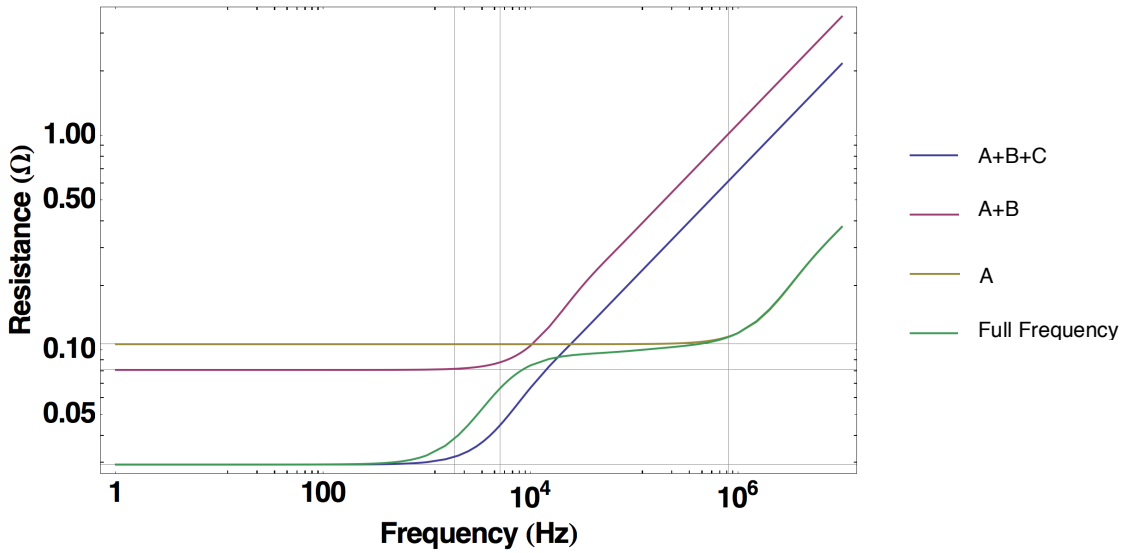

Figure 8: Full Frequency Average Structural Analysis of an arbitrary three layer multipath conductor. The full frequency curve can be approximated through interpolation. This is achieved by tracing the lowest value per frequency point across all the plots, transitioning between knee point (skin depth) frequencies

A further outcome from this is that the low frequency values of resistance and internal inductance can be calculated through established methods to provide the impedance value for each structural scenario. Coupled with the ability to identify the skin depth frequency – which is a good measure of where the valuable frequency points are – a Salient Point Analysis can be identified requiring only n pairs of frequency-resistance values (and frequency-internal inductance values) in order to quickly analyse the structures. Salient Point Analysis is presented further in Section 4.3.1.

Average Structural Analysis, Salient Point Analysis and the Peel Off Method are demonstrated in Section 5 showing their agreement with the Full Frequency Analytical Method as validation of the estimation methodology.

2.3 Design Ability

The design approach makes use of two concepts identified thus far.

- The resistance calculation to find the effective conductivity and effective thickness properties.
- The skin depth equation given that the structure can be represented as a single layer.

The input parameters for design are the frequency-resistance pairs (similar to Salient Point Analysis). The design equations are found by manipulating the equations for skin depth and resistance of effective materials. The system however is underspecified and relies on the designer to make trade-off decisions based on the availability or practicality of the designed-for material properties. A note on practical considerations

for design is given with the identification of feasible regions in this high-dimensional space marked as future work.

2.4 Summary

Figure 9 captures the flow through the concepts of this section diagrammatically. This visual guide to the document is intended to act as a reference figure that the reader can refer to throughout the document.

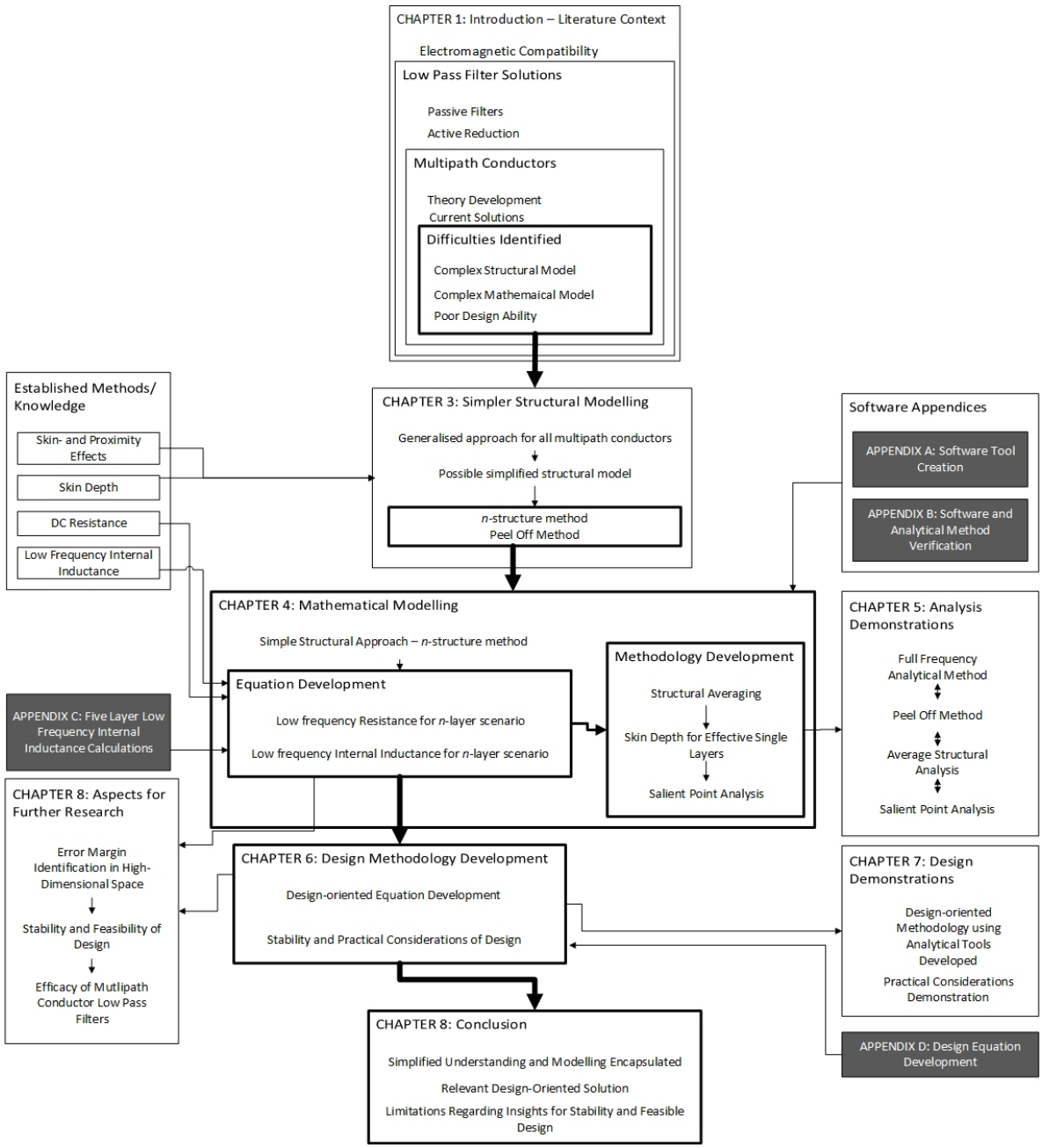

Figure 9: Flow diagram illustrating the flow of the argument with major components identified.

3. Modelling a Simpler Understanding of Multipath Theory

This section aims to develop a simpler theoretical understanding of multipath conductor behaviour. A simpler understanding provides a basis upon which mathematical models can approximate the system. The simplification is aimed at a generalised understanding of all multipath conductors for any number of layers. This section focuses on:

- Reasonable theory development with appropriate argument – in order to gain confidence in the validity of the progression.
- Development of a procedural methodology to enhance how the developed theory is relevant – create a step-by-step approach to using the theory.

This section covers these by first developing a generalised model and then codifying it into an approach termed the Peel Off Method.

At the end of this section, the more simple understanding will form the foundational reasoning behind the methodologies developed in later sections. The Peel Off Method provides a succinct demonstration of the theory, which reinforces the simpler perspective on multipath conductors.

3.1 Generalised Model

A generalised model is necessary to identify that the simplified understanding is relevant across planar multipath conductors of any number of layers. The theory is developed for differential- and common mode operation due the similar nature of the current migration. Differential mode is proceeded with in this work, noting that, although it is suspected that the methodology is portable to common mode operation, it should be verified as future work.

The approach taken begins by inspecting the behaviour of many layers of the exact same material. The layer boundaries are inspected and the characteristic resistance profile is inspected from a current migration perspective. Comparing whole structures against partitioned structures is key to this theory development. It is reasoned that when considering different layers, the current migrations and resistance values over various frequency ranges behave in a similar way.

This section identifies that each subsequent layer of a multipath conductor becomes irrelevant as current migrates with increasing frequency. The layers can, at an estimate, be ignored from the system after a certain frequency as the impact of the current that they conduct is negligible to the overall resistance profile. This is the basis for the Peel Off Method that follows as a means of applying this understanding as a repeatable approach.

3.1.1 Behavioural equivalency of similar single layer conductors

Consider two separate conductors, A and B, each energised by their own current source, I_A and I_B, respectively, as per Figure 10. The two conductors have the same values of conductivity ($\sigma_A = \sigma_B$) and permeability ($\mu_A = \mu_B$), yet A is thicker than B ($w_A > w_B$). The current sources are set to the same value, $I_A = I_B$. Both A and B conduct the full terminal current as per the current source. At DC, A has a lower resistance, R_A, than B, R_B, due to the indirect relationship of resistance and cross-sectional area as seen in Figure 12.

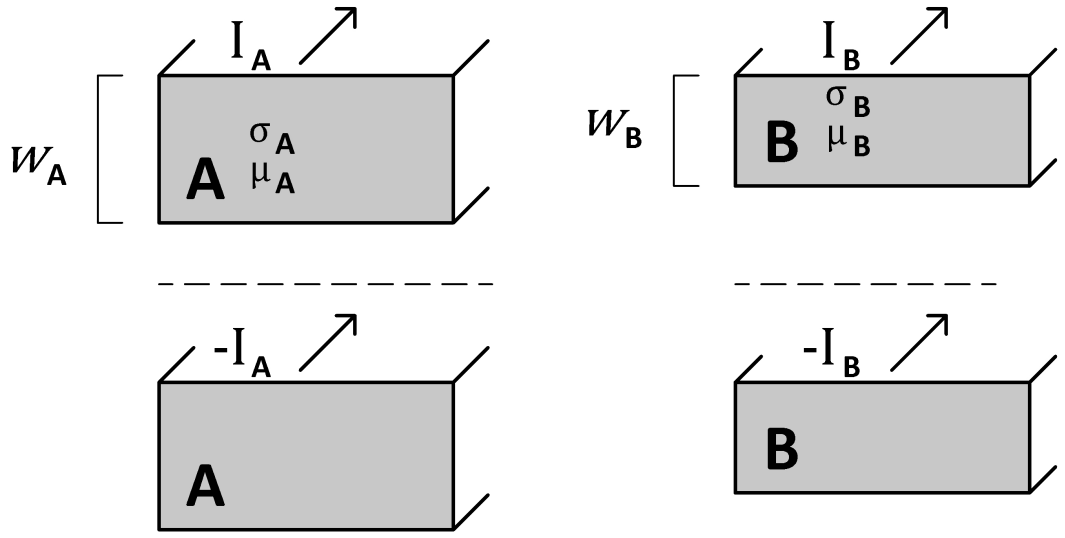

Figure 10: Two conductors of the same conductivity and permeability, yet of different thicknesses powered by their own current source.

Across all conducting frequencies, the full terminal current is conducted. As the frequency of the current sources increase, skin- and proximity effects become more prevalent, causing the conducting cross-sectional area of A and B to decrease. Once skin- and proximity effects result in the conducting cross-sectional area to be less than that of the conductor itself, both A and B, begin to increase in resistance value. This can be seen in Figure 12.

Conductor B is equivalent to A with the exception of its thickness. However, at a certain frequency, the conducting cross-sectional area of A will begin to decrease with increasing frequency, resulting in the same conducting cross-sectional area of B at some frequency higher. At this frequency, the two conductors can be considered truly equivalent in terms of their resultant behaviour – their physical structure, of course, has not changed. For frequencies greater than this equivalency frequency, A and B

behave identically as they are equivalent over the higher frequencies. This concept is comparable to the case of two identical conductors, which will therefore have the same resistance profile across all frequencies. Only in this case, the equivalency frequency is not at DC but at a certain (identified later) higher frequency (and resistance) value. A difference in thickness results in different resistance values at lower frequencies but will become the same value at higher frequencies.

The concept described here illustrates the frequency-dependent nature of resistance due to skin- and proximity effects. A similar effect occurs with internal inductance of the conductor as seen in Figure 13 due to the decreasing conducting cross-sectional area.

It is known that the skin depth frequency is an indicator of when resistance begins to increase for a conductor. Skin depth, δ, is an indication of where the majority of current lies in the structure due to skin- or proximity effects.

The skin depth frequency represents the frequency at which $e^{-1} \cong 0.37$ of the current is in the inactive layers and $1 - e^{-1} \cong 0.63$ of current is within the skin depth thickness of the layers. The total thickness of the active layers is used as the skin depth to find a skin depth frequency for the scenario. More current moves into the active layers as the frequency increases above the skin depth frequency. The resistance value rises and the conducting cross-sectional area decreases. Once the 63% of current has migrated into the active layers (layers that fall within the skin depth thickness), the outer layer is considered inactive. The frequency range over which the rest of the current migrates is not considered any further beyond this point. The range is considered negligible in these simplification methods as the convenience of the skin depth frequency point will suffice as the estimated point at which that scenario contributes its impedance value to the overall profile. Consider a two-layer single material property case shown by Figure 7. The one-layered structural scenario, composed only of A, can be considered to estimate the total resistance for frequencies greater than A's skin depth frequency. It is known, however, that this is not accurate yet the convenience of the A's skin depth frequency is more valuable in this work than eliminating the error introduced. The introduction of this type of error is shown in Figure 11, which is seen in the high level summary (Figure 7) and is repeated here for convenience.

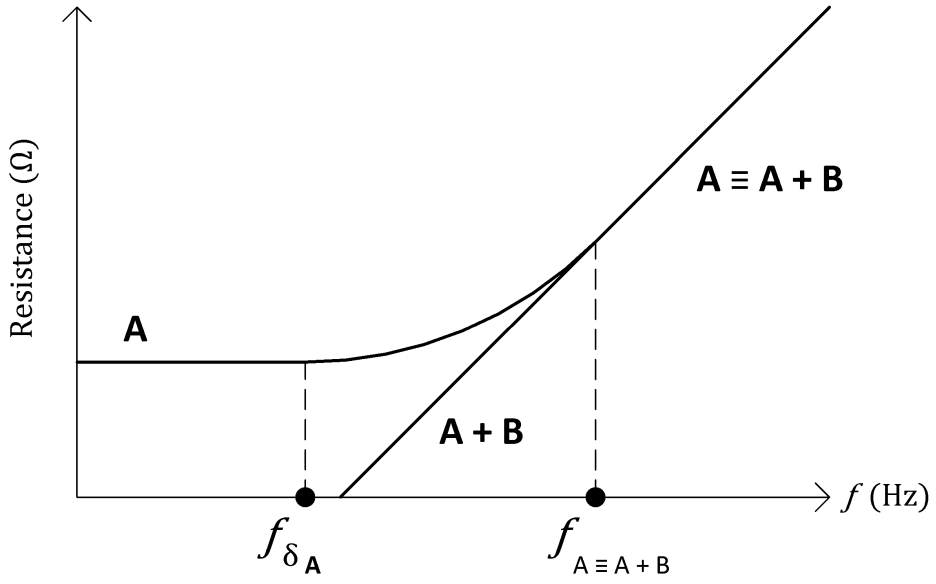

Figure 11: Skin depth approximations of frequency boundaries whereby the structural scenarios can approximately represent the full impedance profile.

A decreased conducting cross-sectional area occurs when the majority of current is being conducted in a thickness less than the physical thickness of the conductor. This means that when the skin depth thickness is less than the physical thickness, the resistance begins to rise. The frequency at which this occurs is the skin depth frequency, f_δ, of the conductor and is observed by the knee-point in Figure 12 and Figure 13. In reference to conductors A and B, R_{ac} will begin to increase at f_{δ_A} and A and B will be behaviourally equivalent for all frequencies greater than f_{δ_B}.

For frequencies below f_{δ_B} the behaviour of the two conductors is different and they need to be treated separately, however, above f_{δ_A} conductor B can be used to fully describe the behaviour of the system. Both conductors carry the full terminal current from the current source and have the same resistance values for frequencies higher than f_{δ_B}. The physical differences in thickness are not visible at these frequencies meaning that the existence of A's greater thickness is irrelevant over the higher range.

The following intuitive key points are a result of the discussion so far:

1. The skin depth frequency, f_δ, describes the knee-point where resistance begins to increase
2. The conducting cross-sectional area decreases for frequencies above f_δ.
3. The behavioural state can be represented by a different physical state of the conductor in certain frequency ranges.

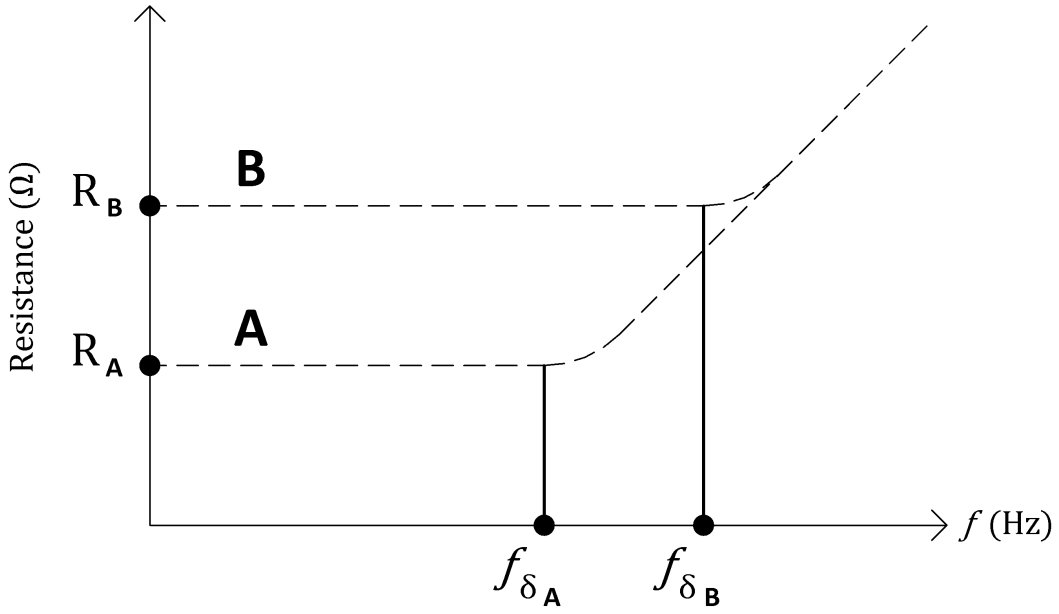

Figure 12: Common frequency dependent resistance profile of conductors A and B over a large generalised frequency range.

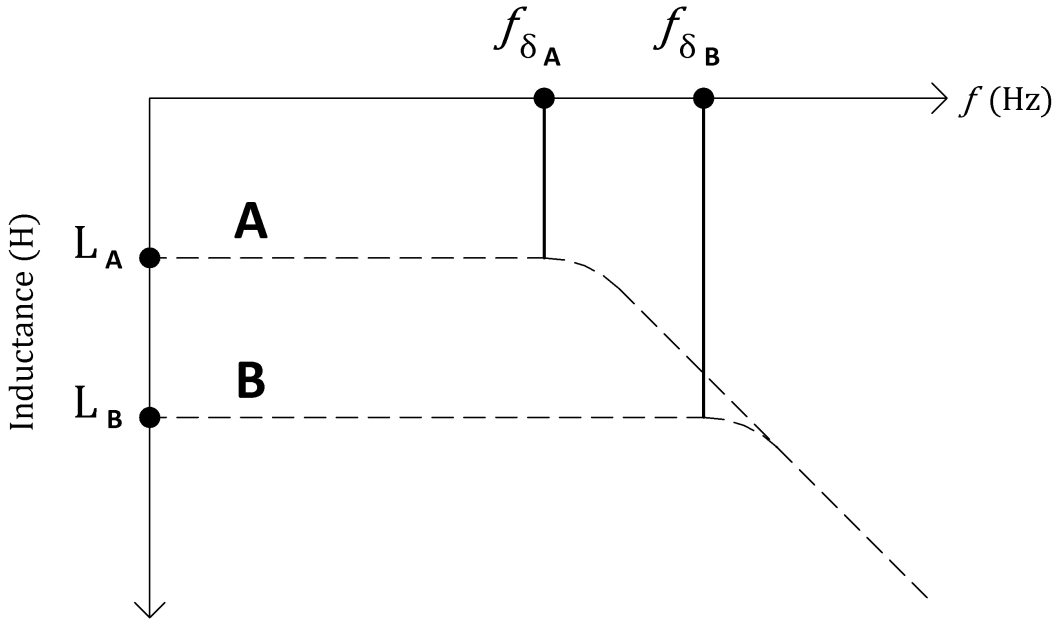

Figure 13: Common internal inductance profile of conductors A and B over a large generalised frequency range.

3.1.2 Behavioural equivalency within partitions of single layer conductors

Now consider the thickness of conductor A being split into n partitions, namely $p_1, p_2, p_3 \ldots p_n$ each with a thickness of $w_{p_1}, w_{p_2}, w_{p_3} \ldots w_{p_n}$ such that the total thickness is

the sum of all the thicknesses, Equation (5). This is represented in Figure 14. The partitions can be collected to compose conductor A or all successive thicknesses of the conductor, A, where an outer partition is left out, as described in Equation (6), making A_n equivalent to A. All partitions have the same conductivity and permeability allowing for incremental (or decremented) thicknesses of conductor A to be investigated as A_i. The resistance profile of each conductor, A_i, is plotted in Figure 15.

$$w_A = \sum_{j=1}^{n} w_{p_j} \tag{5}$$

$$A_i = \sum_{j=1}^{i} p_j \tag{6}$$



Figure 14: Conductor A divided into n partitions.

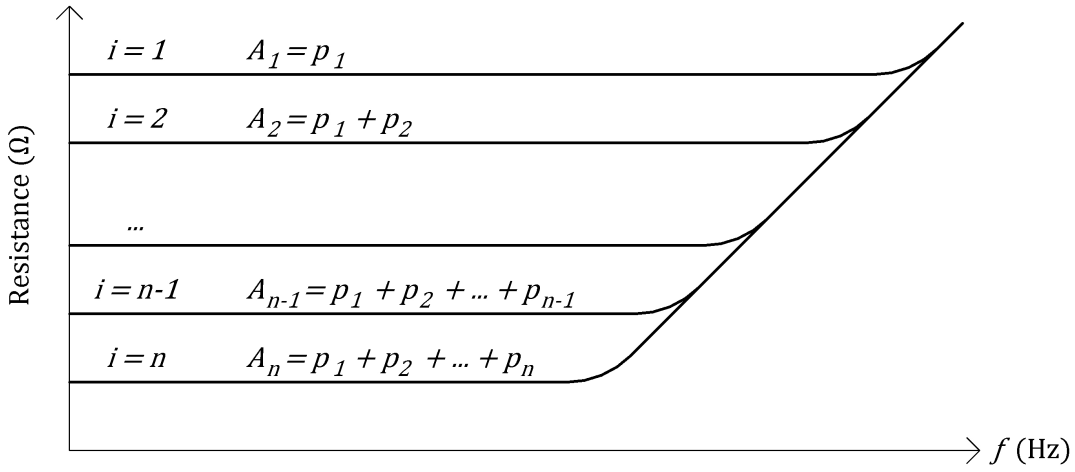

Figure 15: Resistance profile of conductor A's n partitions.

The n resistance profiles in Figure 15 are as expected, with the same comparable findings as with conductor B. In the same way that conductor A can be composed of n partitions, so can conductor B. In this case conductor B is equivalent to some combination of A's n partitions and thus A is composed of B from a behavioural perspective. The behavioural state of B describes A above B's skin depth frequency, from before, as does n partitions of A or B. The result here is that A can be represented as an n layered conductor with one of those layers being the conductor B, and is fully describable by B after B's skin depth frequency. This is illustrated in Figure 16 below and by Equation (7). This assumes the rules from the first step such that A must be thicker than B, therefore $\delta_A > \delta_B$, and with increasing frequency current tends towards p_1, making B the final layer to conduct. Given that B can also be partitioned, it is not required that it is the final layer as another resistance profile could be found for any portion of B's thickness. For the purposes of Figure 17, B will be the final layer.

$$B = \sum_{i=1}^{k} p_i \tag{7}$$

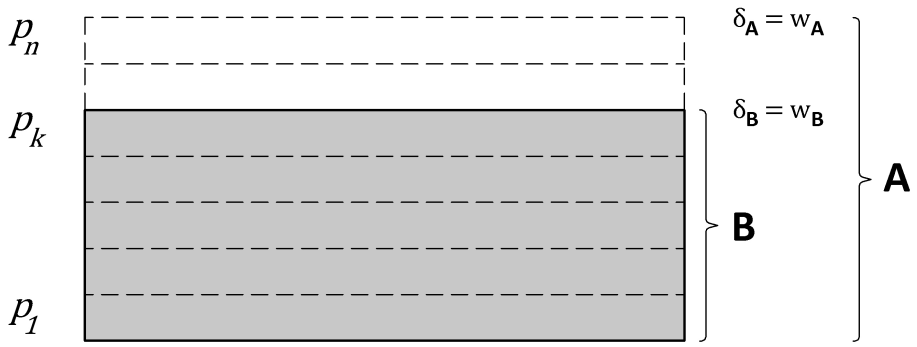

Figure 16: An n layered conductor A composed of conductor B as it is equivalent to partitions p_1 to p_k of A's n layers in the case that p_1 will conduct all the current at the highest frequency and that $\delta_A > \delta_B$.

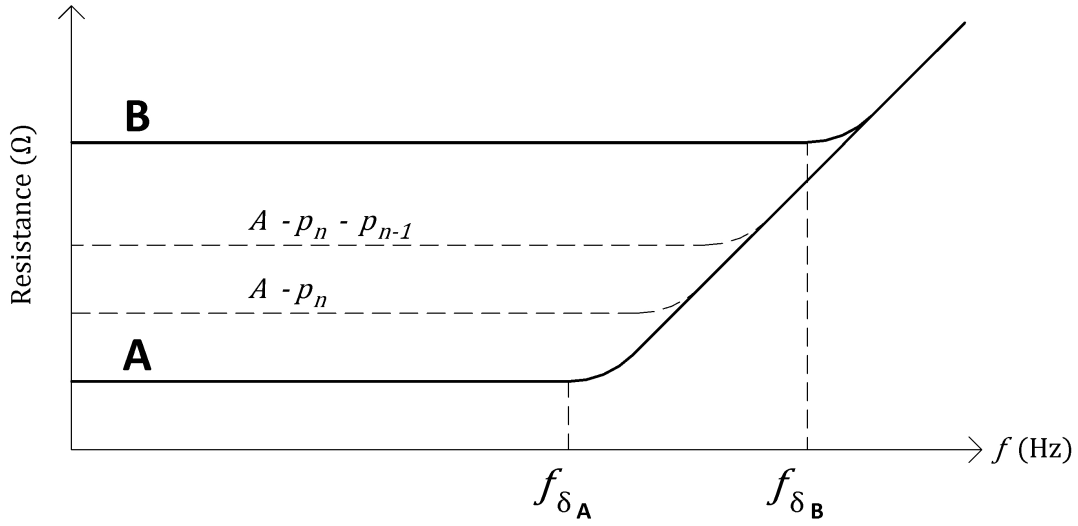

Figure 17: Resistance profile of conductor A composed of n-k-1 partitions and conductor B.

3.1.1 Behavioural equivalency in multipath conductors

It is clear that as frequency increases, the resistance through the structure increases, as the conducting cross-sectional area decreases due to the current migration. As in the previous examples, conductor B fully describes the behaviour when $f > f_{\delta_B}$. Consider **different** material properties of conductivity and/or permeability of B to A – and A being an outer layer to B. The value of skin depth for the composed conductor will be different, however, the movement of current will still continue in the same direction and $\delta_A > \delta_B$. This means that B describes the system for $f > f_{\delta_B}$. This is where the majority of the current has migrated into conductor B, to the extent that A is considered to not be in the system. This is only feasible as an estimate when the frequency is higher than the skin depth frequency of B alone.

For $f < f_{\delta_B}$, the resistance is a result of the combined effect of the materials that are conducting current. This is the materials of A and B – and any other layers included in the frequency range in other cases. Similarly, B can be composed of different layers and have the same effective results. Consider the example that only the resistance value is known between some arbitrary frequency value, z, and f_{δ_B} where $z < f_{\delta_B}$. This value is equal to R_A. If z is greater than DC, infinitely many combinations of materials exist to compose the resistance value. But if z is at DC then no other layers exist and R_A is composed only of A and B where the material properties combine in a certain way resulting in R_A. In examples of more layers, all the layers will be present in the resistance calculation at DC – as expected.

The manner in which the materials combine in order to predict the behaviour is described later in the work. This logic presents a core understanding of multipath

conductors that is applicable to *n* layers: as frequency increases beyond the first skin depth, the portion of the conductor larger than the skin depth, can be considered to not be conducting and the conducting layers govern the behaviour of the impedance. Should the conducting layers be composed of various material layers, these will, in order, no longer conduct, whilst the left over layers govern the behaviour. This explains the frequency-dependent nature of impedance in multipath conductors.

Creating *n* partitions of the same material is not necessary. By allowing the various layers to be the separations one can view the behavioural action of the multipath conductor as having a *peeling off* nature with increasing frequency. The material layers are the minimum resolution needed in order to understand the general behaviour of the multipath system. This is shown in the Figure 18 for differential- and common mode. This action is equivalent to structurally-different conductors as previously explained. Simulation of resistance and internal inductance of the separate structures and the combined structure is shown in Figure 19 and Figure 20 respectively. Demonstrated by simulation, the Peel Off Method is an understanding of multipath that the approached developed in this work is based on.

Figure 18 shows the basis of the *n-structure* method. The approach shows *n*-structures that can be simulated and the resulting profiles modelling a component of the overall behaviour. The structures decrease by one layer as the skin depth frequency of its equivalent single layer is reached. This makes a series of structures with *n, n-1, n-2, …, 2, 1* layers each. This is, in essence, the simplified behavioural understanding of multipath conductors with a relatable simple structural model for the system. The generalised approach encompasses *n-layered* multipath conductors – which would have *n*-structural scenarios.

Multipath conductor domain is made accessible by modelling different material properties for multipath layers in a simpler manner. It is this aspect that is developed by mathematically modelling the *n*-structures that this method enables. These models will be explored in later sections.

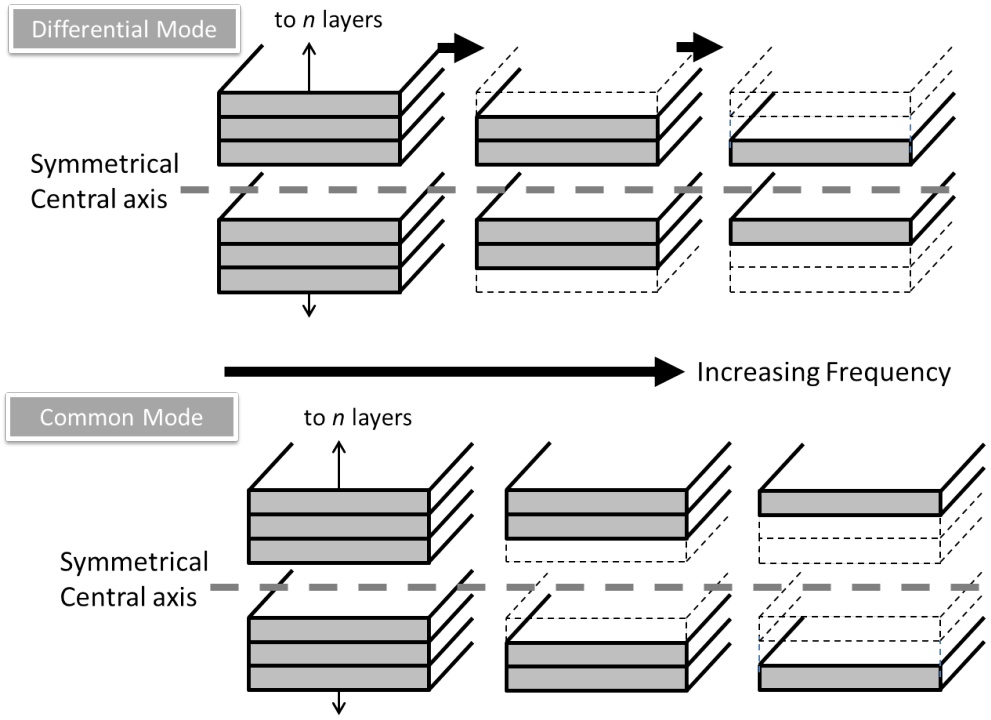

Figure 18: Differential- and common mode peel off action of multipath conductors with increasing frequency. Layers are peeled off as the frequency increases beyond the conducting structure's skin depth.

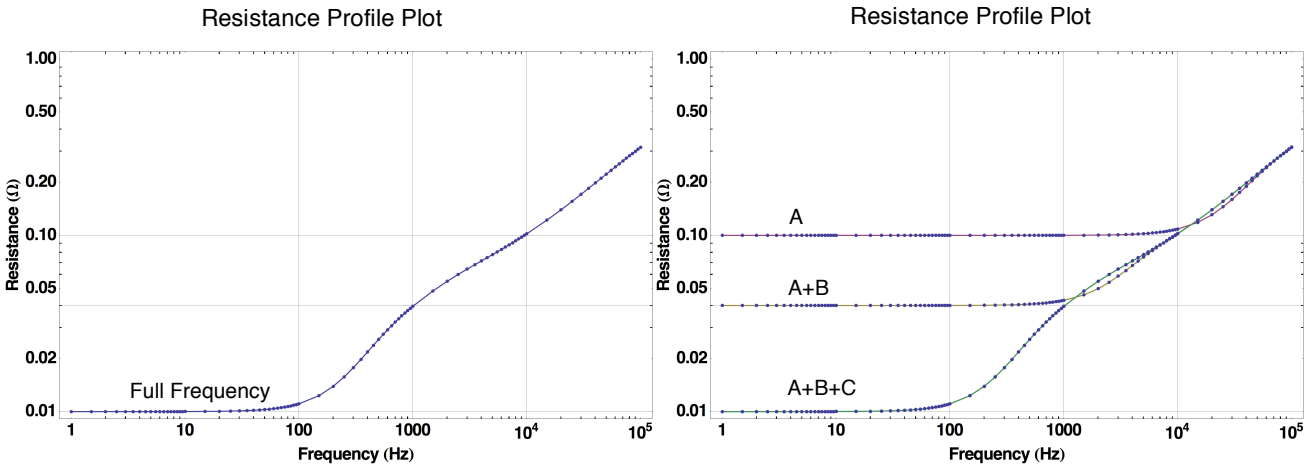

Figure 19: (left) Resistance profile of a multipath conductor with different material properties for each layer in differential mode operation. (right) The Peel Off approach of the same structure illustrating each layer's contribution to the overall impedance profile.

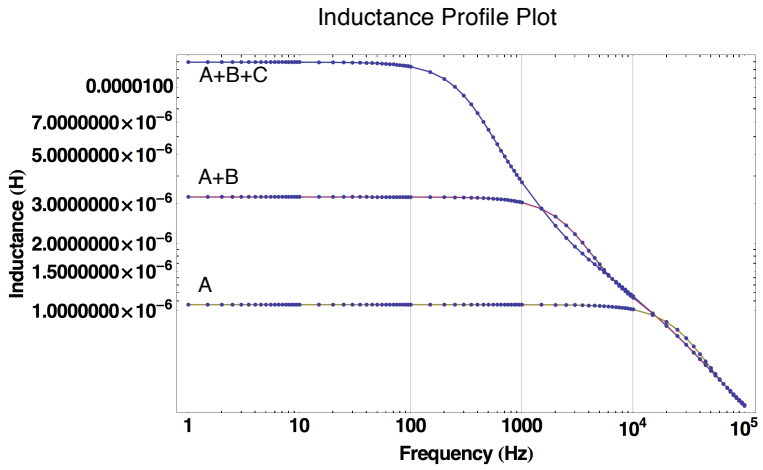

Figure 20: internal inductance profile for the same structure measured in Figure 19, with each layer's contribution illustrated using the peel off method.

3.2 The Peel Off Method

This section presents a procedural methodology to encapsulate the theory developed in the previous section. It is easier to grasp the theory in terms of a step-by-step method and thus be able to refer to it in explanations that stem from this theory. The Peel Off Method is a validation of the *n-structure* method from the previous section. Simulating each of the n-structures, using the complex Full Frequency Analytical Method, and investigating the agreement of profiles against the whole structure's behaviour is how the validation is found.

The generalised approach and understanding described above shows that any planar conductor:

1. Can be represented by n separate layers.
2. Can be composed of layers of different material properties.
3. Can be understood that with increasing frequency, certain layers are estimated to not contribute to the conducting cross-sectional area.
4. Can be understood that the conducting component of the structure as a whole can be used to find the resistance and internal inductance values.

The first two points here are specific to multipath conductors and the last two points are specific to an understanding of multipath conductors. The points form the foundation of what is discussed here.

An important simplification of the generalised approach is that layers of different materials (true structural layers) will no longer conduct with increasing frequency, one-at-a-time, as the skin depth of the structure becomes smaller than the whole structure. This is extrapolated to be true for n layers of different materials. Figure 21 illustrates how various structural scenarios arise when eliminating non-conducting layers from the conductor as frequency increases. An n-layered conductor gives rise to

n structural scenarios through *n* skin depth frequencies that mark the transition between the scenarios. Figure 18 shows primarily the migration of current between layers and is part of the theory development. Figure 21 is a description of the method derived from the theory development showing that the *n*-structure method is not considering current migration but rather that the layer does not exist for purposes of the analysis.

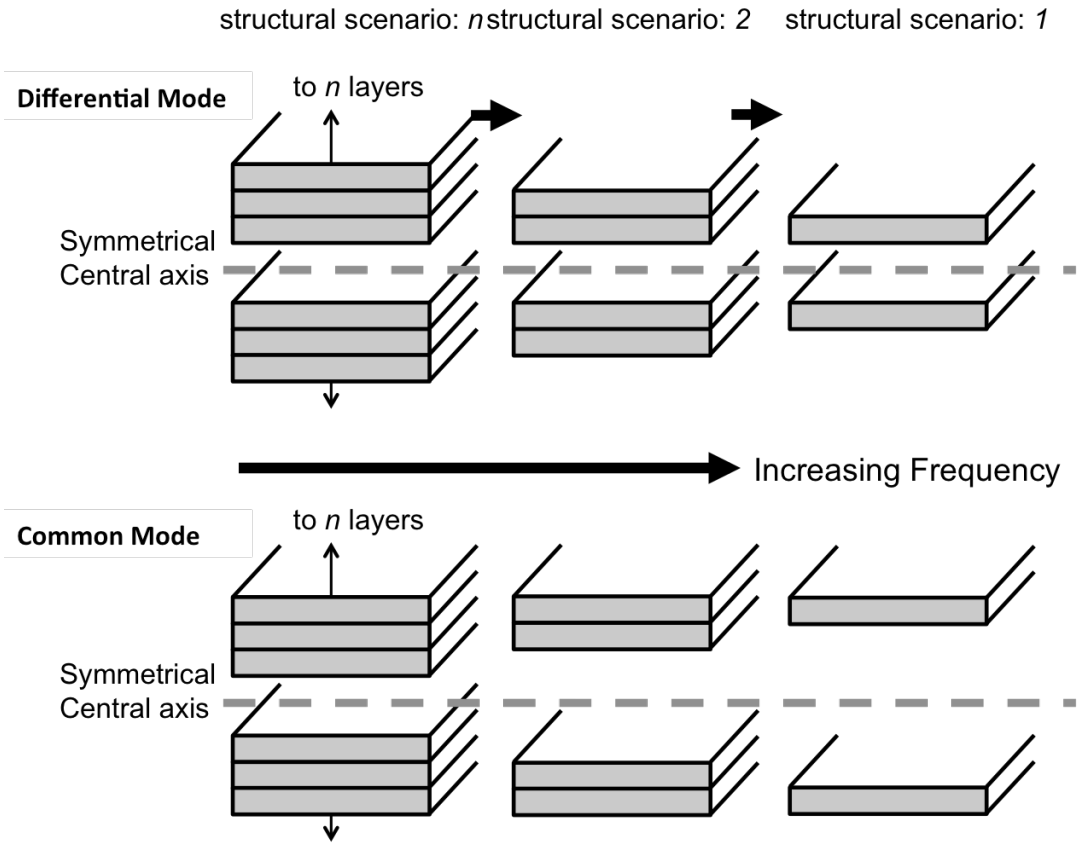

Figure 21: Creation of structural scenarios by eliminating non-conducting layers over various frequency ranges.

This approach of modelling *n* structural scenarios over *n* defined frequency ranges (governed by the skin depth frequencies of each structural scenario) is termed the *n-structure method*, however, simulating these structural scenarios is termed the *peel off method*. The structural scenarios present a manageable way to deal with (and understand) multipath conductors through its approach of isolating only relevant aspects of the conductor.

The combined effect of each structural scenario's material properties is a constant resistance- and internal inductance value. Although the value is not truly constant, the estimations presented in the generalised approach using a log scale show that the values can be considered constant over the given frequency range, and equal to the low frequency (near DC) value. This characteristic is found in clear-cut cases yet provides the necessary understanding such that in more obscure cases (with

noticeably increasing profiles), the behaviour can still be understood. The structural scenarios can be analysed with the net effect of all the scenarios composing the impedance profile of the conductor. The Peel Off Method also simplifies away the need to model skin- and proximity effects on the current distribution, allowing for analytical approaches to use low frequency (DC) approximation methods to model the structure.

It is clear that there exists a means to determine the constant resistance- and internal inductance values by using the material properties of the layers that comprise each scenario. This is identified in the next section. Understanding how the individual layers come together in a given structure is important for the modelling approaches considered in this work. The manner in which material properties behave together and, also, modelled as an aggregation for averaged effective properties, is discussed in the sections that follow.

4. Mathematically Modelling the *n*-structure Method

In the previous section, a generalised understanding of multipath conductors using the Full Frequency Analytical Method and the Peel Off Method is explained. The theory is developed to gain insights into the behaviour of the structure and identify ways of simplifying the understanding of it. The aim of this section is to apply a mathematical understanding to the simplified, general understanding that is developed in the previous sections. Development of the mathematical model is founded on using equations that make use of the material properties of the layers directly. The benefits of using the material properties directly gives the analyst (or designer) the ability to directly relate material properties that one has control over to the behavioural impact that a change effects – as is achieved in [9]. This takes preference to using equations based on properties that abstract from the material properties such as having lumped parameter resistance values – which later suffers from a dependency on FEM analysis to identify material properties, as elaborated on in the introduction of this work.

The first equations needed are developed from the application of established methods of resistance (using material property parameters) and Ampere's Law (for finding the internal inductance equation) to the simplified structural scenarios from the *n*-structure method. These equations provide a means to calculate the impedance magnitudes for each of the *n* structures at low frequency such that the values agree with near constant (plateau) values of the Peel Off Method. The immediate benefit of this method is that the constant values of the Peel Off Method can be found using simple mathematics instead of carrying out complex mathematics over multiple frequencies. Yet the structure of the equations themselves provides a key simplification to unlock the greater findings of this work.

By parameterising terms that involve summations and relationships between layers, an equation can be represented in a simpler manner, whilst maintaining its overall correctness. This parameterisation encapsulates relationships and can be understood as replacing many layers with an effective single layer. The relationship between the layers in the case of resistance happens to represent a weighted average of material properties, with the weighting being the layer thickness compared to the total thickness. This weighted average, when viewed from a structural perspective, is essentially a *structural averaging* of layer properties to find a single, representative set of properties. This is described in the Section 4.2.

The ability to approximately reduce a multipath conductor to a single-layer conductor enables the solution to be further understood using established single layer methods. A full frequency analysis using established methods is possible and is explained in Section 4.2.3 in a method termed Average Structural Analysis. The concept of skin depth (only intuitive for single layers) and the frequency at which it is comparable to the thickness of the structure is reviewed in Section 4.3. The ability to find the skin

depth frequency is combined with the low frequency methods to give rise to the method termed Salient Point Analysis in Section 4.3.1. Later, the ability to find the skin depth frequency, possible through the use of structural averaging, is key to identifying the design solution of this work.

4.1 Low Frequency Impedance of Structural Scenarios Using Material Properties

The purpose of this section is to apply the concepts resistance and internal inductance to develop equations that model the simplified structures. The structures are based on the *n*-structure method of compartmentalising a multipath conductor system up into *n*-structures each with {*n, n-1, n-2, …, 2, 1*} layers – from Section 3.

Consider a single structural scenario having *n* layers, with each layer potentially having different material properties of conductivity (σ), permeability (μ), and thickness in the vertical direction (*w*). For analysis purposes, it is desirable to find the total impedance of the scenario and is therefore required that the total resistance and total internal inductance be found using the material properties of the structure.

Finding the total impedance of the *n*-layered scenario can either be determined:

- Through a closed-form solution where the variable can be substituted for any number of layers
- Or through a generalised approach that can be iterated to a solution for any number of layers.

Resistance and internal inductance are orthogonal and are considered separately in this approach. Finding the total resistance and internal inductance using each of the layers' properties for each of the scenarios can be visualised using Figure 22. Figure 22 will be contrasted to another method later, which finds the combined effective material properties instead of the total impedance.

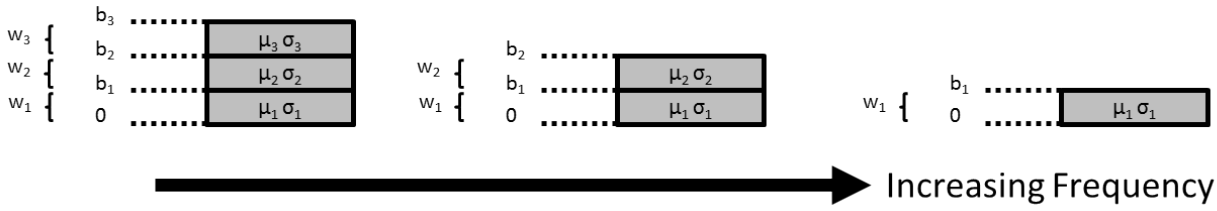

Figure 22: Structural basis for finding the total impedance using the material properties.

A method for finding resistance and internal inductance values for low frequency of structural scenarios is presented in the sections that follow. In this approach there is no means of identifying valid frequency ranges for the structural scenario, only the

impedance magnitudes. In later sections, a method of identifying the frequency ranges is developed using skin depth theory.

4.1.1 Development of resistance equations

At DC the total resistance of the structure can be found in the same way that total resistance can be found for resistors in parallel, see Figure 23. This assumption can be made due to the well-known effect that, at DC, current distributes itself across paths according to the conductance of each path. The DC value can be approximated to remain constant over the frequency range considered. Equation (8) describes the resistance for the structural scenario by using the material properties in the resistor equation for *n* resistors in parallel.

$$r_n = \frac{l}{width \sum_{i=1}^{n} w_i \sigma_i} \tag{8}$$

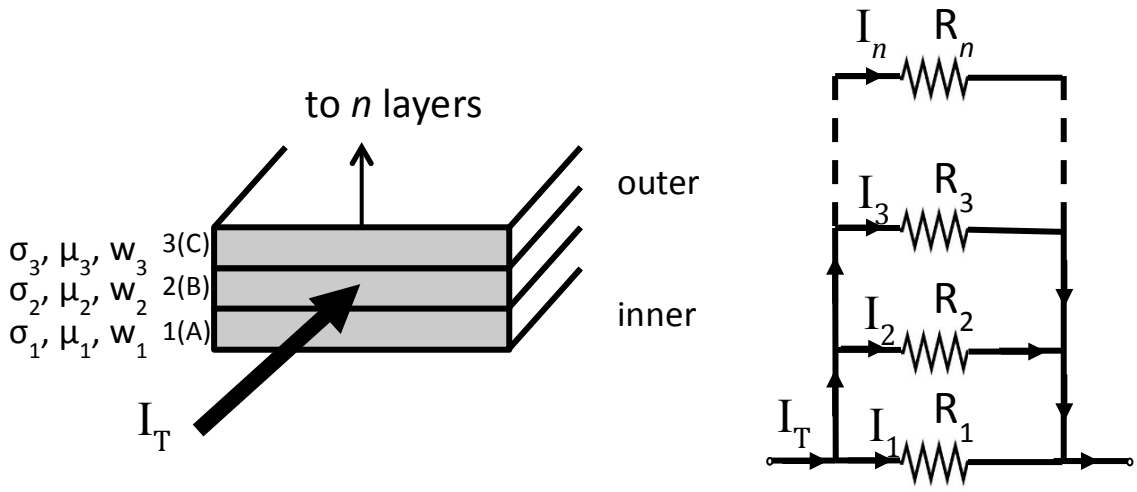

Figure 23: Modelling the resistance of a multipath conductor as each layer being a resistor in parallel with the next. The resistance of each resistor in parallel is found from the material properties of its corresponding layer.

4.1.2 Development of internal inductance equations

The internal inductance is related to the material properties of the structure and is the structure's contribution to total inductance. External inductance is a result of the structure's layout mainly depending on length of- and air gap between conductors. External inductance is not considered here, as it is specific to the implementation and construction of the conductor, however, it is important to not neglect its contribution as it becomes largely responsible for the inductance component at high frequency. Modelling the internal inductance is more involved than the resistance component and requires the application of Ampere's Law, Equation (9), to determine the magnetic field intensity (H field) across the structure. The H field is then used to find the energy stored in the structure, *W*, and hence the inductance, *L* – Equations (10)-(11).

$$\oint H \bullet dl = I_{enc} \tag{9}$$

$$W = \frac{1}{2}\mu \int H^2 dV \tag{10}$$

$$L = \frac{2W}{I^2} \tag{11}$$

In this approach it is important to define references from the outer boundary of the layer that will next be peeled off and is where the H field truly is zero. The reference definitions for the mathematics are shown in Figure 24, along with explanatory examples of the current density (J)- and H field profiles through the multipath conductor.

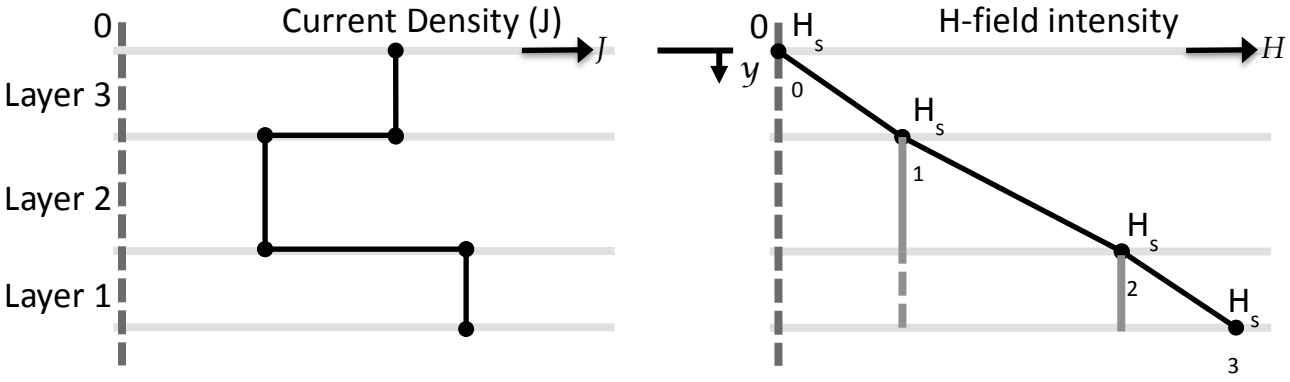

Figure 24: A structural scenario modelled at DC showing explanatory profiles of current density and magnetic field intensity. The reference definitions used in the solution of the maths is shown. This is shown for one half of the symmetrical layout of the conductor.

The following is under the assumption that planar multipath conductors can be resolved to a two dimensional problem. The contour integral in Equation (10) can be simplified through Equations (12)-(14) by considering that the thickness is very much smaller than the width of the conductor. This allows for approximating the length of the loop, *l*, to be twice the width of the conductor – see Figure 25. Equation (13) shows a direct relationship between J- and H for each layer. As depicted in Figure 24, the relationship is only linear between the layer boundaries, creating an overall piecewise linear H field. This is important to remember when finding the energy stored in the conductor. The current, *i*, in Equation (14) is a proportion of the total current due to the conductance contribution of the layer to the overall structure. This proportional value is found later yet the proportional current concept should be kept in mind throughout this derivation.

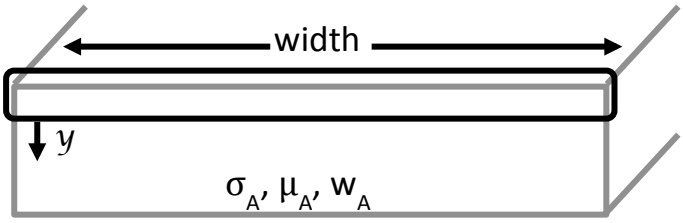

Figure 25: Simplification of the contour integral due to the width being much larger than the thickness. The loop length is approximately two times the width, since the thickness (in y-direction) is negligible over these dimensions.

$$2\,H\,width = J\,y\,width \tag{12}$$

For both halves of the conductor: $H = J\,y$ (13)

$$J = \frac{i}{width\,y} \tag{14}$$

Equation (10) is used to find stored energy of a magnetic field. This uses a reference defined for y where the H field is zero and increasing in the positive direction. Given that the length and width of the conductor are known constants, the volume integral simplifies to an integral over the thickness only, Equation (15). With increasing y, the current density changes at the layer boundaries as each layer conducts a different portion of the current, Figure 24. The gradient of the H field differs at these layer boundaries resulting in the stored energy of Equation (15) being modified to take into account, firstly the layer boundaries, Equation (16) and secondly the gradients, Equation (17). An illustration of the summation of the integrals is shown in Figure 26 by the total area between layers being the sum of the rectangular area (the constant terms within the integral) and the triangular area (the term in the integral with y variable). Note that this can also be solved geometrically.

$$W = \frac{1}{2}\mu\,length\,width\int H^2\,dy \tag{15}$$

$$W = \frac{1}{2}\mu_n\,length\,width\int_0^{w_n} H^2\,dy + \frac{1}{2}\mu_{n-1}\,length\,width\int_{w_n}^{w_n+w_{n-1}} H^2\,dy + \cdots + \frac{1}{2}\mu_1\,length\,width\int_{w_n+w_{n-1}+\cdots+w_2}^{w_n+w_{n-1}+\cdots+w_1} H^2\,dy \tag{16}$$

$$W = \frac{1}{2}\mu_n \, length \, width \int_0^{w_n} \left(\frac{i_n}{width \, w_n} y\right)^2 dy + \frac{1}{2}\mu_{n-1} \, length \, width \int_{w_n}^{w_n+w_{n-1}} \left(\frac{i_n}{width \, w_n} w_n + \frac{i_{n-1}}{width \, w_{n-1}} (y - w_n)\right)^2 dy + \cdots + \frac{1}{2}\mu_1 \, length \, width \int_{w_n+w_{n-1}+\cdots+w_2}^{w_n+w_{n-1}+\cdots+w_1} \left(\frac{i_n}{width} + \frac{i_{n-1}}{width} + \cdots + \frac{i_1}{width \, w_1}(y - (w_n + w_{n-1} + \cdots + w_2))\right)^2 dy \quad (17)$$

Let n be the total number of layers.

$$W = \sum_{j=n}^{1} \left(\frac{1}{2} length \, width \, \mu_j \int_{\sum_{z=n}^{j+1} w_z}^{\sum_{z=n}^{j} w_z} \left(\left[\frac{1}{width} \sum_{z=n}^{j+1} i_z \right] - \left[\frac{i_j}{width \, w_j} \sum_{z=n}^{j+1} w_z \right] + \left[\frac{i_j}{width \, w_j} y \right] \right)^2 dy \right) \quad (18)$$

Where the proportion of current can be found in terms of the total current, I_T, between each layer boundary as per Equation (19). This calculation divides the total current proportionally, due to the weighted contribution of thickness and conductivity to the total. Equation (19) shows how the conductivity property of each layer contributes to the overall stored magnetic energy, Equation (18), within the structure by the weighted proportioning of total current. Substituting Equation (19) into Equation (18) shows the stored magnetic energy in terms of all thickness, conductivity and permeability.

$$i_j = \frac{w_j \sigma_j}{\sum_{z=1}^{n} w_z \sigma_z} I_T \quad (19)$$

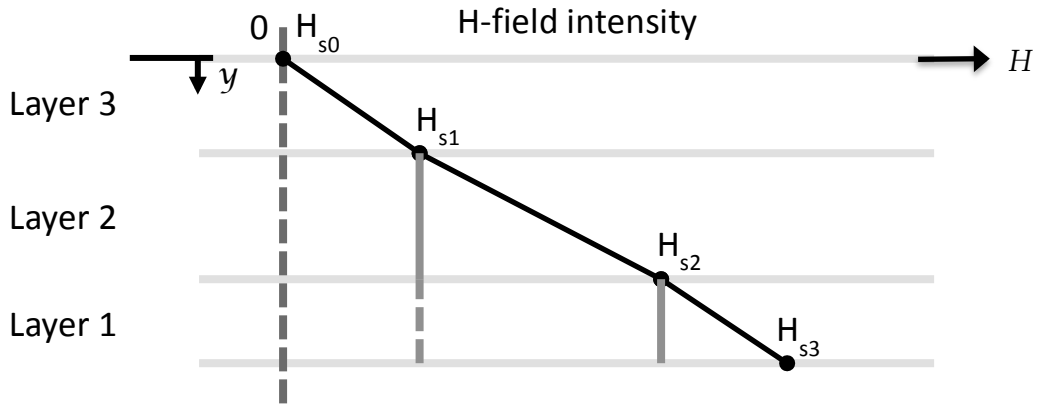

Figure 26: Layer boundaries and different gradients within the piecewise linear H field result in different integrals describing the area below the curve.

The stored energy of (18) is substituted into Equation (11) in order to find the total inductance for the structural scenario, Equation (20)-(21). Note that this is independent of the total current since the conditions in Equation (21) are also squared once substituted in Equation (20) and are cancelled out by the denominator.

The general form of this solution allows for the total inductance of any number of layers to be present in the structural scenario. The modelling approach and the Peel Off Method results in n structural scenarios over each of the n frequency ranges for an n-layered structure. The total inductance solution found for an n-layer structural scenario allows for the solution of all structural scenarios by simply setting the non-conducting layers' conductivities to zero in the general solution, in order to eliminate them from the total inductance for the scenario under consideration.

$$L = \frac{2}{I_T^2}\sum_{j=n}^{1}\left(\frac{1}{2}length\ width\ \mu_j \int_{\sum_{z=n}^{j+1} w_z}^{\sum_{z=n}^{j} w_z}\left(\left[\frac{1}{width}\sum_{z=n}^{j+1} i_z\right] - \left[\frac{i_j}{width\ w_j}\sum_{z=n}^{j+1} w_z\right] + \left[\frac{i_j}{width\ w_j} y\right]\right)^2 dy\right) \tag{20}$$

Where

$$i_j = \frac{w_j \sigma_j}{\sum_{z=1}^{n} w_z \sigma_z} I_T \tag{21}$$

4.2 Aggregation of Material Properties in Structural Scenarios

This section makes use of the equations developed for resistance and internal inductance to n layers in the previous section. Where the goal in the previous section was to find a magnitude for the impedance components, the purpose of this section is

to find, rather, a single layer structure that, when analysed using the developed equations, is representative of the *n*-layered structure. This section makes use of algebraic substitutions to parameterise out the inter-layer relationships of the developed equations. This transforms the equation into the same structure as single layer (low frequency) equations, thereby finding single material properties for a single layer that is representative of the underlying multipath conductor.

The aggregation of material properties is a means of identifying the net effect of all the layers using the impedance behaviour. The net effect is a reduction to a single effective conductivity, permeability and thickness for an *n*-layered structural scenario. The effective material properties give rise to a conceptual effective single layer that represents multiple layers such that the impedance behaviour is maintained. Choosing to model the behaviour as opposed to modelling the structure is key to this solution.

The importance of effective properties lies in the identification of the skin depth frequency for the structural scenario – since a single layer equivalent structure is conceptualised. Beyond the requirement for identifying a skin depth frequency, this method is significant in simplifying the structure to a single layer that can be simulated over the full frequency range.

An alternative means of finding the total resistance and inductance (as in the previous section) for the structural scenario is to combine all the material properties such that only a single layer needs to be analysed. The benefit of a single layer solution is that the literature and computational tooling in this domain are well established. This approach simplifies the combination of the material properties within a structural scenario. The simplification is such that the resultant effective material properties have the correct low frequency impedance and skin depth characteristics. Figure 27 describes this approach showing each structural scenario represented by a single value for conductivity, permeability and thickness calculated from the materials that comprise the scenario – this is in contrast to that seen in Figure 22. This approach too considers an n-layer structural scenario such that its solution can be applied to all scenarios.

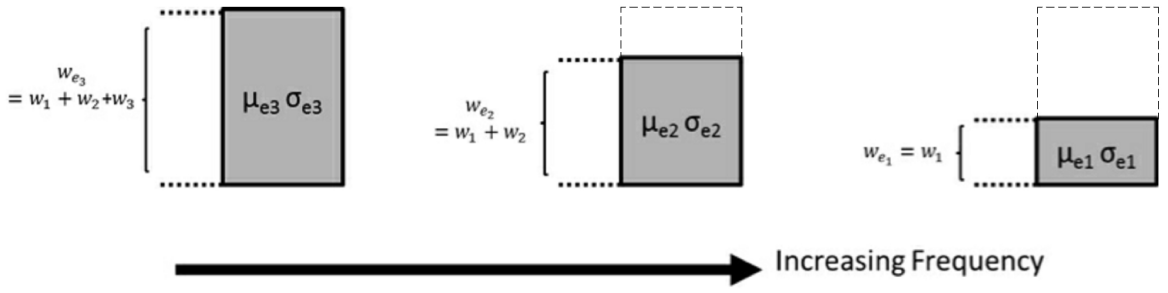

Figure 27: Structural basis for the aggregation of material properties for the reduction of a multipath conductor to a single layer conductor.

4.2.1 Resistance using effective material properties

Essentially this approach is a weighted average of the material properties using each layer's thickness contribution to the total thickness as the weighting. This effect is already at play with the standard resistance equation. Parameterising the weighted average creates a single-layer perspective on the resistance equation, which can then be analysed in terms of skin depth. This is seen as an enabling aspect of the method.

To re-iterate the concept of effective property values, the net behavioural effect is a reduction to a single effective conductivity, permeability and thickness for an *n*-layered structural scenario. Each property is considered in terms of the combined property values that are active in the scenario to identify an effective property value that has the same effect as all the property values.

Consider an *n*-layered structural scenario with effective material properties of conductivity, permeability and thickness as $\sigma_{e_n}, \mu_{e_n}, w_{e_n}$ respectively. The total resistance of the structure represented as a single layer is described by Equation (22) and is the same format as any single layer resistance equation.

$$r_n = \frac{l}{width\, w_{e_n} \sigma_{e_n}} \tag{22}$$

In comparison with Equation (8), the summation can be rearranged as shown in Equation (23). Here, each term in the summation is divided by the sum of all the thicknesses present in the scenario and multiplied by the sum too. This is effectively a multiple of one. Each term, however, is now structured as a weighted average according to thickness. It is this manipulation that allows for the parameterisation and therefore structural averaging of the structural scenarios.

$$r_n = \frac{l}{width \left(\frac{w_1\sigma_1}{w_1+w_2+\cdots+w_n}+\frac{w_2\sigma_2}{w_1+w_2+\cdots+w_n}+\cdots+\frac{w_n\sigma_n}{w_1+w_2+\cdots+w_n}\right)(w_1+w_2+\cdots+w_n)} \tag{23}$$

Letting an effective thickness be equal to the sum of all *n* thicknesses, see Equation (24), simplifies the resistance equation to Equation (25). It is important to define effective thickness as the sum of the thicknesses present in the scenario as it needs to be compared against the skin depth of the structure later – a fundamental assumption discussed in the generalised approach – section 3. Letting the effective conductivity of all the conductivities in the structure be a weighted average, using the thickness of the layer as a weighting, Equation (26), then the simplification shown in Equation (27) agrees with that found in Equation (22).

$$w_{e_n} = w_1 + w_2 + \cdots + w_n = \sum_{i=1}^{n} w_i \tag{24}$$

$$r_n = \frac{l}{width\left(\frac{w_1\sigma_1}{w_{e_n}} + \frac{w_2\sigma_2}{w_{e_n}} + \cdots + \frac{w_n\sigma_n}{w_{e_n}}\right)(w_{e_n})} \tag{25}$$

$$\sigma_{e_n} = \frac{w_1\sigma_1}{w_{e_n}} + \frac{w_2\sigma_2}{w_{e_n}} + \cdots + \frac{w_n\sigma_n}{w_{e_n}} = \sum_{i=1}^{n} \frac{w_i\sigma_i}{\sum_{j=1}^{n} w_j} = \frac{1}{w_{e_n}} \sum_{i=1}^{n} w_i\sigma_i \tag{26}$$

$$r_n = \frac{l}{width\, w_{e_n}\sigma_{e_n}} \tag{27}$$

Equations (24) and (26) provide a means of aggregating the material properties of thickness and conductivity. This abstraction of the individual material properties into a single figure allows for the DC resistance for any structural scenario, up to *n* layers, to be calculated in the standard way.

The benefit of the single layer approach is to simulate the single layer over all frequencies (not just at DC) using standard full frequency equations. Full frequency resistance simulations take into account skin- and proximity effects and require a value for permeability as well as conductivity and thickness. An effective permeability parameter is required to be found using the layer properties.

A simple approach is to model the structure as a magnetic circuit with parallel branches in which flux can flow. Reluctance is analogous to resistance, as is flux to current and permeability to conductivity when considering a magnetic circuit. An effective permeability is found, using this analogy, in the same manner that the effective conductivity is found. This progression is seen in Equations (28)-(30) and uses the same definition of equivalent thickness found in Equation (24). This method of simplifying the calculations by using a magnetic circuit rather than the low frequency inductance equations is that the equations are too complex to work with. It is difficult to identify a pattern (similar to that of the weighted average seen in the resistance equation) within the equations and parameterise it such that a general form of the equation can be found. The identification of the parameterised internal inductance equation is not critical to the progression of this method yet does introduce more error into the approach. This simplification using a magnetic circuit model limits the scope of application for structural averaging, as it does not contain as much detail as the full equation. Structural averaging for internal inductance is elaborated on in the section following.

$$\Re = \frac{length}{width\, w\, \mu} \tag{28}$$

$$\Re_{tot} = \frac{length}{width\, \sum_{i=1}^{n} w_i\mu_i} = \frac{length}{width\, w_{e_n}\mu_{e_n}} \tag{29}$$

$$\mu_{e_n} = \left(\frac{w_1\mu_1}{w_{e_n}} + \frac{w_2\mu_2}{w_{e_n}} + \cdots + \frac{w_n\mu_n}{w_{e_n}}\right) = \frac{1}{w_{e_n}}\sum_{i=1}^{n} w_i\mu_i \tag{30}$$

The full frequency single layer resistance can now be found using the effective conductivity, permeability and thickness parameters identified in this section. These material properties are proportionally related in the skin depth equation. The skin depth frequency describes the significant frequency points in the analysis and is identified when simulating the equations over the full frequency range. The magnetic circuit model assists as a different approach to finding a simplified value for permeability. The permeability value found by this method only allows for the full frequency resistance to be simulated. Finding the internal inductance for the structure is explained in the next section, although the full frequency analysis of an effective single layer is not possible using the permeability parameter found here.

4.2.2 Internal inductance using effective material properties

Internal inductance cannot be explained as simply as a parameterisation of the existing mathematics. The underlying low frequency mathematics for single- to many layers does not produce an identifiable, manageable pattern – as is seen by the weighted average pattern found in the resistance case. The approach to finding effective properties for their use in the internal inductance calculations is no simple task and does not have a simple underlying mathematical 'trick' that will more readily describe the layer interactions.

The effective conductivity is found, given an effective thickness definition, through the comparison of the single layer DC resistance equation and the n-layered DC resistance in Equation (8). It would be ideal if, in the same vein, the single layer low frequency internal inductance equation, Equation (31), were comparable with the n-layered inductance equation, Equations (20) and (21), in order for a similar abstraction approach to be followed. One can see that this is no simple task as the total internal inductance is not represented as a closed form solution and contains many summations. Even considering two or three layers with the integrals simplified does not present any simple means of encapsulating terms with single parameters. This approach of finding the effective permeability through the internal inductance equation is not considered further. The total internal inductance therefore cannot be found using this approach as there are more parameters and terms to consider that are at play than those simply described in Equation (31) when moving to multiple layers. This means that even with an effective permeability, Equation (31) is simply inadequate to describe the multipath structure's total internal inductance by encapsulating it in a single parameter.

This is not of much consequence as there is already a computationally easy mechanism for finding total inductance of the structure. Extra effort in this approach does not contribute to the overarching goal of a design-oriented analytical approach but rather

limit the scope of its application as error margins are suspected to become large when there are largely contrasting material property values. Identifying a way to better parameterise the permeability, without reliance on the magnetic circuit simplification, will enhance the approach presented in this work. However, the magnetic circuit approach does allow for a value to be found and suffices in the context of this work. The need to identify the enhanced approach is seen as non-critical for the further development of this work. Future work in this field to minimise error margins should consider this aspect.

$$L = \frac{1}{3\,wid} w\mu \tag{31}$$

Note that the effective permeability cannot be used in an equation such as Equation (32) to find the DC value either. The equation is invalid, has no mathematical grounding, and will produce incorrect values of total DC internal inductance.

$$L = \frac{1}{3\,wid} w_{e_n}\mu_{e_n} \tag{32}$$

4.2.3 Averaged Structural Analysis Concept Development

This section aims to consolidate the findings of structural averaging (in multipath conductors) by an analytical method termed *Averaged Structural Analysis*. Structural averaging is the ability to represent a multipath conductor, which is composed of many different material properties, as a single set of effective material properties. The method applies the concepts, developed above, to form an analytical approximation to the Full Frequency Analytical Method by [9] with the intention of simplifying the analysis of structures.

Structural averaging is only successful in approximating the resistance profile of structures. Only layers that do not have vast (orders of magnitude) differences in their property values are applicable for this approach.

The approach is as follows:

1. Apply the *n*-structure method to a given multipath conductor of the appropriate nature to obtain *n* structural scenarios of {*n*, *n-1*, *n-2*, …, *3*, *2*, *1}* layers.
2. Calculate the structural average for each of the structural scenarios present.
3. Determine the resistance profile through simulation by applying established methods to the effective single layer structural averages.
4. Interpolate the curves to approximate the full frequency response by plotting the effective single layer resistance profiles on the same set of axes.

Finding the structural average for each scenario is a simple task based on Equations (24)-(30). The approach is defined as a systematic means of plotting all the

structural scenario's resistance profiles on a single set of axes. The interpolation follows the lowest valued resistance profile and transitions between curves after when the skin depth frequencies are reached. This transition relates to the migration of the majority of current out of an outer layer – approximately, such that it is no longer conducting. This method is demonstrated in Section 5.1.2.

This method is not capable of producing the internal inductance profiles and requires another method (developed later) to complement it's resistance profile in this sense to identify the full impedance behaviour of the conductor as an approximation.

The analysis of multipath conductors is made simpler by the systematic nature of this approach coupled with the simplified internal mathematics. This method makes use of established methods and as such is more accessible to people working in this field. The skin-depth-frequencies are intrinsic to the simulation of the effective single layers and therefore does not require further calculations to find that frequency bounds of each structural scenario. Other approaches that follow on from here do require this information. Further to this, the analytical approach lends itself to parametric design capabilities by iterating through material property values for multipath structures. These concepts are later used in a different manner to find an analytical design approach.

4.3 Skin Depth Using Effective Material Properties

The generalised approach and basis for the *peel off method* makes the approximation that the full thickness of a layer can be considered to be conducting current until the frequency at which skin depth of the whole structural scenario is less than the physical thickness of the structure. After the skin depth frequency, the next structural scenario is considered. If only the last layer is left conducting, a single layer analysis should be followed. Equation (33) is the standard skin depth equation for a single layer. This is rearranged to solve for the frequency at which the skin depth is equal to the layer thickness in Equation (34).

$$\delta = \sqrt{\frac{1}{\pi f \sigma \mu}} \tag{33}$$

$$f_\delta = \frac{1}{\pi \sigma \mu w^2} \tag{34}$$

The equivalent single layer properties found in this section provide a means to find a value for the skin depth frequency and solve the missing component in the model. Finding effective material properties is necessary for reducing a multipath conductor to an effective single layer – this is for each structural scenario. Skin depth makes intuitive sense only when considering a single layer, or effective single layer, in order to make use of it's attributes. A means of finding the effective material properties is

presented in the next section. The concept of skin depth however is necessary for the skin depth frequencies to be found.

It seems strange that the behaviour occurs in this way when considering the physical underlying structure of the conductor. The previous section on the low frequency approach to modelling was tightly coupled to the structure itself. Using effective materials is tightly coupled to the behaviour while making use of the underlying structure. This suggests that the same behaviour may be obtained through the use of different physical aspects of the structure – as in, different thicknesses of different conductivities, and permeabilities may result in the same resistance value and skin depth frequency. Using a single layer to now represent behaviour is a more manageable concept, given the behavioural aspects over the physical aspects.

The effective material properties essentially abstract/transform each structural scenarios into separate single layers each with the total physical thickness maintained. The skin depth figure can then be compared against the effective thickness (the total thickness of the structural scenario) to find the frequency at which the scenario is no longer an applicable model. Equation (35) finds the skin depth frequency for an *n*-layered structure using the effective material properties identified in this section. Equation (35) shows strong resemblance to Equation (34) as both represent a single layer.

$$f_{\delta_n} = \frac{1}{\pi \sigma_{e_n} \mu_{e_n} w_{e_n}^2} \tag{35}$$

4.3.1 Salient Point Analysis Concept Development

The purpose of this section is to develop an analysis methodology that allows the analyst to make use of only the salient points in multipath conductor impedance profiles such that it approximates the structure's behaviour as a whole. The Averaged Structural Analysis methodology requires a full frequency simulation of the structures yet has the benefit of not requiring the skin depth frequency to be calculated separately as the frequency bounds are a natural consequence of simulating single layer structures over across the frequency range. This method aims to make use of simpler, point analysis to achieve a similar approximation.

The low frequency resistance and internal inductance values can be found for any structure – and therefore any structural scenario using the *n*-structure method. This is achieved by using Equations (8) and (20)-(21) respectively. At this point the frequency bounds under which each structural scenario is defined are unknown – yet the bounds are known to exist.

Structural averaging allows each structural scenario to be represented as an effective single layer. With this single layer perspective, a skin depth can be found using Equation (35). The skin depth has no intuitive value for a multi-layered structure, yet for a (effective) single layer it can be compared to the (effective) thickness of the structure. The *skin depth frequency* is calculated here when the skin depth of the effective structure is equal to the effective thickness of the structure. This frequency represents the upper frequency bound for which the structural scenario is defined. The combination of the impedance values and the corresponding skin depth frequency values are the salient points in the structure's impedance profile.

The approximation method is therefore as follows:

1. Apply the *n*-structure method to the multipath conductor.
2. Calculate the low frequency resistance and internal inductance for each of the structural scenarios.
3. Determine the effective material property values for each of the structural scenarios
4. Calculate the skin depth frequency of structural scenario using the effective single layer material properties and the skin depth equation.
5. Plot the intersection of each structural scenario's resistance/internal inductance and skin depth frequency.
6. Add in a point at the lowest resistance value and 0 Hz
7. Interpolate these salient points in a piecewise linear fashion.

This approach is developed by interpolating a small number of points, 1+*number of layers present*, to approximate a resistance or internal inductance profile. The requirement for full frequency analysis is not present, yet the approach relies heavily on the concept of structural averaging. This approach is demonstrated in Section 5.1.3.

4.4 Significance of DC modelling and Effective Material Properties

A lot of information is presented in the preceding sections pertaining to the modelling of *n*-layered multipath conductors. This section aims to contextualise the approaches in terms of:

- Which information is useful specifically to the model
- Which information is more appropriate for one to analyse a multipath conductor.

The aim is to successfully approximate the impedance behaviour of a multipath conductor using the theory outlined by the generalised approach. In order to do so, one should follow these steps:

1. Create *n* structural scenarios according to the Peel Off Method.

2. Find a constant resistance value for each structural scenario. This can be achieved by
    a. Low frequency analysis using each layer's material properties – Equation (8).
    b. Low frequency analysis using effective material properties for all the layers – Equation (27).
    c. Full frequency single layer analysis using effective single layer material properties for all the layers from Equations (24)(26)(30).
    d. Full frequency multipath conductor analysis using the actual material properties – Peel Off Method optional.
3. Find a constant internal inductance value for each structural scenario. This can be achieved by:
    a. Low frequency analysis using each layer's material properties – Equation (20) and Equation (21).
    b. Full frequency multipath conductor analysis using the actual material properties – Peel Off Method optional.
4. Find the skin depth frequency of each structural scenario. This can be achieved by:
    a. Using the single layer skin depth frequency with effective material properties – Equation (35) using Equations (24)(26)(30).
    b. Identifying the skin depth knee point frequency in a full frequency single layer analysis using effective single layer material properties for all the layers from Equations (24)(26)(30).
5. On a log-log scale magnitude vs frequency set of axes, plot for each structural scenario:
    a. The DC resistance values.
    b. The low frequency internal inductance values.
    c. The skin depth frequency.
6. Interpolate the plot over the valid frequency ranges for the scenarios:
    a. Starting at the low frequency figure for the structural scenario with the most number of layers. This will also be the lowest value for resistance, and the highest value for internal inductance.
    b. Plot a constant value across all frequencies lower than the skin depth frequency of the current structural scenario and above the skin depth frequency of the preceding scenario.
    c. Many different interpolations of the data can be used to best match it to the true values.

This section summarises the various means that an analyst can choose to use when analysing a multipath conductor. The methods are based on the concepts developed thus far in this work. It is up to the analyst to decide which approach is more suited to the needs or tooling available to them. This section acts as a guide to utilising the methodologies developed. Actual demonstration of the methods is presented in

Section 5 that follows in order to give the analyst a practical understanding of these methodologies summarised here.

5. Analysis Capabilities

This section aims to demonstrate specific examples of theory developed thus far for up to *n* layers. The reader is exposed to methods and typical representations of multipath behaviour that one would make use of when applying this (and existing) theory. The extent to which these approximate, yet simple, analysis methods frame the actual behaviour of the structure is qualitative and is primarily assessed by the reader through graphical analysis and interpretation.

The impedance behaviour across the frequency domain describes the behaviour of the structure and allows for predictable results. It is worth noting that the ability to analyse a structure creates the ability to design through iteration – although a closed form design solution is to follow in this work. This allows for a parametric design tool that could be used in experiments of a similar style to [10], with the added ability to simulate and account for potential material parameter error margins.

5.1 Demonstration of Methods

A demonstration of the analysis methods presented in previous sections is given here. Table 1 specifies the details of the configuration used for the demonstration with regard to the setup. Table 2 contains the material properties of the structure used in the demonstration – these values are represented separately as they are the key factors governing the impedance profiles. A demonstration of each method is presented separately.

Table 1: Configuration parameters used in the demonstration.

Description	Value
Terminal Current	8 A
Mode of Operation	Differential
Width of Conductor	30 mm
Conductor Length (send and receive)	4 m
Gap between Conductors (send and receive)	250 μm

Table 2: Property values used in simulations that are in the normal range of real world values – however the materials themselves cannot typically be named.

Layer Index	Layer Position	Thickness (μm)	Relative Permeability	Conductivity (Siemens/meter)
1	Outer	50	~1	5.80E+07
2	Middle	50	600	7.95E+06
3	Inner	250	1	5.00E+06

5.1.1 Peel Off Method

The Peel Off Method is a conceptual understanding tool. The method illustrates the migration of current due to skin- and proximity effects within the conductor. Understanding the migration is key to understanding the general behaviour of multipath conductors and provides the essential insights that allow for the approximation methods to exist.

Figure 28 demonstrates the Peel Off Method from three layers to one across the frequency range for resistance. Its internal inductance counterpart is demonstrated in Figure 29. Upon visual inspection of the profiles it is obvious that the underlying structure scenarios of three, two and one layers show good agreement with the overall profile (equivalent to the three layer profile) over the appropriate frequency ranges. This plot was created using the complex full frequency method for the same structure with only three, two and one layers present in the respective simulations.

The Peel Off Method agrees with the intuitive knowledge of skin and proximity effects and provides the necessary insights to visually assess that an estimate using the structural scenarios is feasible. The profiles in this method suggest definite salient points that can be used in some relationship to estimate the exact curve.

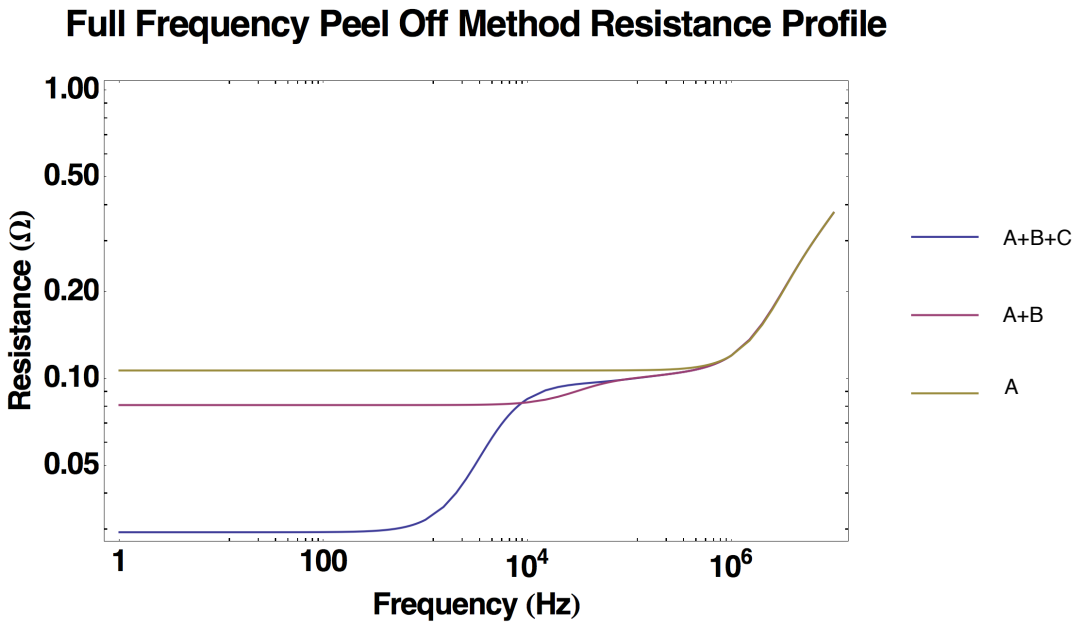

Figure 28: Full frequency resistance profile of the structure using the peel off method. This illustrates how the migration of current in the conductor can be estimated as being peeled away. The full response for the structure is the three-layer response as shown.

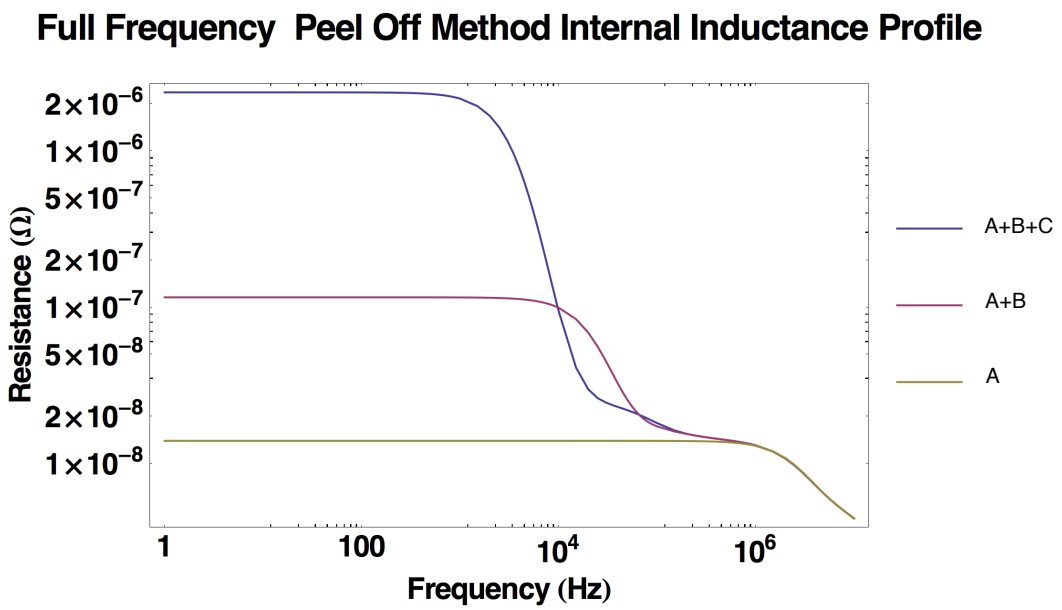

Figure 29: Full frequency inductance profile of the structure using the peel off method. This illustrates how the migration of current in the conductor can be estimated as being peeled away. The full response for the structure is the three-layer response as shown.

5.1.2 Averaged Structural Analysis

The Averaged Structural Analysis method effectively combines the material properties present in the structural scenarios into single values that represent the structure as a single layer. This simplification (or reduction) of materials to a single effective material is demonstrated here. The results of Equations (35)(24)(26) and (30) using the values in Table 1 and Table 2 are presented in Table 3 and illustrates how the material properties of an n-layered structure can be combined mathematically into *n* single layers. The skin depth frequency is calculated here as it is found using this method and used in subsequent demonstrations.

Table 3: Effective material values calculated for an approximate representative single layer – used in the Average Structural Analysis Method.

Number of Layers	Present Thickness (μm)	Effective Thickness (μm)	Present Relative Permeability	Effective Relative Permeability	Present Conductivity (Siemens/meter)	Effective Conductivity (Siemens/meter)	Skin Depth Frequency (Hz)
3	50	350	~1	87	5.80E+07	1.29E+07	1838
	50		600		7.95E+06		
	250		1		5.00E+06		
2	-	300	-	101	-	5.49E+06	5082
	50		600		7.95E+06		
	250		1		5.00E+06		
1	-	250	-	1	-	5.00E+06	810569
	-		-		-		
	250		1		5.00E+06		

Figure 30 illustrates the three single layer full frequency plots using the effective material property values from Table 3. The benefit here is that single layer mathematics and simulation is well established and can be easily achieved currently. Figure 30 demonstrates that the single layer plots can be interpolated – through visual inspection – to estimate the full frequency multipath profile. The vertical lines in Figure 30 are the skin depth frequencies from Table 3, which also mark the skin frequency of the single layer plot. The Averaged Structural Analysis method is necessary in order to find that skin depth frequency is used in the Salient Point Analysis method that follows.

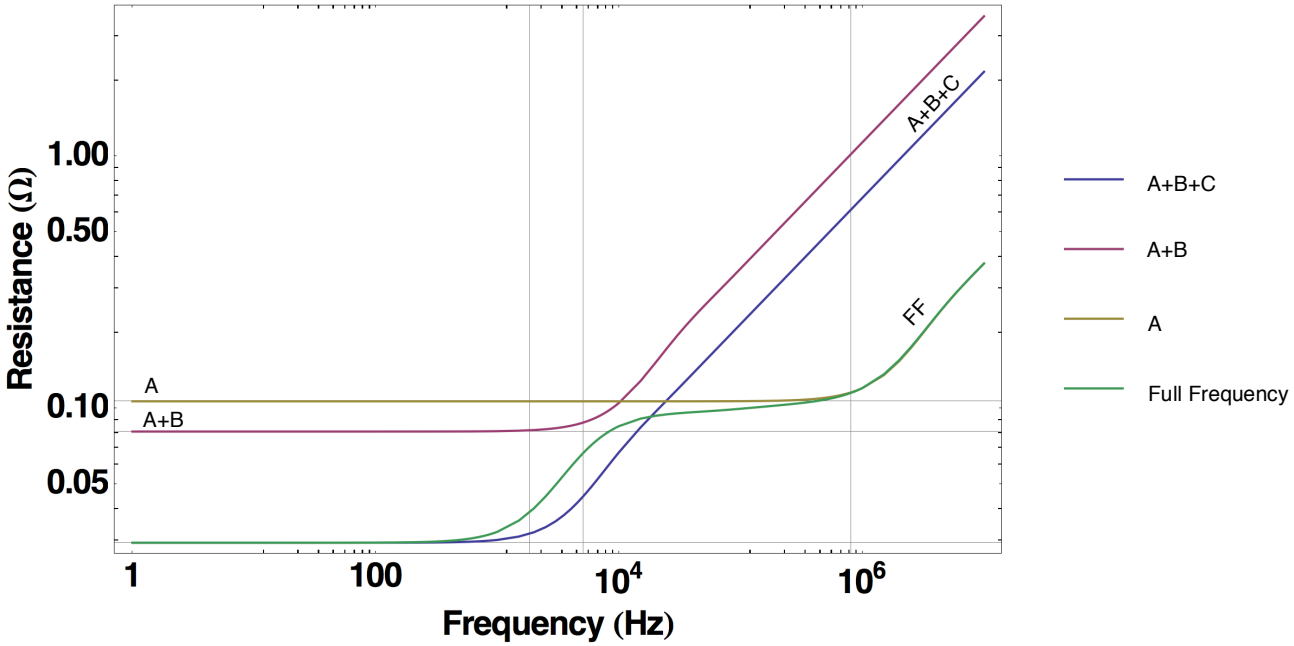

Figure 30: Resistance profile of the Average Structural Analysis method where the combined equivalent material property values are used for each of the three scenarios present.

Figure 31 illustrates an important procedural error that a user of the Average Structural Analysis method may fall into. The Averaged Structural Analysis method provides effective parameters for resistance and not internal inductance. As mentioned in the description of the method, the relationships in the internal inductance are too complex and provide little value for the user, as other methods are available. Figure 31 shows no agreement to the full frequency multipath profile and acts as a demonstration that the Averaged Structural Analysis method cannot be used in this manner.

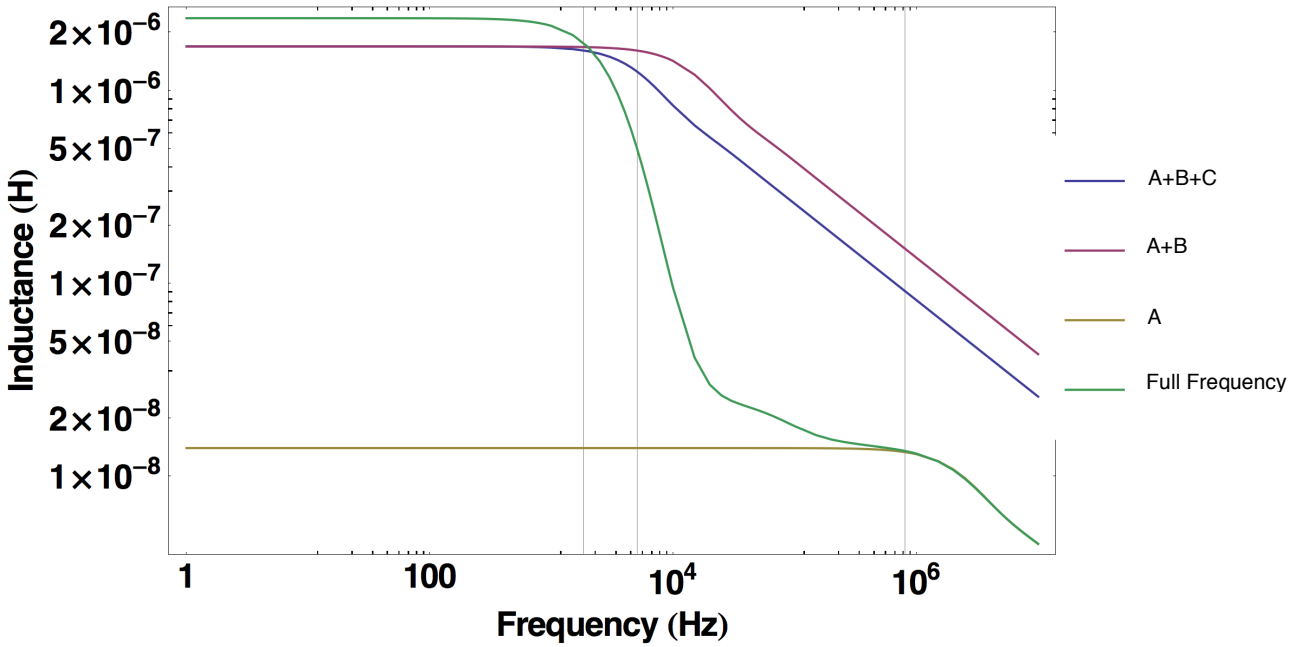

Figure 31: Error Case: Illustration of applying the Averaged Structural Analysis method to model the internal inductance. As mentioned previously this has no mathematical grounding but could be an easy mistake using this method.

5.1.3 Low Frequency Salient Point Analysis Method

The purpose of the Salient Point Analysis method is to calculate the low frequency (very near to DC) values for structural scenarios identified from the Peel Off Method. Table 4 extends Table 3 to show the low frequency- resistance and internal inductance values for each structural scenario. These values are calculated using Equations (8)(20) and (21) and are plotted in Figure 32 and Figure 33 with reference to the full frequency profile that they estimate in this method.

Table 4: Calculated low frequency values of resistance and inductance with reference to their structural scenario.

Number of Layers	Present Thickness (μm)	Effective Thickness (μm)	Present Relative Permeability	Effective Relative Permeability	Present Conductivity (Siemens/meter)	Effective Conductivity (Siemens/meter)	Skin Depth Frequency (Hz)	Low Frequency Resistance (mΩ)	Low Frequency Internal Inductance (H)
3	50	350	~1	87	5.80E+07	1.29E+07	1838	29.3	2.36E-06
	50		600		7.95E+06				
	250		1		5.00E+06				
2	-	300	-	101	-	5.49E+06	5082	80.9	1.16E-07
	50		600		7.95E+06				
	250		1		5.00E+06				
1	-	250	-	1	-	5.00E+06	810569	106.7	1.39E-08
	-		-		-				
	250		1		5.00E+06				

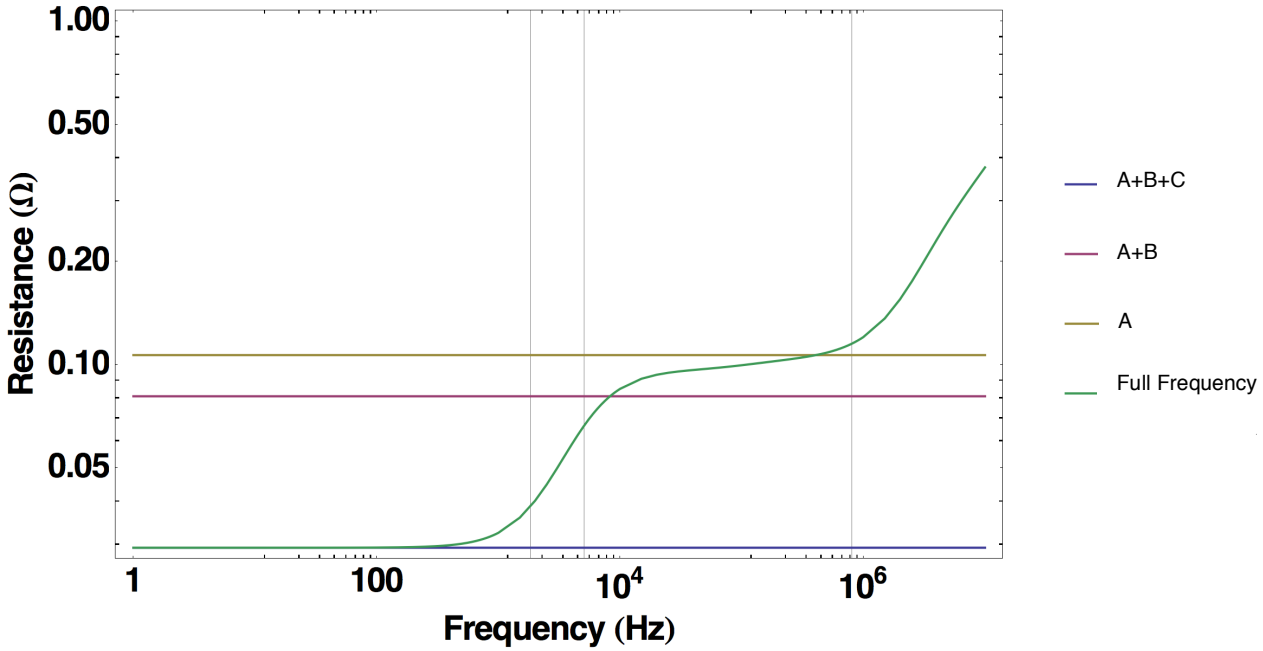

Figure 32: The horizontal lines represent the DC value of resistance for each structural scenario using the Salient Point Analysis method. The vertical lines are the skin depth frequencies found using the combined parameter approach from the Average Structural Analysis Method.

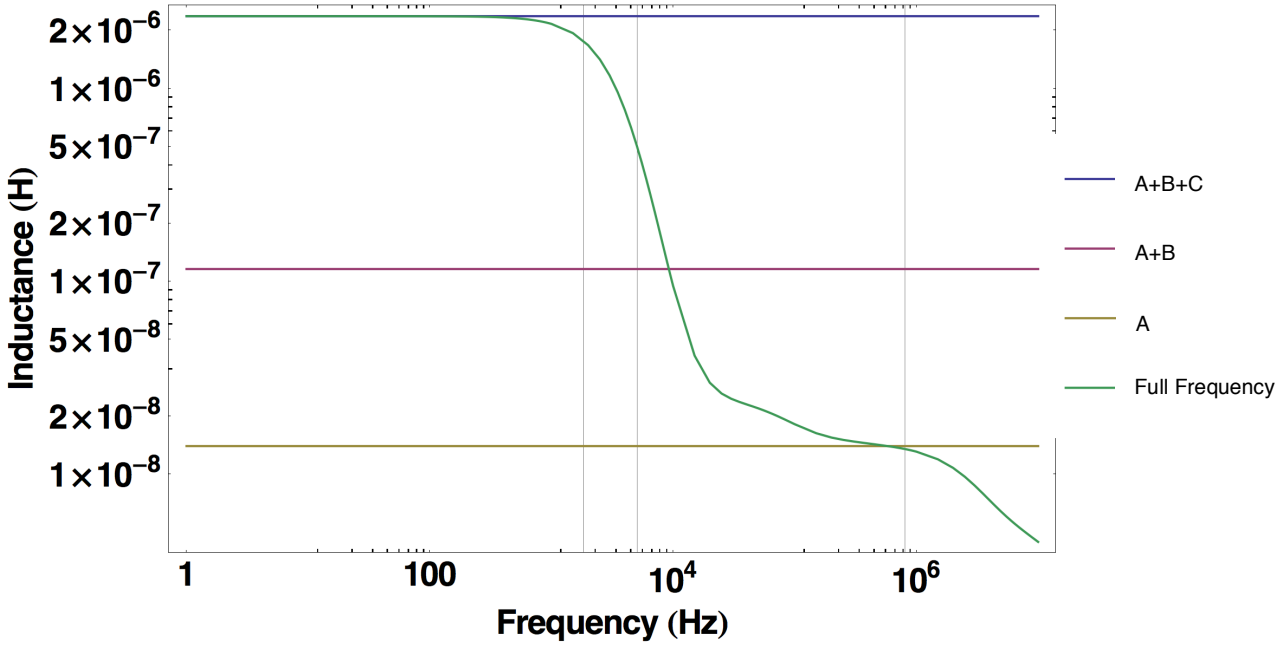

Figure 33: The horizontal lines represent the low frequency value of internal inductance for each structural scenario using the Salient Point Analysis method. The vertical lines are the skin depth frequencies found using the combined parameter approach from the Average Structural Analysis Method.

The skin depth frequency and low frequency value pairs form the salient points that estimate multipath behaviour. A basic approach to interpolating these pairs is demonstrated in Figure 34 and Figure 35 showing a typically simple approach to analysis using the Salient Point Analysis method for resistance and internal inductance respectively. This interpolation approach can also be applied when using the Average Structural Analysis Method, as the salient points are nearly the same, and is demonstrated in Figure 36. Figure 37 shows a close up how the curve around the knee point from the Average Structural Analysis Method is a region and is compared to the single point from the Salient Point Analysis. The region and the point differ due to different simulations being used that involve different levels of modelling, yet are consistently very close to one another.

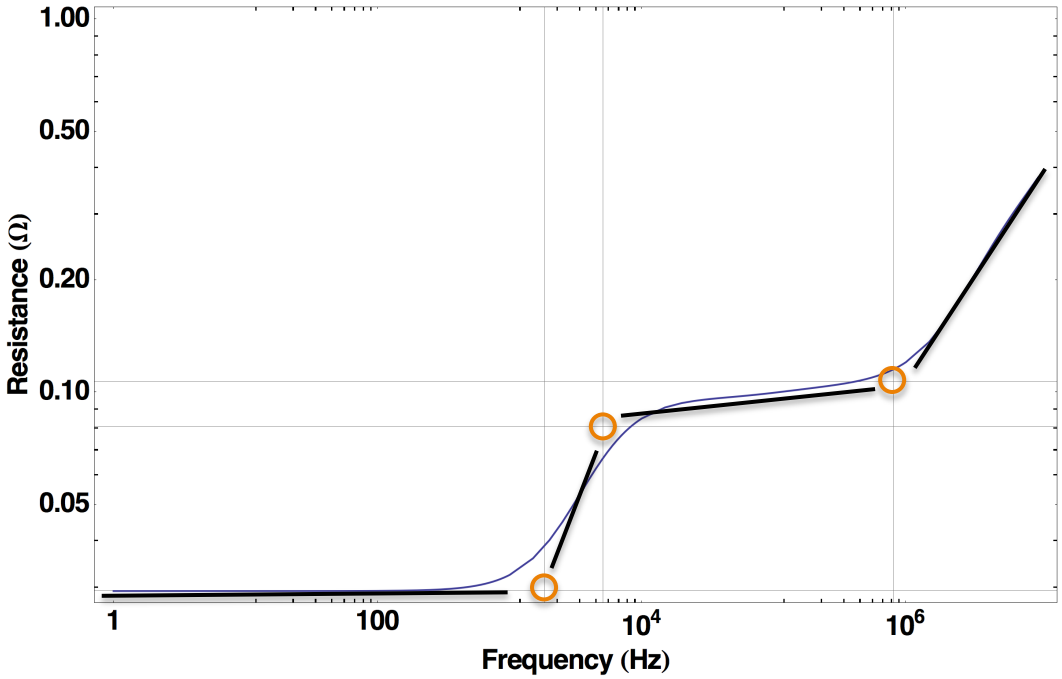

Figure 34: Frequency-resistance pairs of the Salient Point Analysis method used with straight-line interpolation to demonstrate simple estimation of the full frequency multipath behaviour.

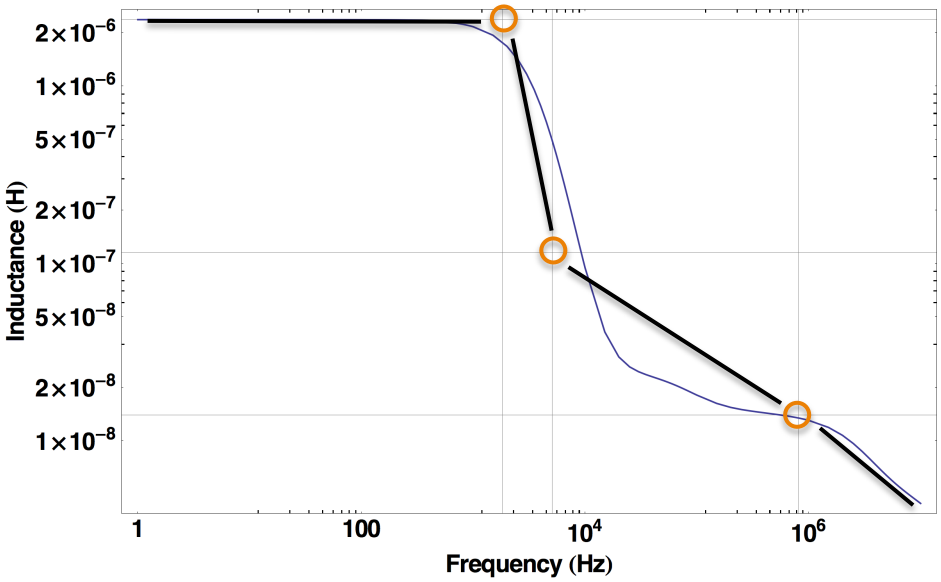

Figure 35: Frequency-inductance (internal inductance) pairs of the Salient Point Analysis method used with straight-line interpolation to demonstrate simple estimation of the full frequency multipath behaviour.

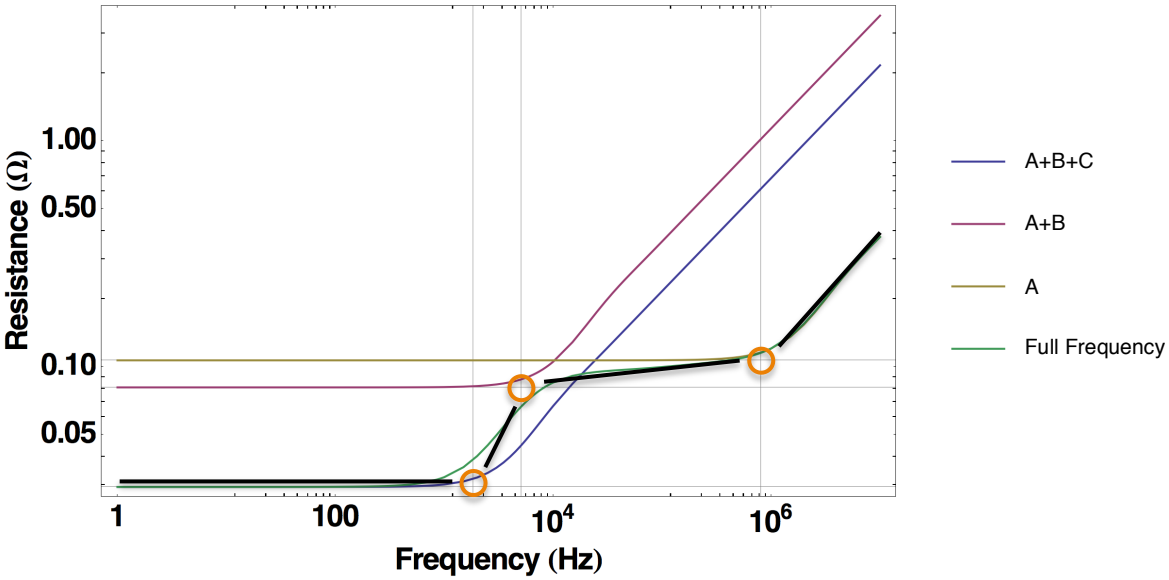

Figure 36: Agreement between the frequency-resistance pairs and the skin depth knee-points of the Average Structural Analysis method. Both methods can be interpolated in the same basic manner to estimate the full frequency profile.

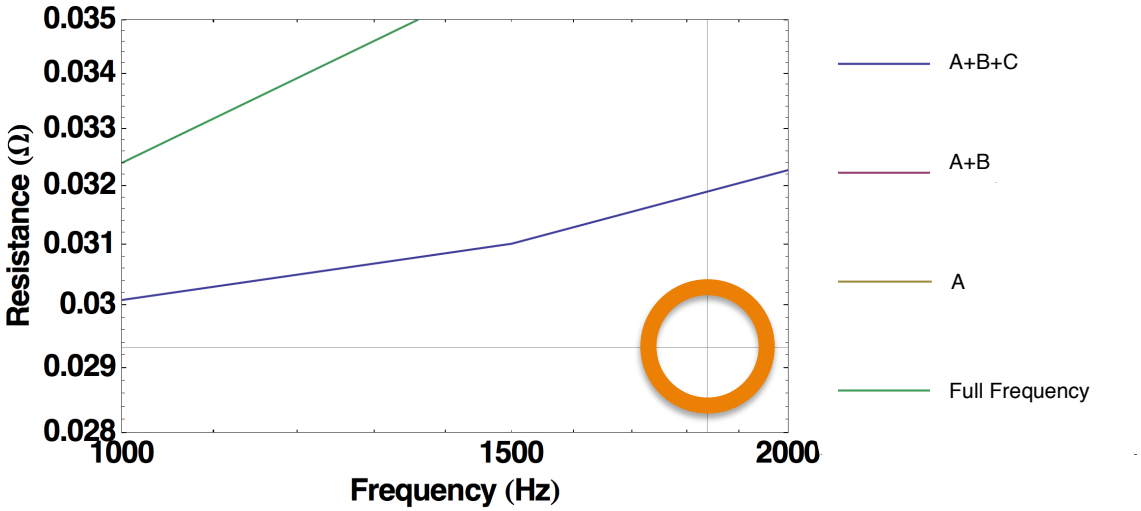

Figure 37: Enlargement of Figure 36 at the first frequency bound showing how the single layer's (A+B+C) knee point frequency of its full frequency curve of Averaged Structural Analysis does not pass exactly through the point defined by the Salient Point Analysis.

6. Mathematical Design Methodology

To draw back to the initial problem, multipath conductors are explored as a means of implementing a low pass filter without the drawbacks experienced in lumped parameter passive filters. A low pass filter is a well-established and supported means of eliminating high frequency noise. The application lies in EMI mitigation for improved EMC. A successful mathematical design solution to multipath conductors does not exist and it is the purpose of this work to present a method of designing multipath conductors to an approximate specification. The structural and analysis theory, developed in sections thus far, is drawn upon in the development of this method – with key reliance on structural averaging, the skin depth equation applied to equivalent single layer representations of multipath conductors.

The *analysis* of multipath conductors focuses on predicting the impedance profile – primarily focussing on resistance profile – of a given structure composed of certain material properties. The *design* of multipath conductors specifies a desired impedance profile, again more specifically the resistance profile, in order to calculate the material properties required for the underlying layers. Usually the resistance profile is specified and the internal inductance profile will be left out of the specification, as it is a resulting consequence of the desired resistance.

This section focuses on the design methodology and considers practical aspects that the designer should be aware of when making use of this approach.

It is easiest to specify the desired resistance profile in terms of increasing resistance- and frequency pairs that can be interpolated. This is aligned to the use of the DC methods presented in this work. These salient points of the profile provide the inputs for the design.

The effective material property calculations of Equations (24)(26)(30) and the generalised skin depth equation, Equation (35), are key to the identification of a design solution.

The design principles make use of the following identified features from the *n*-structure approach:

- The Peel Off Method.
- The composable nature of the multipath conductors by many layers.
- The ability to represent each structural scenario as an effective single layer.
- The skin depth of a single layer – with true or effective properties – approximates the transition frequency between layers.

Typical frequency-resistance pairs that describe a desired response are shown in Figure 38. The designer specifies these pairs of values in accordance with the desired behaviour. Each pair has the effect of adding another layer to the underlying structure.

The pairs used in Figure 38 results in a four-layer multipath conductor being designed. The full frequency behaviour of the structure would follow a curve similar to the interpolation of these pairs, as shown in Figure 39. It is this resulting full frequency behaviour that the designer desires and the frequency-resistance pairs are a means of applying this design methodology.

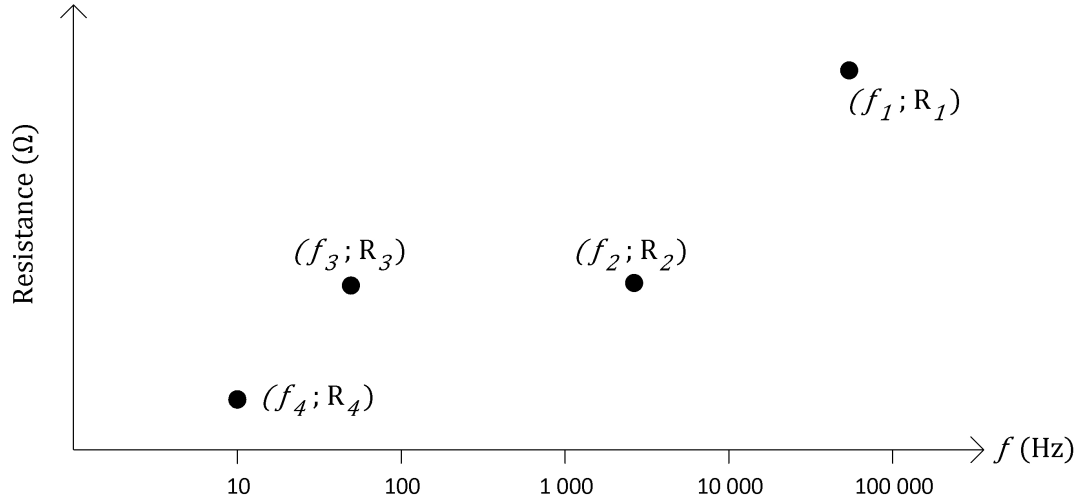

Figure 38: Frequency-resistance pairs used to specify the salient points for a desired resistance profile.

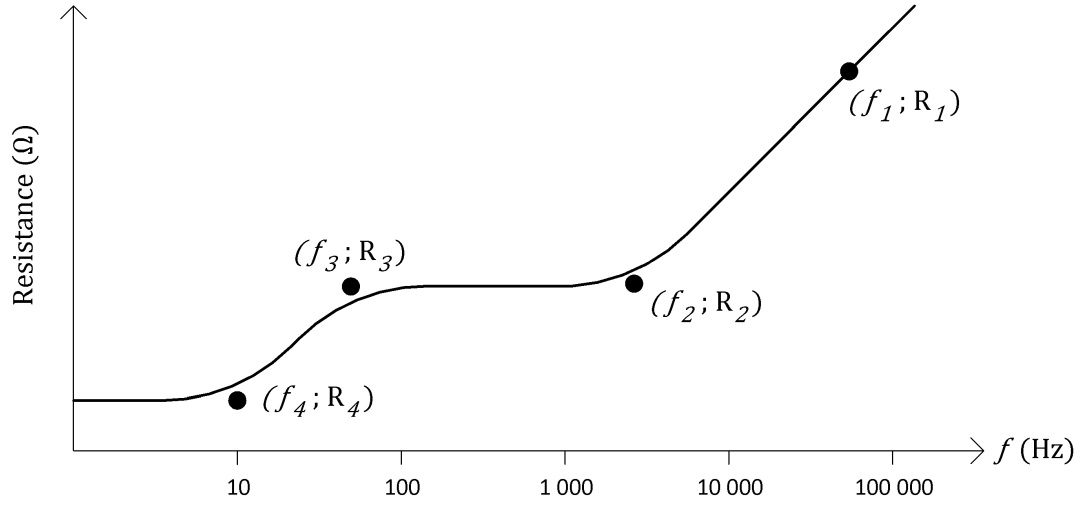

Figure 39: Interpolation of the specified salient points for an improved visual understanding of the desired curve.

6.1 Development of Design Equations

Given the paired inputs of frequency and resistance, the output of conductivity, permeability and thickness for each of the n layers is required. The pairs are defined

by the highest frequency pair starting at 1 and the lowest being n. This is aligned to the structural definition where layer 1 is the only contributing layer to the resistance profile in the highest frequencies for either differential or common mode. Conversely, the lowest frequency contribution to the resistance profile is composed of weighted contributions from all of the layers since the whole structure is active.

The three output variables require three independent equations to be resolved at each point. The desired inputs only specify the resistance profile and defining frequencies, which leaves the system underspecified. This design solution is aimed at the designer and so specifying a frequency is most desirable, rather than defining values for internal inductance. Specifying the frequency encapsulates two concepts in one parameter:

- The desired transition frequency.
- The required permeability / thickness combination.

The skin depth equation relates the variables in this way and is used in the design methodology. The resistance equation provides another equation. Only two equations are available for use in this case. The system is under-defined using only these equations and creates trade-off decisions that the designer will be required to make. There is no single result using this approach due the requirements on the internal inductance being relaxed. Having specified the internal inductance pairs as well as the resistance pairs, another equation could be used and the system would be fully specified. This, however, is not desirable for a designer who would not typically know the exact value of internal inductance required and may not be relevant given the external inductance from how the structure is actually constructed. Trade-offs provide flexibility in the design which better suits practical considerations when sourcing materials and implementing the solution.

The required permeability and required thickness equations can be found by solving Equation (36), resulting in Equation (37) and Equation (38) respectively. This is for each of the n layers in terms of the input pairs. Where n is zero, the term is considered to be zero, as the layer does not exist. Note that Equation (38) is only an algebraic change to Equation (37) in order to find the required thickness. This is an example where the flexibility of the design solution lies. Often it is simpler to manufacture a certain required thickness of a layer than it is to manufacture for a required permeability. In such a case, the permeability is already specified by the available values that can be manufactured and Equation (38) should be used to solve for the required thickness. A more in-depth development of the design equations can be found in Appendix D.

$$\mu_{e_n} = \frac{1}{w_{e_n}} \sum_{i=1}^{n} w_i \mu_i = \frac{1}{\pi \sigma_{e_n} f_{\delta_n} w_{e_n}^2} \tag{36}$$

$$\mu_n = \frac{wid}{\pi\, l\, w_n}\left(\frac{r_n}{f_{\delta_n}} - \frac{r_{n-1}}{f_{\delta_{n-1}}}\right) \tag{37}$$

$$w_n = \frac{wid}{\pi\, l\, \mu_n}\left(\frac{r_n}{f_{\delta_n}} - \frac{r_{n-1}}{f_{\delta_{n-1}}}\right) \tag{38}$$

Equation (39) provides the basis for the finding the required conductivity in a design – Equation (40) – given the desired input pairs. As before, an algebraic manipulation allows for Equation (41), which specifies the required thickness in terms of the available conductivities. The thickness found in Equation (38) and Equation (41) will, of course, need to be the same value if such an approach is followed.

$$r_n = \frac{l}{width\ \sum_{i=1}^{n} w_i \sigma_i} \tag{39}$$

$$\sigma_n = \frac{l}{width\, w_n}\left(\frac{1}{r_n} - \frac{1}{r_{n-1}}\right) \tag{40}$$

$$w_n = \frac{l}{width\, \sigma_n}\left(\frac{1}{r_n} - \frac{1}{r_{n-1}}\right) \tag{41}$$

These concise design equations are solved for n input pairs requiring n layers of materials in the multipath conductor. Each layer can be solved for independently given that the input pairs remain fixed. This allows for flexibility around the physical design of each layer in the overall conductor. The interplay between parameter values is seen clearly through this concept in that each variable can compensate for another in order to obtain the same result. Although this flexibility is desirable in terms of potential manufacturing benefits, it does give way to potentially risky designs, practically.

6.2 Practical Design Considerations

Solving for exact single values of the material properties allows for a theoretically correct design that theoretically results in the desired behaviour. A single value for each designed parameter is not ideal as there is usually some error margin associated with material properties, practically. The error margin should be accounted for by identifying the designed behaviour within the error margins.

From the literature review, FEM analysis is a popular simulation tool. FEM can be used iteratively for design purposes and can simulate many different values around a single set of designed material properties to check for stability. Parametric design procedures suffer from a similar transparency issue as the exact structure under experimentation may have slightly unexpected property values or repeated experiments may not have the exact property values and result in a different behaviour. Analytical relationships, such as equations, contextualise single point values in terms of their stability. The effect of small changes to the parameter value can

be seen using the mathematical relationship. Taking the stability of the design into account is an important design consideration.

Consider the relationship captured by Equation (40) for calculating the third layer conductivity value. The equation is simplifies to the Equation (42) when the thickness of the layer is held constant, as shown in Equation (43):

$$\sigma_3 = C\left(\frac{1}{r_3} - \frac{1}{r_2}\right) \tag{42}$$

$$where \quad C = \frac{l}{width\ w_3}\ and\ is\ a\ constant\ for\ constant\ thickness, w_3 \tag{43}$$

Equation (42) captures the relationships at play for the conductivity of only one of the n layers. This shows the high-dimensional nature of the simplified equations as more layers are introduced into the system. Equation (42) can be visualised in Figure 40, which shows the relationship for conductivity, given the inputs, can vary from a stable, low gradient, to an unstable, steep gradient. The context of the point in which the designer chooses a value should be investigated to check for fast-rising gradients and their potential impact.

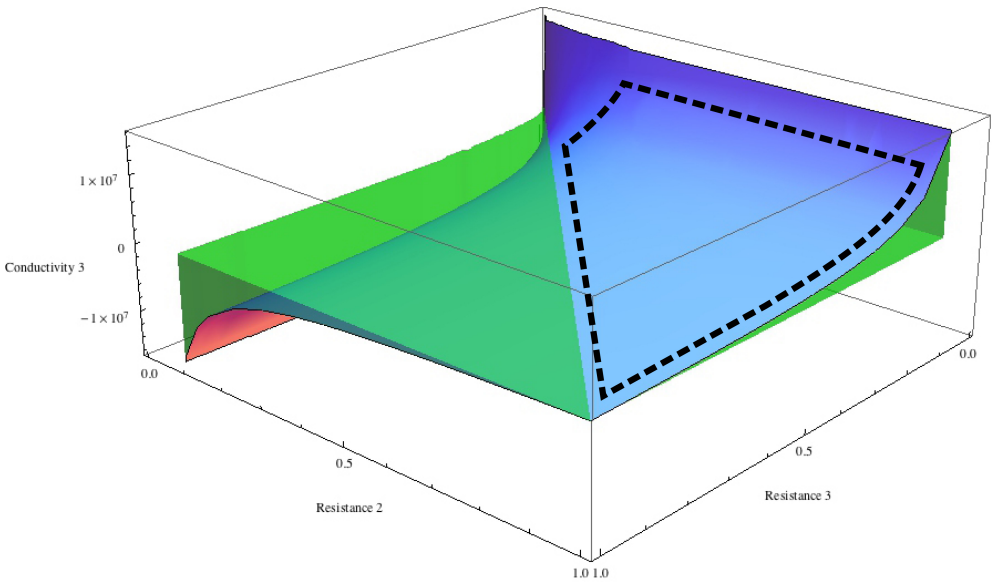

Figure 40: Stability considerations for designed properties. An estimated stable region in the relationship is shown by the dotted line. Here, the relationship between r_2 and r_3 and the effect they have on the required conductivity of layer 3 under constant thickness conditions.

Another concept shown in Figure 40 is the design limitations on multipath conductors. Not all inputs result in feasible values for material properties. It is shown that r_3 cannot be larger than r_2. This is in agreement with the underlying definitions of the structure

and cannot be designed for due to negative values of conductivity being infeasible. Very large (and possibly impractical) values of conductivity, in this example, result when r_3 is very small. The designer should be aware of this in order to avoid designing for- and expect impractical performance.

Figure 40 shows limitations based on the relationship between three variables only. This is only one component of the combined relationships at play in the whole system. Identifying these limitations can be very complex, considering that the design Equations (37) and (40) introduce seven inter-related parameters into the system for each layer added. These seven variables are $\sigma_n, \mu_n, w_n, r_n, r_{n-1}, f_{\delta_n}, f_{\delta_{n-1}}$. The system of variables exists in a high dimensional space that is currently unexplored in this work. Current management of the limitations is to identify when infeasible scenarios result – such as negative values of conductivity, permeability and thickness. Examples of these limitations and their identification are demonstrated in Section 7.2.

However, understanding these relationships over the high dimensional space could possibly allow the designer to identify more stable regions in relationships. This could lead to more stable designs and possible identification of the applicability multipath conductors as dissipative filters, should the limitations be quantifiable.

These limitations are noted in one relationship but are required to be found to all relationships before it can be used as an effective design tool. This presents a new mathematical challenge in solving the high dimensional space. This is presented as future work in Section 8.2 where feasible designs are considered.

7. Design Capabilities

The main goal of this work is to present a design-oriented solution that can estimate the material property values of each layer in a multipath conductor system given a desired output. The design equations (Equations (37)(38)(40)(41)) are developed in the previous section. The derivation of the equations uses concepts developed in this work stemming from:

- The Peel Off Method.
- Structural scenario modelling.
- Combined parameter simplification – for the Average Structural Analysis method.
- The understanding and use of the skin depth equation.

The design capability of the equations is demonstrated in this section.

Table 5 contains the input and output values for various designs that illustrate different components of the design equations. The frequency-resistance pairs specify the general desired behaviour and drive the design equations in order to obtain material properties. When simulated, these material properties result in the desired behaviour of the multipath conductor.

Table 5: Values used and calculated in design demonstrations for differential mode operation.

		Input (Resistance-Frequency pairs)			Output			
Demo Number	Input Pair Number	Skin Depth Frequency (Hz)	Low Frequency Resistance (Ω)	Chosen Thickness (μm)	Layer Number	Conductivity (S)	Relative Permeability	Consequential Internal Inductance (H)
DESIGN 1								
1	1	100 000	1	100	1	1.33E+06	190	1.06E-06
	2	1 000	0.1	100	2	1.20E+07	1710	1.06E-05
	3	10	0.01	200	3	6.00E+07	8549	1.06E-04
DESIGN 2								
2	1	100 000	1	700	1	1.90E+05	27	1.06E-06
	2	1 000	0.1	50	2	2.40E+07	3420	1.06E-05
	3	10	0.01	2000	3	6.00E+06	855	1.06E-04
DESIGN 3								
3	1	100 000	1	100	1	1.33E+06	190	1.06E-06
	2	5 000	0.1	100	2	1.20E+07	190	3.73E-06
	3	2 000	0.01	100	3	1.20E+08	-285	4.71E-06
DESIGN 4								
4	1	10 000	1	100	1	1.33E+06	1900	1.06E-05
	2	100 000	1.3	100	2	-3.07E+05	-1653	7.55E-06
	3	100	1.6	100	3	-1.92E+05	303 717	9.33E-05
DESIGN 5								
5	1	100 000	1	100	1	1.33E+06	190	1.06E-05
	2	1 000	0.8	15000	2	2.22E+03	100	4.67E-06
	3	100	0.1	70	3	1.67E+06	543	2.17E-04

7.1 Conceptual design and trade-off considerations

Equations (37)(38)(40)(41) present an interesting trade-off scenario for the designer as they underspecify the multipath system. The designer needs to specify a value for either the thickness, permeability or conductivity for each layer in order for the equations to solve for the other property values. The decision should be based on:

- With how much certainty a property is known – e.g. permeability values often differ from specifications or is specified over a large range.
- The ability to manufacture the property values with the most precision.

It is important to note at this point that material properties are most likely not as configurable as suggested by the designs and mathematics. Materials are also unlikely to be fabricated directly for the design but probably selected from an already existing source of material, perhaps from a catalogue. The most flexible material property is the thickness of the layers as there are well-established technologies to achieve this. This section demonstrates the design ability by manipulating all of the properties for theoretical purposes and to demonstrate the interplay of the properties.

Designs 1 and 2 from Table 5 use unrealistic input figures but allow for good demonstration of the input frequency-resistance pairs and the output layer properties. The chosen layer thicknesses in Design 2 differ vastly from Design 1. Figure 41 is a Salient Point Analysis method analysis of the structure using the designed material property values. The output of the Salient Point Analysis method is maintained for both Design 1 and Design 2 with the required conductivity and permeability values compensating for the layer thickness differences.

Designs 1 and 2 demonstrate how the designer can trade-off a parameter for other parameters until satisfied with all material property values. The design equations are structured such that any parameter can be traded-off against the others.

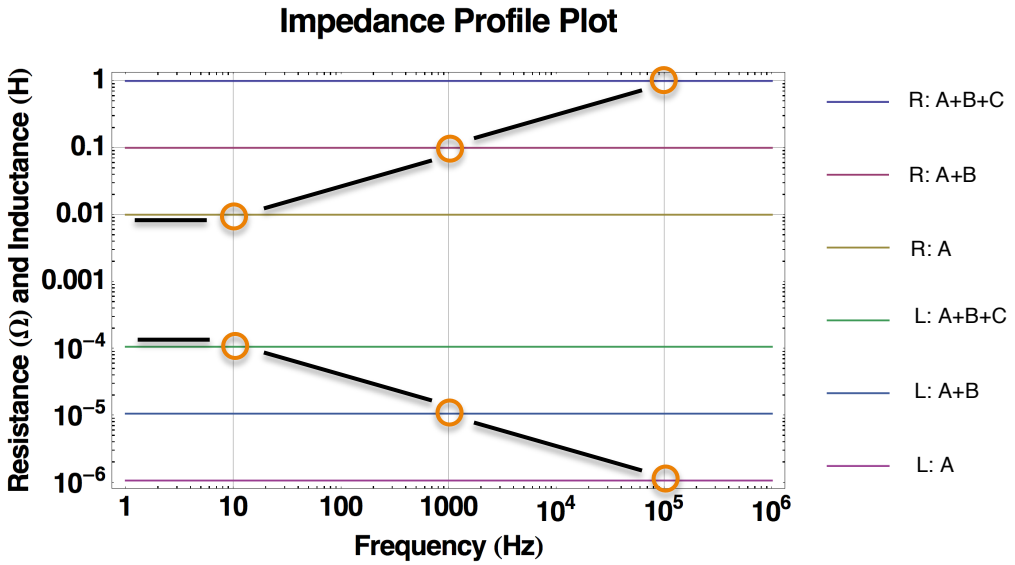

Figure 41: Design 1-2: Salient Point Analysis Method resistance and internal inductance plots using from resulting, designed-for, material properties values. The desired output is maintained even though layer thicknesses vary between designs – illustrating the designer's choice in trade-offs.

Figure 42 and Figure 43 show the exact analytical method of the different structures from design 1 and 2. The curves are shown to lie on top of one another, indicating that the two different structures have been designed for the same behaviour. This capability is seen in the relationships present in Equations (37)(38)(40)(41). Scaling the width by a factor will result in the other parameters being scaled by the inverse of that factor if the behaviour is to be kept constant. Table 6 shows this scaling factor specifically for Designs 1 and 2. This aspect of the design shows that it is the proportion of the values to one another that dictate the behaviour. Scaling the magnitude of the values does not change the behaviour, yet the difference in proportions between the properties does.

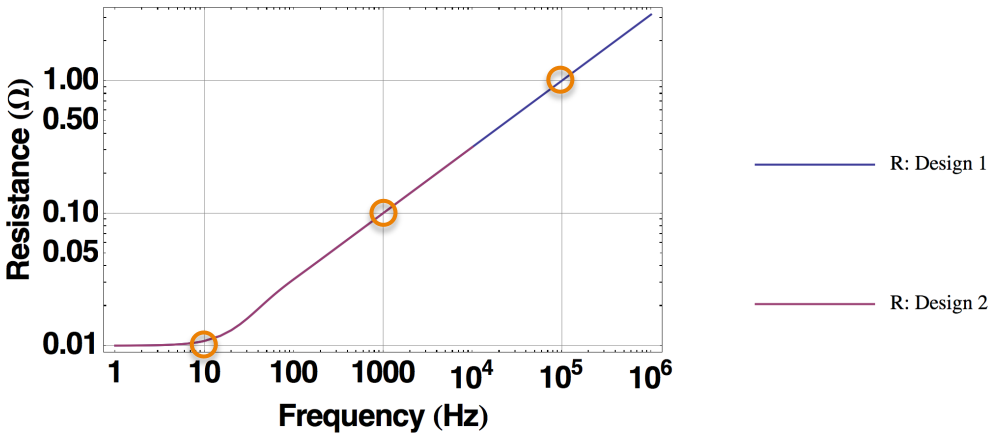

Figure 42: Resistance profile of Design 1 and 2 showing full agreement between the vastly different structures. The structures are found using the design equations with the same frequency-resistance pair inputs and using different thicknesses. All material properties are different between designed conductors.

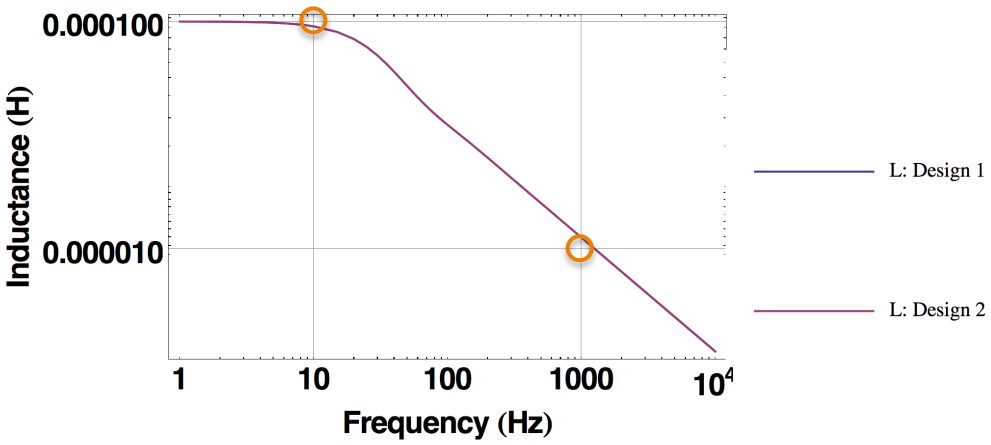

Figure 43: Internal inductance profile of Design 1 and 2 showing full agreement between the vastly different structures. The structures are found using the design equations with the same frequency-resistance pair inputs and using different thicknesses. All material properties are different between designed conductors.

Table 6: Scaling proportions between Design 1 and 2 that result in the same impedance behaviour.

	w1 (μm)	σ1 (S)	μ1	w2 (μm)	σ2 (S)	μ2	w3 (μm)	σ3 (S)	μ3
DESIGN 1	100	1.33E+06	190	100	1.20E+07	1710	200	6.00E+07	8549
DESIGN 2	700	1.90E+05	27	50	2.40E+07	3420	2000	6.00E+06	855
PROPORTION	**1/7**	**7**	**7**	**2**	**1/2**	**1/2**	**1/10**	**10**	**10**

7.2 Validation and Error Cases

Designs 3 and 4 from Table 5 demonstrate how the design equations, although only an estimation, can be used to identify desired cases that are impossible due to the nature of the underlying physics governing the behaviour.

Design 3 shows a negative value for the permeability of the outer layer. A negative permeability is impossible yet the full frequency resistance plot, Figure 44, using the designed figures looks correct and tracks the desired points with reasonable accuracy. Resistance is often perceived as the important plot yet the internal inductance plot completes the impedance model and in this design illustrates the impossible nature of the desired response. Figure 45 shows an increasing internal inductance value in the full frequency three-layer plot of the whole structure, which arises from the negative permeability value – an infeasible outcome.

Design 4 deliberately requests a design for a decreasing resistance, forcing the conductivity values to be negative – impossible. The physical nature of the structure is that it increases in resistance with increasing frequency through a decreasing conducting area. The desired frequency contradicts this by requesting that structural scenario 2 (inner two layers present) be valid at a higher frequency than structural scenario 1 (all layers present), again impossible. This impossibility is identifiable by

the negative permeability value required for such behaviour. Impossibilities are also apparent in resulting negative values for conductivity and thickness.

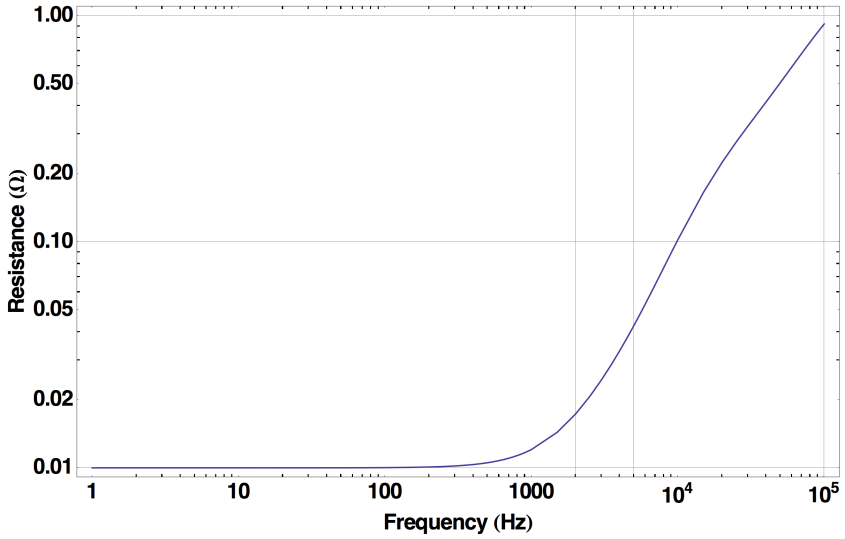

Figure 44: Design 3: Resistance plot using designed material values follow the desired points in an approximate sense. Unsuspecting in the resistance profile, this design is actually impossible and is identified in the negative permeability value, which is more apparent in the internal inductance profile.

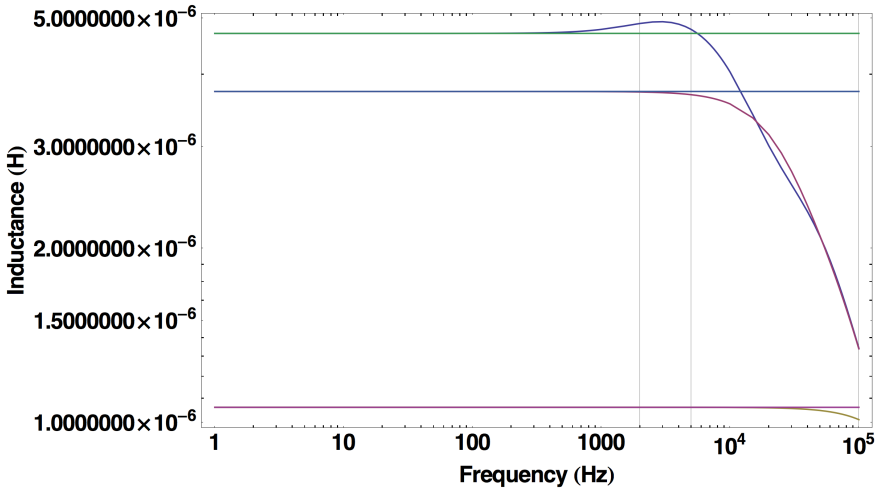

Figure 45: Design 3: Internal inductance plot with an impossible increase around 1 KHz. This impossibility is identifiable in the negative design value for permeability in layer 3 – see Table 5.

7.3 Working design

Design 5 aims to satisfy the design requirements of:

- A pass band of 0-70 Hz
- 8 or more times the low frequencies losses for frequencies higher than 2 kHz.

Table 5 contains the desired frequency-resistance pairs to satisfy the design criteria (illustrated using the Salient Point Analysis method and Full Frequency Analysis Method in Figure 46). The designed material values fall within common ranges of values – however this is not to say that a single material with those exact properties is easily obtainable, but is used here for demonstration purposes. Figure 46 shows a full frequency analysis of the resistance profile and how it tracks the desired input frequency-resistance pairs shown in grey by the Salient Point Analysis method. The internal inductance counterpart is presented in Figure 47 for completeness.

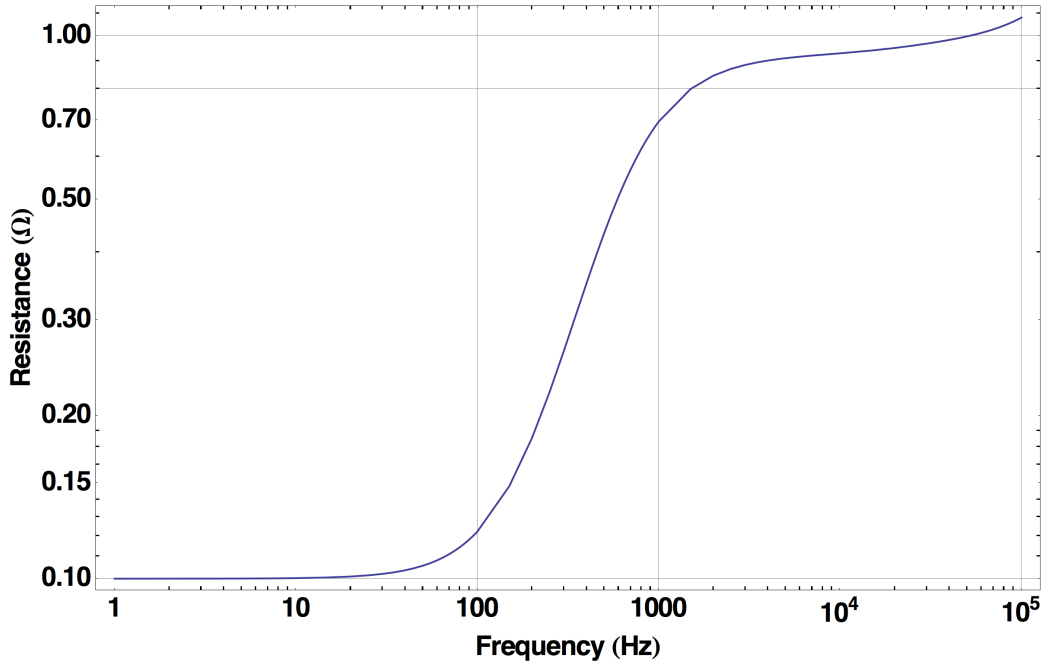

Figure 46: Design 5: High performance resistance profile using commonly valued material properties. Note how the desired design points are tracked in the full frequency simulation using the resulting designed material properties.

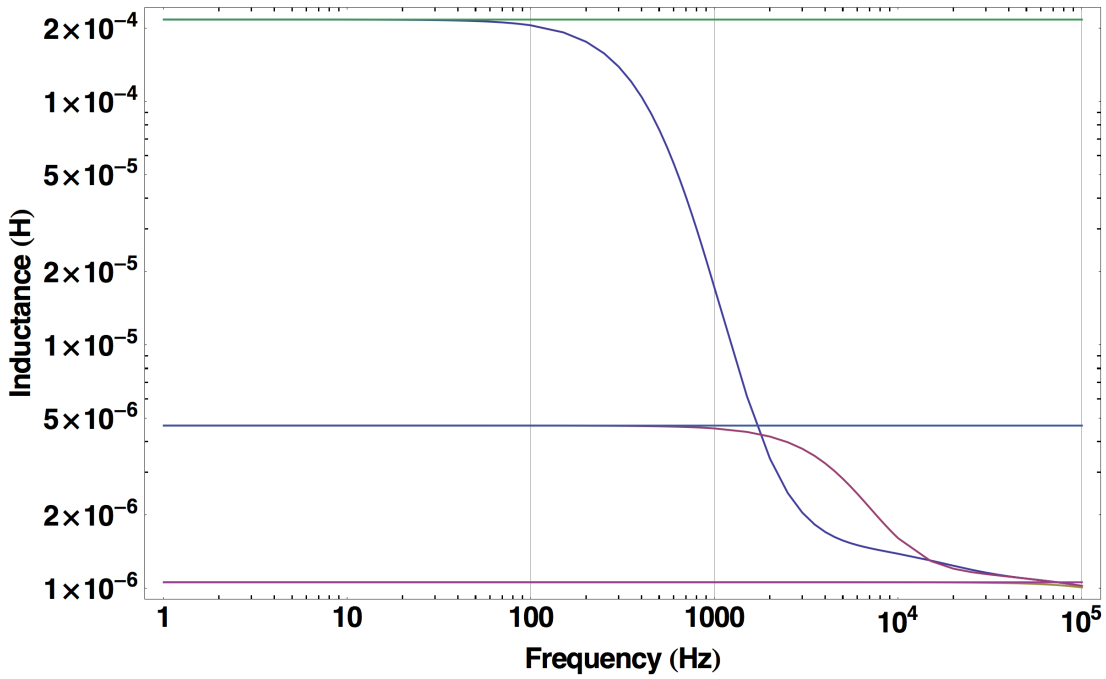

Figure 47: Design 5: High performance internal inductance profile using commonly valued material properties.

8. Conclusion

This work is conducted with the main objective to find a means to design multipath conductors, given a desired characteristic frequency-resistance profile and applicable log-log scale. The high-level design ability is the focus of this work. The high accuracy requirements in other solutions often hinders the design ability predominantly by:

- The dependence on simulating lumped parameter values using FEM analysis.
- The complexity of the system of equations.

This work identifies the need for a simple modelling technique of multipath conductors such that the governing equations are simpler and can be used for design.

The pertinent findings of this work are summarised in this section. The discovery process of this work has revealed aspects that require further attention and is presented in this section as recommended future work.

8.1 Summary of findings

The *n*-structure method defines the simplifications used in this work and is justified through its agreeable comparison against the full frequency analytical method using the Peel Off Method. This method contributes to the simplified understanding of multipath conductors to provide a foundational structural model for further development of mathematical models.

Applying the established methods of low frequency resistance and internal inductance (both using the material properties of the layers) to multipath structures allows the various structural scenarios that stem from the use of the *n*-structure method to be modelled mathematically. The impedance magnitudes for each of the n structural scenarios agree with the Peel Off Method and full frequency analytical method, thereby validating the correctness of the equation development.

The developed equations can be manipulated to provide a sense of structural averaging. Finding an effective single layer (using effective material property values) representation of a multipath conductor over a given frequency band is key to having the ability to analyse and design in a simple manner. The effective single layer representation is a structural average as it is found by using a weighted average of all the present layer's conductivity and permeability values. The weighting is found using each present layer's thickness against the sum of the thicknesses present in the structural scenario (multipath conductor). This ability to average the material properties is achieved through the parameterisation of summation terms within the equations that are based on established methods. The structural averaging is a mere perspective on established mathematical equations through algebraic manipulations. This manipulation is easily found for the resistance equation (to obtain an average conductivity value) yet is more difficult using the internal inductance equation. It is

suspected that applying the same parameterisation approach to the internal inductance can result in a more robust method of structural averaging – this is presented as future work. However due to the complexity this introduces a further simplification is used by modelling the structure as a magnetic circuit in order to find an average permeability value.

Simpler analysis methods result from the simplified structural model. The Average Structural Analysis method arises by simulating each of the n averaged material property scenarios across the full frequency domain using established methods. These curves can be interpolated by tracing the lowest curve and transitioning between curves at the skin depth knee points. This method uses the simplified method of finding the average permeability and is thus expected to have a larger error in magnitude and skin depth frequency when analysing highly contrasting materials. The Salient Point Analysis method applies established concepts of resistance and internal inductance at low frequency to calculate agreeably similar values of resistance and inductance as determined by the full frequency analytical Peel Off Method. This approach uses a more involved calculation finding the internal inductance, which is too complex to derive a permeability value from. The internal inductance magnitude is therefore more robust when using largely contrasting materials, however, the skin depth frequency is associated with a greater error margin as it is calculated using the structural averaging methodology.

The error that is introduced by simplifying the behavioural understanding of the system is acceptable provided that the method is used in conjunction with iterations of accurate simulation methods before a final design is settled upon. Accurate simulation methods are more suited to assessing the impact of refinement tweaks whereas this approximation method provides a base design where high-level design decisions are explored. Although the designed layers' material properties theoretically do provide a solution, the sensitivity of the design equations and error margins still need to be assessed to properly conclude the efficacy of this design method. The sensitivity- and error margins analysis is presented, as possible future work due to the high dimensionality of the multipath conductor domain and the further complexities it introduces that would defocus this work.

8.2 Aspects for Further Research

A design-oriented methodology for designing multipath conductors is presented in this work. The methodology is under the assumptions of [9] and addresses identified design limitations in the multipath field. A simplified analytical approach is an added benefit to developing the design-oriented approach.

The two most pertinent aspects for further research that could improve this work lie in the concepts of:

- Error understanding and mitigation.
- Feasibility of design.

The developed equations for different material properties introduce error into the findings due to its simplified nature. The ability to assess this error margin allows the designer or analyst to know whether they are working with feasible inputs or results that are relevant to their work. The need for identifying the structural averaging approach when using the low frequency internal inductance equation has not been relevant in this exploratory work. This work uses a basic estimation (magnetic circuit theory) to that simplification in order to develop the greater methodology. The estimation is being made to an already simplified structure, which causes a larger error margin than necessary in the calculations. To complete the model and improve the unnecessary introduction of further error, it is recommended that an improved means of finding the structural average (or equivalent) be determined.

Further feasibility studies include the stability of the resulting material properties in relation to one another. The equations result in many possible unstable regions due to the way in which they are related within the system. These relationships are identified mathematically, which reveals their infeasibilities. At a superficial level to the design methodology presented here, a mathematical approach could be developed to check the multi-dimensional relationships for unstable or impossible design requirements. This could better scope the solution domain that multipath conductors holds and limit unnecessary design requirements faster.

From a practical perspective, additional feasibility studies are required as designs are not necessarily viable due to stability, fabrication, cost and appropriateness to the problem domain. These aspects are relevant much further on from the research problem presented here however.

Improvements in the understanding of current migration and its relation to resistance could better characterise the transition zones of the behaviour. This would require a deeper knowledge of the underlying physics at play rather than the black-box approach used in this work.

Although the approach shows merit it has by no means been assessed as the best method for design. The analytical solution of [9] enabled the insights for this work. In order to further the body of the knowledge an investigation into other approaches is required in order to identify whether this approach can be followed or if there are better methodologies to be discovered.

The greater research question that underpins the field of multipath conductors as dissipative filters is to investigate the extent to which multipath solutions are effective, practically. Can multipath methodologies truly be used to mitigate the effects of EMI in accordance with EMC regulation when considering the required material

specifications, fabrication, effective costing and feasible design performance? Or perhaps multipath conductor technology is more suited to applications that are not focussed on the realm of EMI mitigation?

9. References

[1] W. Kodali, *Engineering Electromagnetic Compatibility:Principles, Measurements, Technologies, and Computer Models*, 1st ed.: Wiley-IEEE Press, 2001.

[2] H. M. Schlicke and H. Weidmann, "Compatible EMI Filters," IEEE Spectrum, pp. 59-68, October 1967.

[3] L. Rossetto, P. Tenti, and A. Zucatto, "Electromagnetic compatibility issues in industrial equipment," Industry Applications Magazine, IEEE, vol. 5, no. 6, pp. 34-36, Nov/Dec 1999.

[4] H. M. Schlicke, "Assuredly Effective Filters," IEEE Transactions on Electromagnetic Compatibility, vol. EMC-18, no. 3, pp. 106-110, Aug 1976.

[5] P.J. Wolmarans, J.D. van Wyk, van Wyk jr. J. D., and Campbell C. K., "Technology for Integrated RF-EMI Transmission Line Filters for Integrated Power Electronic Modules," in Industry Applications Conference, 37th IAS Annual Meeting, 2002, vol. 3, 2002, pp. 1774-1780.

[6] J. L. Schanen, T. De Oliveira, J. M. Guichon, S. Mandray, and A. B. Thales, "Active Reduction of Common Mode Current in Power Modules," CIPS, March 2010, Paper 7.3.

[7] J.D. van Wyk jr, W. A. Cronje, J. D. van Wyk, C. K. Campbell, P. J. Wolmarans, "Power Electronic Interconnects: Skin- and Proximity Effect-Based Frequency Selective Multipath Propagation," IEEE TRANSACTIONS ON POWER ELECTRONICS, vol. 20, no. 3, pp. 600-610, May 2005.

[8] P. Schiffres, "A dissipative coaxial RFI-filter," IEEE Transactions on Electromagnetic Compatibility, vol. EMC-6, no. 1, pp. 55 -61, 1964.

[9] E. A. Brink and I. W. Hosajer, "Analytical Approach for Determining the Frequency-Dependent Characteristics of Multipath Conductive Structures," Power Electronics, IEEE Transactions, vol. 29, no. 11, pp. 5835-5845, Jan 2014.

[10] Y. Liang, J. D. van Wyk, and K. Ngo, "Parametric Characterization of Differential-Mode Transmission Line EMI Filter," The Bradley Department of Electrical and Computer Engineering, Virginia Polytechnic Institute and State University, 2007.

[11] F. Luo, R. Robutel, S. Wang, F. Wang, and D. Boroyevich, "Integrated input EMI Filter for a 2 kW DC-fed 3-phase motor drive," College of Electrical and Electronics Engineering, Huazhong University of Science and Technology, Wuhan, Hubei, China, 2009.

[12] J.D. van Wyk jr, W.A. Cronje, J.D. van Wyk, P.J. Wolmarans, and C.K. Campbell, "Integrated Power Filters Utilizing Skin- and Proximity Effect Based Low-pass Interconnects," in Conference on Integrated Power Systems, 2002.

[13] L. Zhao and J.D. van Wyk, "Electromagnetic modeling of an integrated RF EMI filter," in IEEE Industry Applications Conference, 2003, pp. 1601-1607.

[14] C.K. Campbell, J.D. van Wyk, and P.J. Wolmarans, "Improved transmission line attenuators for integrated power filters in the RF band," IEEE Trans on Components and Packaging Technologies, vol. 27, no. 2, pp. 311-316, 2004.

[15] A. C. Baisden, D. Boroyevich, and J. D. van Wyk, "High Frequency Modelling of a Converter with an RF-EMI filter," in IEEE Industry Applications Conference, 2006, pp. 2290-2295.

[16] A. C. Baisden, D. Boroyevich, and J. D. van Wyk, "Enhanced Design of an Integrated Transmission-Line Bus Filter," in IEEE Power Electronics Specialists Conference, 2007, pp. 3029-3033.

[17] C. Hebedean, C. Munteanu, A. Racasan, and O. Antonescu, "Technologies to increase HF losses in planar structures and their limitations," in 13th Intl. Conf on Optimization of Electrical and Electronic Equipment, 2012, pp. 48-53.

[18] D. Xu, Z. Wen, Y. Okuma, and K. Mino X. Wu, "Design, Modelling, and Improvement of Integrated EMI Filter With Flexible Multilayer Foils," IEEE Trans. on Power Electronics, vol. 26, no. 5, pp. 1344-1354, May 2011.

[19] R. Chen, J.D. van Wyk, S. Wang, and W.G. Odendaal, "Improving the Characteristics of Integrated EMI Filters by Embedded Conductive Layers," IEEE Trans. on Power Electronics, vol. 20, no. 3, pp. 611-619, May 2005.

[20] F. Luo et al., "Design of a Hybrid Busbar Filter Combining a Transmission-Line Busbar Filter and a One-Turn Inductor for DC-Fed Three-Phase Motor Drive Systems," IEEE TRANSACTIONS ON POWER ELECTRONICS, vol. 28, no. 12, pp. 5588-5602, Dec 2013.

Appendix A – Multipath Software Development and Implementation

1. Introduction

This appendix is presented in a procedural manner by laying down progressive logical steps to verify the correctness of the software calculator developed. The work does not validate the analytical method itself but rather that the software produces the same results as the analytical method. This is done to demonstrate the thoroughness of the solution. Repeatability of this work is aimed to be improved by assisting the reader with a step-by-step guide to recreating or improving this software.

A basic guide to implementing the analytical approach as software, specifically using *Mathematica* is presented. Here, the analytical methodology of [1] is recapped with the in-depth mathematics explored. The implementation is validated against the work of [1] to provide a reliable software implementation. Repeatable and less error prone coding practices are elaborated on in order to gain confidence in the software and allow for faster adoption of future work in this domain. This is shown for up to three layers only. The equations for four- and five-layer multipath conductors are not displayed here, as they cannot be made sense of in this medium. There are an overwhelmingly large number of terms in these functions, taking up to 76 pages to describe the coefficients, making it inappropriate to house in the written appendix

Multipath conductive structures have been modelled by [1] and provide an analytical solution of how the electric and magnetic fields distribute themselves in a multipath conductor. Computing these fields and the calculations that stem from them, however, has not been achieved. Mathematical software lends itself to the computational side of the model where the calculations can help with visualisation of the internal workings of the mathematics in the model, and predict the behaviour of different input scenarios. Derived works that fall within the scope of the model and from computing the model therefore depend on a well-developed, trustworthy calculator.

This appendix presents how software is used to implement the calculations required by [1] and the verification thereof. [1] is presented briefly in Section 2.1 along with how the expressions and equations involved are translated into software that can compute them. Section 2.2 lists and explains some noteworthy points when using the software and areas where better coding practices could be adhered to for a more maintainable solution. Sections 2.3-2.6 presents the verification of the software solution by comparing simulations using the implemented solution with other established computational tools. The software solution is verified with some basic experimental data. The implications of having this computational tool is explained in Section 3 with concluding points on what can be assumed for work that makes use of this computational software solution.

2. Translating the Analytical Methodology into Workable Software

The methodology in [1] for modelling multipath conductors along with the equations developed for certain structures is summarised here. This provides a basis for the development of the software solution. An explanation of how the model is implemented in software is given. Aspects regarding the choices made in implementing the software and the operation of the mathematical package used is shown to give insight into how the software is executing.

2.1 Summary of Analytical Method

[1] defined four steps to developing the necessary equations to model the structure, listed here:

1. The magnetic field intensity of the two exterior boundaries is determined depending on the configuration. This allows for *two* equations in terms of constants to be developed.
2. Continuity of the electric fields is enforced across layer boundaries. This is in accordance with Faraday's Law because neighbouring layers will be equated. This gives rise to *n-1* equations.
3. Continuity of the magnetic fields is enforced across layer boundaries. This is in accordance with Ampere's Law and produces *n-1* equations.
4. The above steps develop *2n* equations and therefore allow for simultaneous equations to be developed and the unknown coefficients solved for.

The general solution of the above four steps is given by Brink is shown below, where i is the layer number ($i \geq 1$). This is for a flat, semi-infinite conductor.

$$E_{x_i}(y) = L_i cosh\big(D_i(y - b_{i-1})\big) + M_i sinh\big(D_i(y - b_{i-1})\big)$$

$$H_{z_i}(y) = \frac{L_i D_i}{j\omega\mu_i} cosh\big(D_i(y - b_{i-1})\big) + \frac{M_i D_i}{j\omega\mu_i} sinh\big(D_i(y - b_{i-1})\big)$$

$$J_{x_i}(y) = \sigma_i L_i cosh\big(D_i(y - b_{i-1})\big) + \sigma_i M_i sinh\big(D_i(y - b_{i-1})\big)$$

where, $D_i = (1 + j)\sqrt{\frac{\omega\mu_i\sigma_i}{2}} = \frac{(1+j)}{\delta_i}$ and $b_{i-1} \leq y \leq b_i$

and μ represents permeability and σ represents conductivity.

This general solution is shown for simpler flat, semi-infinite conductive structures in the following sections.

2.2 The Use of *Mathematica* as an Appropriate Mathematical Package

Good software design is key to the reducing the risk of errors within a system. For this reason careful consideration has been taken to implement the solution according to established principles of best practice.

The code is structured into three major components:

- a custom library of usable equations as functions
- a business logic layer that handles the calling (of library functions) and passing around of data.
- a data persistence layer – this actually resides externally to the codebase.

This structures allows for the mitigation of errors by:

1. Structurally centralising the common code components thereby not requiring duplication of code and its inherent risk of error.
2. Allowing for testing access to the centralised library.
3. Simplifying the responsibility of storing output data and the conditions under which it occurred.

A library is implemented to house the valid equations and has benefits in centralising the functions. This enables a multitude of business logic layers to use the library (coded against an interface to the library) that can view the data in various ways. This is ideal for research work as different experiments can be implemented in different client layers with their own logic to find new understandings. A second advantage to this is that the equations can be tested by one set of client code and used seamlessly by another without code duplication. Code duplication increases the maintenance required in the upkeep of valid code and increases the room for human error, both in the transfer and maintenance of it. Version control of a centralised repository allows for properly storing, accessing and maintaining the code base.

The requirements of the software package take into account the design aspects for how the implementation is structured but more importantly its ability to compute. *Mathematica* was chosen for its:

- Symbolic math capabilities – allowing fully specifiable computational precision.
- Functional programming capabilities to execute pure mathematical concepts – as in the analytical method from [1].
- Fast compute time – allowing for tighter feedback in processing data and faster experimental iterations.
- Ability to create functions.
- Ability to extend core functionality to incorporate a custom library (known as *Mathematica packages*) where the functions could be housed.
- Interpreted execution of code allows for segments of calculations to be explored in isolation.

2.3 Flat Single Layer Structure

Using the general solution from [1], the equations for a single layer structure were developed. Using *Mathematica,* the code for the equations is implemented as shown below in Figure 1. Table 1 gives brief explanation on the naming convention used.

Table 1: Explanation of variables used in software.

Notation	Meaning
J	Current Density
H	Magnetic Field Intensity
E	Electric Field
x,y,z	Cartesian co-ordinates representating where the field lies
1,2,3,4…	The layer number being considered
Jx1	Current density in the x direction for layer 1
Hz1	Magnetic Field Intensity in the z direction for layer 1
Ex1	Electric Field strength in the x direction for layer 1

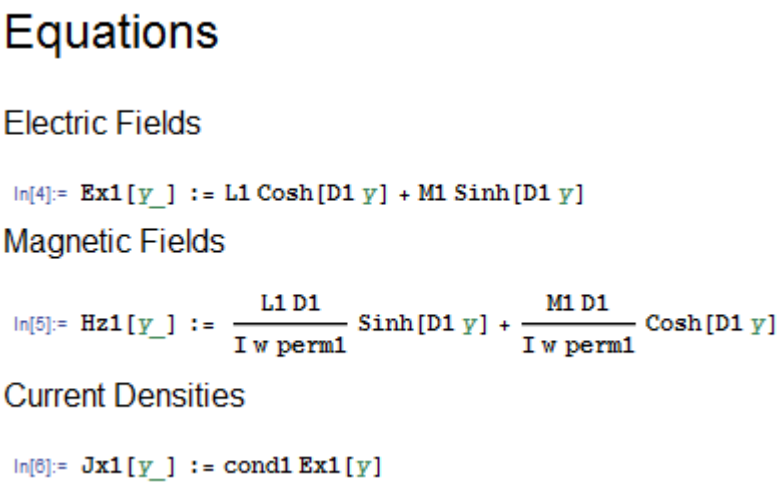

Figure 1: Mathematica implementation of field equations from [1].

These equations are then used in the four steps [1] has defined. In the single layer case there are no boundaries where the fields are defined to be continuous and therefore only steps 1 and 4 are shown below in Figure 2. Hz1 is calculated where y=0 and where y=b1 in order to find the boundary magnetic field intensity values. This allows for the values of Hs0 and Hs1 to be found and substituted into the equations to find the M1 and L1 coefficients, as shown in step 4. These coefficients match up to the results found in [1].

Solving

Step 1 outer boundaries

In[7]:=
```
Hz1[0]
```

Out[7]=
$$-\frac{i\ D1\ M1}{perm1\ w}$$

In[8]:=
```
Hz1[b1]
```

Out[8]=
$$-\frac{i\ D1\ M1\ Cosh[b1\ D1]}{perm1\ w}-\frac{i\ D1\ L1\ Sinh[b1\ D1]}{perm1\ w}$$

Step 4 get and solve simultaneous equations

In[9]:=
```
simultaneousEquations = {Hs0 == Hz1[0], Hs1 == Hz1[b1]}
unknowns = {M1, L1};
solution = Solve[simultaneousEquations, unknowns]
```

Out[9]=
$$\left\{Hs0==-\frac{i\ D1\ M1}{perm1\ w},\ Hs1==-\frac{i\ D1\ M1\ Cosh[b1\ D1]}{perm1\ w}-\frac{i\ D1\ L1\ Sinh[b1\ D1]}{perm1\ w}\right\}$$

Out[11]=
$$\left\{\left\{M1\to\frac{i\ Hs0\ perm1\ w}{D1},\ L1\to-\frac{i\ (Hs0\ perm1\ w\ Coth[b1\ D1]-Hs1\ perm1\ w\ Csch[b1\ D1])}{D1}\right\}\right\}$$

Confirm the simultaneous equations have solved for the correct values and assign their values from the list.

In[12]:=
```
M1 = M1 /. solution
L1 = L1 /. solution
```

Out[12]=
$$\left\{\frac{i\ Hs0\ perm1\ w}{D1}\right\}$$

Out[13]=
$$\left\{-\frac{i\ (Hs0\ perm1\ w\ Coth[b1\ D1]-Hs1\ perm1\ w\ Csch[b1\ D1])}{D1}\right\}$$

Figure 2: Software implementation of steps 1 and 4 for a single layer equation.

Although these coefficients can be found relatively easily using a symbolic math tool, the strength of the calculator is in putting the coefficients into a more workable form so that they can be used in functions and thus simulate the electromagnetic characteristics of the structure. By examining the functions it is identifiable that the key variables that can influence the response of the structure, and analysis of it, are those found in Table 2 below.

Table 2: Key variables of influence in a single layer structure.

Variable	Variable Symbol
Frequency of input current	f
Conductivity of each layer	σ
Permeability of each layer	μ
Thickness of each layer	b
Point of analysis in y-direction through the layer	y
Layer number	1,2,3…n

These variables are therefore incorporated into the coefficients and the functions so that their values can be inputs to the functions and therefore simulate the different scenarios. The functions are developed using the SetDelay symbol and thus maintain the symbolic nature of the functions, only evaluating them when needed and therefore preserving the precision of the calculations. The inputs of the functions are shown to be incorporated into them in Figure 3 below. Note that the coefficients have also been modified as this change needs to propagate to all terms within the function calls.

```
w[f_] := 2 Pi f;
D1[f_, σ1_, μ1_] := (1 + I) Sqrt[w[f] σ1 μ1 / 2];
```

Electric Fields

```
Ex1[y_, f_, σ1_, μ1_, b1_] := L1[f, σ1, μ1, b1] Cosh[D1[f, σ1, μ1] y] +
   M1[f, σ1, μ1] Sinh[D1[f, σ1, μ1] y];
```

Magnetic Fields

```
Hz1[y_, f_, σ1_, μ1_, b1_] := L1[f, σ1, μ1, b1] D1[f, σ1, μ1] / (I w[f] μ1) Sinh[D1[f, σ1, μ1] y] +
   M1[f, σ1, μ1] D1[f, σ1, μ1] / (I w[f] μ1) Cosh[D1[f, σ1, μ1] y];
```

Current Densities

```
Jx1[y_, f_, σ1_, μ1_, b1_] := N[σ1 Ex1[y, f, σ1, μ1, b1]];
```

Coefficients

```
M1[f_, σ1_, μ1_] := i Hs0 μ1 w[f] / D1[f, σ1, μ1];

L1[f_, σ1_, μ1_, b1_] :=
  -1 / D1[f, σ1, μ1] i (Hs0 μ1 w[f] Coth[b1 D1[f, σ1, μ1]] - Hs1 μ1 w[f] Csch[b1 D1[f, σ1, μ1]]);
```

Figure 3: Implementation of the functions and solved coefficients into workable software what depends on input parameters.

The fields and current density can now be calculated and the effects of changes to each of its variables can be determined. But this level of detail can be overwhelming and difficult to understand if used in isolation. Well known concepts of impedance and power within the conductor can be derived from the functions that are given in Figure 3. These derived functions also accept the input variables to allow the values to change in all places in the functions and interact with other. Figure 4 below contains these derived equations.

Power Equations for the layers

```
P1[f_, σ1_, μ1_, b1_] :=
 length width / (2 σ1) NIntegrate[Abs[Jx1[y, f, σ1, μ1, b1]^2], {y, 0, b1},
   WorkingPrecision → numericalPrecision]
PTot[f_, σ1_, μ1_, b1_] := P1[f, σ1, μ1, b1]
```

Resistance Equation

$$\text{RDiff}[f_, \sigma1_, \mu1_, b1_] := \frac{2\,\text{PTot}[f, \sigma1, \mu1, b1]}{\text{netCurrent}^2}$$

Internal Inductance

$$\text{LInt}[f_, \sigma1_, \mu1_, b1_] := N\left[\frac{2\,(2\,\text{WTot}[f, \sigma1, \mu1, b1])}{\text{netCurrent}^2}\right]$$

External Inductance

$$\text{LExt} := \frac{\text{perm0 length gap}}{\text{width}}$$

Total Inductance

```
LTot[f_, σ1_, μ1_, b1_] := LInt[f, σ1, μ1, b1] + LExt
```

Total Impedance

```
ZTot[f_, σ1_, μ1_, b1_] :=
 RDiff[f, σ1, μ1, b1] + I 2 w[f] LTot[f, σ1, μ1, b1]
```

Figure 4: Impedance and power equations for a single layer solution in usable simulation form.

2.4 Flat Two Layer Structure

The same methodology used for single layers was applied to two layer structures. Again the steps started from [1]'s method and are as follows:

1. Develop the exterior magnetic field intensity boundary equations
2. Develop the electric and magnetic field equations for each layer, enforcing continuity of the fields at the internal boundaries.
3. Solve for the M and L coefficients of the layers symbolically
4. Convert the coefficients, derived equations and higher level power and impedance equations into a form that can be simulated using a symbolic math tool.

Conversion of the various calculations required can be achieved at various levels of automation. The simplest being the find and replace too with some manual manipulations. As the number of layers in the structure increases the size of the code starts to increase quickly as the solution becomes more complex. It may be better in this situation to look at scripting

changes to the text form of the code in order to manage the conversion more efficiently and accurately.

The two layer equations are shown below in Figure 5.

Equations

Electric Fields

$$Ex1[y_] := L1\,\text{Cosh}[D1\,y] + M1\,\text{Sinh}[D1\,y]$$

$$Ex2[y_] := L2\,\text{Cosh}[D2\,(y - b1)] + M2\,\text{Sinh}[D2\,(y - b1)]$$

Magnetic Fields

$$Hz1[y_] := \frac{L1\,D1}{I\,w\,perm1}\,\text{Sinh}[D1\,y] + \frac{M1\,D1}{I\,w\,perm1}\,\text{Cosh}[D1\,y]$$

$$Hz2[y_] := \frac{L2\,D2}{I\,w\,perm2}\,\text{Sinh}[D2\,(y - b1)] + \frac{M2\,D2}{I\,w\,perm2}\,\text{Cosh}[D2\,(y - b1)]$$

Current Densities

$$Jx1[y_] := cond1\,Ex1[y]$$

$$Jx2[y_] := cond2\,Ex2[y]$$

Figure 5: Two-layer field equations as software.

Implementing and solving [1]'s method for finding the coefficient expressions is achieved in the following four steps, Figure 6:

Step 1 outer boundaries

$$Hz1[0]$$

$$-\frac{i\,D1\,M1}{perm1\,w}$$

$$Hz2[b2]$$

$$-\frac{i\,D2\,M2\,\text{Cosh}[(-b1 + b2)\,D2]}{perm2\,w} - \frac{i\,D2\,L2\,\text{Sinh}[(-b1 + b2)\,D2]}{perm2\,w}$$

Step 2 Faraday's Law electric fields continuous at boundaries

$$Ex1[b1]$$

$$L1\,\text{Cosh}[b1\,D1] + M1\,\text{Sinh}[b1\,D1]$$

$$Ex2[b1]$$

$$L2$$

Step 3 Ampere's Law, tangential magnetic field continuous at b1

```
Hz1[b1]
```

$$-\frac{i\ D1\ M1\ \text{Cosh}[b1\ D1]}{perm1\ w}-\frac{i\ D1\ L1\ \text{Sinh}[b1\ D1]}{perm1\ w}$$

```
Hz2[b1]
```

$$-\frac{i\ D2\ M2}{perm2\ w}$$

Step 4 get and solve simultaneous equations

```
simultaneousEquations = {Hs0 == Hz1[0], Hs2 == Hz2[b2], Ex1[b1] == Ex2[b1], Hz1[b1] == Hz2[b1]}
unknowns = {M1, L1, M2, L2};
solution = Solve[simultaneousEquations, unknowns]
```

$$\left\{Hs0 == -\frac{i\ D1\ M1}{perm1\ w},\ Hs2 == -\frac{i\ D2\ M2\ \text{Cosh}[(-b1+b2)\ D2]}{perm2\ w}-\frac{i\ D2\ L2\ \text{Sinh}[(-b1+b2)\ D2]}{perm2\ w},\right.$$
$$\left.L1\ \text{Cosh}[b1\ D1]+M1\ \text{Sinh}[b1\ D1] == L2,\ -\frac{i\ D1\ M1\ \text{Cosh}[b1\ D1]}{perm1\ w}-\frac{i\ D1\ L1\ \text{Sinh}[b1\ D1]}{perm1\ w} == -\frac{i\ D2\ M2}{perm2\ w}\right\}$$

$$\left\{\left\{L1 \to \left(i\left(D1\ Hs2\ perm1\ perm2\ w - D1\ Hs0\ perm1\ perm2\ w\ \text{Cosh}[b1\ D1]\ \text{Cosh}[(-b1+b2)\ D2] - D2\ Hs0\ perm1^2\ w\ \text{Sinh}[b1\ D1]\ \text{Sinh}[(-b1+b2)\ D2]\right)\right)/\right.$$
$$\left.(D1\ (D1\ perm2\ \text{Cosh}[(-b1+b2)\ D2]\ \text{Sinh}[b1\ D1]+D2\ perm1\ \text{Cosh}[b1\ D1]\ \text{Sinh}[(-b1+b2)\ D2])),\right.$$
$$M2 \to \left(i\left(D1\ Hs2\ perm2^2\ w\ \text{Sinh}[b1\ D1]+D2\ Hs0\ perm1\ perm2\ w\ \text{Cosh}[b1\ D1]^2\ \text{Sinh}[(-b1+b2)\ D2] - D2\ Hs0\ perm1\ perm2\ w\ \text{Sinh}[b1\ D1]^2\ \text{Sinh}[(-b1+b2)\ D2]\right)\right)/$$
$$(D2\ (D1\ perm2\ \text{Cosh}[(-b1+b2)\ D2]\ \text{Sinh}[b1\ D1]+D2\ perm1\ \text{Cosh}[b1\ D1]\ \text{Sinh}[(-b1+b2)\ D2])),$$
$$L2 \to \left(i\left(Hs2\ perm1\ perm2\ w\ \text{Cosh}[b1\ D1] - Hs0\ perm1\ perm2\ w\ \text{Cosh}[b1\ D1]^2\ \text{Cosh}[(-b1+b2)\ D2] + Hs0\ perm1\ perm2\ w\ \text{Cosh}[(-b1+b2)\ D2]\ \text{Sinh}[b1\ D1]^2\right)\right)/$$
$$(D1\ perm2\ \text{Cosh}[(-b1+b2)\ D2]\ \text{Sinh}[b1\ D1]+D2\ perm1\ \text{Cosh}[b1\ D1]\ \text{Sinh}[(-b1+b2)\ D2])),$$
$$M1 \to \frac{i\ Hs0\ perm1\ w}{D1}\Big\}\Big\}$$

Figure 6: Software implementation of the four steps presented by [1].

The expressions found for the L and M coefficients of each layer are the result of Step 4 above. The progression from single layer to two layer structures rapidly increases the complexity of the solution. The final step is then carried out for these coefficients, field equations and the necessary power and impedance equations that are required for the simulation and understanding of the structures.

The two layer code used for simulation purposes is shown in Figure 7 below.

Frequency Dependent Factors

```
w[f_] := 2 Pi f;
D1[f_, σ1_, μ1_] := (1 + I) Sqrt[w[f] σ1 μ1 / 2];
D2[f_, σ2_, μ2_] := (1 + I) Sqrt[w[f] σ2 μ2 / 2];
```

Electric Fields

```
Ex1[y_, f_, σ1_, σ2_, μ1_, μ2_, b1_, b2_] :=
 L1[f, σ1, σ2, μ1, μ2, b1, b2] Cosh[D1[f, σ1, μ1] y] +
  M1[f, σ1, μ1] Sinh[D1[f, σ1, μ1] y]

Ex2[y_, f_, σ1_, σ2_, μ1_, μ2_, b1_, b2_] :=
 L2[f, σ1, σ2, μ1, μ2, b1, b2] Cosh[D2[f, σ2, μ2] (y - b1)] +
  M2[f, σ1, σ2, μ1, μ2, b1, b2] Sinh[D2[f, σ2, μ2] (y - b1)]
```

Magnetic Fields

```
Hz1[y_, f_, σ1_, σ2_, μ1_, μ2_, b1_, b2_] :=
 L1[f, σ1, σ2, μ1, μ2, b1, b2] D1[f, σ1, μ1] / (I w[f] μ1) Sinh[D1[f, σ1, μ1] y] +
  M1[f, σ1, μ1] D1[f, σ1, μ1] / (I w[f] μ1) Cosh[D1[f, σ1, μ1] y]

Hz2[y_, f_, σ1_, σ2_, μ1_, μ2_, b1_, b2_] :=
 L2[f, σ1, σ2, μ1, μ2, b1, b2] D2[f, σ2, μ2] / (I w[f] μ2) Sinh[D2 [f, σ2, μ2] (y - b1)] +
  M2[f, σ1, σ2, μ1, μ2, b1, b2] D2[f, σ2, μ2] / (I w[f] μ2) Cosh[D2[f, σ2, μ2] (y - b1)]
```

Current Densities

```
Jx1[y_, f_, σ1_, σ2_, μ1_, μ2_, b1_, b2_] := σ1 Ex1[y, f, σ1, σ2, μ1, μ2, b1, b2]
Jx2[y_, f_, σ1_, σ2_, μ1_, μ2_, b1_, b2_] := σ2 Ex2[y, f, σ1, σ2, μ1, μ2, b1, b2]
```

Figure 7: Parameterised two-layer software solution.

The coefficients are converted to the following form, Figure 8.

Coefficients

```
L1[f_, σ1_, σ2_, μ1_, μ2_, b1_, b2_] :=
 (i (D1[f, σ1, μ1] Hs2 μ1 μ2 w[f] - D1[f, σ1, μ1] Hs0 μ1 μ2 w[f] Cosh[b1 D1[f, σ1, μ1]]
       Cosh[(-b1 + b2) D2[f, σ2, μ2]] -
      D2[f, σ2, μ2] Hs0 μ1^2 w[f] Sinh[b1 D1[f, σ1, μ1]]
       Sinh[(-b1 + b2) D2[f, σ2, μ2]])) /
  (D1[f, σ1, μ1]
    (D1[f, σ1, μ1] μ2 Cosh[(-b1 + b2) D2[f, σ2, μ2]] Sinh[b1 D1[f, σ1, μ1]] +
     D2[f, σ2, μ2] μ1 Cosh[b1 D1[f, σ1, μ1]] Sinh[(-b1 + b2) D2[f, σ2, μ2]]))

L2[f_, σ1_, σ2_, μ1_, μ2_, b1_, b2_] :=
 (i (Hs2 μ1 μ2 w[f] Cosh[b1 D1[f, σ1, μ1]] -
      Hs0 μ1 μ2 w[f] Cosh[b1 D1[f, σ1, μ1]]^2 Cosh[(-b1 + b2) D2[f, σ2, μ2]] +
      Hs0 μ1 μ2 w[f] Cosh[(-b1 + b2) D2[f, σ2, μ2]] Sinh[b1 D1[f, σ1, μ1]]^2)) /
  (D1[f, σ1, μ1] μ2 Cosh[(-b1 + b2) D2[f, σ2, μ2]] Sinh[b1 D1[f, σ1, μ1]] +
   D2[f, σ2, μ2] μ1 Cosh[b1 D1[f, σ1, μ1]] Sinh[(-b1 + b2) D2[f, σ2, μ2]])


M1[f_, σ1_, μ1_] := i Hs0 μ1 w[f] / D1[f, σ1, μ1]

M2[f_, σ1_, σ2_, μ1_, μ2_, b1_, b2_] :=
 (i (D1[f, σ1, μ1] Hs2 μ2^2 w[f] Sinh[b1 D1[f, σ1, μ1]] +
      D2[f, σ2, μ2] Hs0 μ1 μ2 w[f] Cosh[b1 D1[f, σ1, μ1]]^2
       Sinh[(-b1 + b2) D2[f, σ2, μ2]] -
      D2[f, σ2, μ2] Hs0 μ1 μ2 w[f] Sinh[b1 D1[f, σ1, μ1]]^2
       Sinh[(-b1 + b2) D2[f, σ2, μ2]])) /
  (D2[f, σ2, μ2]
    (D1[f, σ1, μ1] μ2 Cosh[(-b1 + b2) D2[f, σ2, μ2]] Sinh[b1 D1[f, σ1, μ1]] +
     D2[f, σ2, μ2] μ1 Cosh[b1 D1[f, σ1, μ1]] Sinh[(-b1 + b2) D2[f, σ2, μ2]]))
```

Figure 8: Software parameterised coefficients for two-layer structures

The power and impedance equations are developed in the following manner so that they apply to two layer structures as follows, Figure 9.

Power Equations for the layers

$$P1[f_, \sigma1_, \sigma2_, \mu1_, \mu2_, b1_] := \frac{\text{length width}}{2\,\sigma1}\,\text{NIntegrate}\left[\text{Abs}\left[Jx1[y, f, \sigma1, \sigma2, \mu1, \mu2, b1, b2]^2\right], \{y, 0, b1\}\right]$$

$$P2[f_, \sigma1_, \sigma2_, \mu1_, \mu2_, b1_, b2_] := \frac{\text{length width}}{2\,\sigma2}\,\text{NIntegrate}\left[\text{Abs}\left[Jx2[y, f, \sigma1, \sigma2, \mu1, \mu2, b1, b2]^2\right], \{y, b1, b2\}\right]$$

$$PTot[f_, \sigma1_, \sigma2_, \mu1_, \mu2_, b1_, b2_] := P1[f, \sigma1, \sigma2, \mu1, \mu2, b1] + P2[f, \sigma1, \sigma2, \mu1, \mu2, b1, b2]$$

Resistance Equation

$$RDiff[f_, \sigma1_, \sigma2_, \mu1_, \mu2_, b1_, b2_] := \frac{2\,PTot[f, \sigma1, \sigma2, \mu1, \mu2, b1, b2]}{\text{netCurrent}^2}$$

Internal Inductance

$$LInt[f_, \sigma1_, \sigma2_, \mu1_, \mu2_, b1_, b2_] := N\left[\frac{2\,(2\,WTot[f, \sigma1, \sigma2, \mu1, \mu2, b1, b2])}{\text{netCurrent}^2}\right]$$

External Inductance

$$LExt := \frac{\text{perm0 length gap}}{\text{width}}$$

Total Inductance

$$LTot[f_, \sigma1_, \sigma2_, \mu1_, \mu2_, b1_, b2_] := LInt[f, \sigma1, \sigma2, \mu1, \mu2, b1, b2] + LExt$$

Total Impedance

$$ZTot[f_, \sigma1_, \sigma2_, \mu1_, \mu2_, b1_, b2_] := RDiff[f, \sigma1, \sigma2, \mu1, \mu2, b1, b2] + I\,2\,w[f]\,LTot[f, \sigma1, \sigma2, \mu1, \mu2, b1, b2]$$

Figure 9: High level equations developed using software for a two-layer structure.

2.5 Three Layer Structures

Again, the same method is applied three layer structures. The steps are presented in the following code snippets.

The electric and magnetic field equations for the layers are developed.

Electric Fields

```
Ex1[y_] := L1 Cosh[D1 y] + M1 Sinh[D1 y]
Ex2[y_] := L2 Cosh[D2 (y - b1)] + M2 Sinh[D2 (y - b1)]
Ex3[y_] := L3 Cosh[D3 (y - b2)] + M3 Sinh[D3 (y - b2)]
```

Magnetic Fields

$$Hz1[y_] := \frac{L1\ D1}{I\ w\ perm1} Sinh[D1\ y] + \frac{M1\ D1}{I\ w\ perm1} Cosh[D1\ y]$$

$$Hz2[y_] := \frac{L2\ D2}{I\ w\ perm2} Sinh[D2\ (y - b1)] + \frac{M2\ D2}{I\ w\ perm2} Cosh[D2\ (y - b1)]$$

$$Hz3[y_] := \frac{L3\ D3}{I\ w\ perm3} Sinh[D3\ (y - b2)] + \frac{M3\ D3}{I\ w\ perm3} Cosh[D3\ (y - b2)]$$

Current Densities

```
Jx1[y_] := cond1 Ex1[y]
Jx2[y_] := cond2 Ex2[y]
Jx3[y_] := cond3 Ex3[y]
```

Figure 10: Field equations implemented as software for three-layer structures.

[1]'s four step solution is applied in order to find expressions for the M and L coefficients of each layer.

Step 1 outer boundaries

```
Hz1[0]
```

$$-\frac{i\ D1\ M1}{perm1\ w}$$

```
Hz3[b3]
```

$$-\frac{i\ D3\ M3\ Cosh[(-b2 + b3)\ D3]}{perm3\ w} - \frac{i\ D3\ L3\ Sinh[(-b2 + b3)\ D3]}{perm3\ w}$$

Step 2 Faraday's Law electric fields continuous at boundaries

```
Ex1[b1]
```

$$L1 \cosh[b1\ D1] + M1 \sinh[b1\ D1]$$

```
Ex2[b1]
```

$$L2$$

```
Ex2[b2]
```

$$L2 \cosh[(-b1 + b2)\ D2] + M2 \sinh[(-b1 + b2)\ D2]$$

```
Ex3[b2]
```

$$L3$$

Step 3 Ampere's Law, tangential magnetic field continuous at b1

```
Hz1[b1]
```

$$-\frac{i\ D1\ M1 \cosh[b1\ D1]}{perm1\ w} - \frac{i\ D1\ L1 \sinh[b1\ D1]}{perm1\ w}$$

```
Hz2[b1]
```

$$-\frac{i\ D2\ M2}{perm2\ w}$$

```
Hz2[b2]
```

$$-\frac{i\ D2\ M2 \cosh[(-b1 + b2)\ D2]}{perm2\ w} - \frac{i\ D2\ L2 \sinh[(-b1 + b2)\ D2]}{perm2\ w}$$

```
Hz3[b2]
```

$$-\frac{i\ D3\ M3}{perm3\ w}$$

Step 4 get and solve simultaneous equations

```
simultaneousEquations = {Hs0 == Hz1[0], Hs3 == Hz3[b3], Ex1[b1] == Ex2[b1],
  Ex3[b2] == Ex2[b2], Hz1[b1] == Hz2[b1], Hz2[b2] == Hz3[b2]}
unknowns = {M1, L1, M2, L2, M3, L3};
solution = Solve[simultaneousEquations, unknowns]
```

$$\left\{Hs0 == -\frac{i\,D1\,M1}{perm1\,w},\ Hs3 == -\frac{i\,D3\,M3\,Cosh[(-b2+b3)\,D3]}{perm3\,w} - \frac{i\,D3\,L3\,Sinh[(-b2+b3)\,D3]}{perm3\,w},\right.$$
$$L1\,Cosh[b1\,D1] + M1\,Sinh[b1\,D1] == L2,\ L3 == L2\,Cosh[(-b1+b2)\,D2] + M2\,Sinh[(-b1+b2)\,D2],$$
$$-\frac{i\,D1\,M1\,Cosh[b1\,D1]}{perm1\,w} - \frac{i\,D1\,L1\,Sinh[b1\,D1]}{perm1\,w} == -\frac{i\,D2\,M2}{perm2\,w},$$
$$\left.-\frac{i\,D2\,M2\,Cosh[(-b1+b2)\,D2]}{perm2\,w} - \frac{i\,D2\,L2\,Sinh[(-b1+b2)\,D2]}{perm2\,w} == -\frac{i\,D3\,M3}{perm3\,w}\right\}$$

Figure 11: Implementation of the four step methodology for three-layer structures.

The solution to the simultaneous equations from step four is given below for each coefficient, Figure 12.

$$L1 \to \left(i\left(D1\,D2\,Hs3\,perm1\,perm2\,perm3\,w - D1\,D2\,Hs0\,perm1\,perm2\,perm3\,w\,Cosh[b1\,D1]\,Cosh[(-b1+b2)\,D2]\right.\right.$$
$$\left.Cosh[(-b2+b3)\,D3] - D2^2\,Hs0\,perm1^2\,perm3\,w\,Cosh[(-b2+b3)\,D3]\,Sinh[b1\,D1]\,Sinh[(-b1+b2)\,D2] -$$
$$D2\,D3\,Hs0\,perm1^2\,perm2\,w\,Cosh[(-b1+b2)\,D2]\,Sinh[b1\,D1]\,Sinh[(-b2+b3)\,D3] -$$
$$\left.D1\,D3\,Hs0\,perm1\,perm2^2\,w\,Cosh[b1\,D1]\,Sinh[(-b1+b2)\,D2]\,Sinh[(-b2+b3)\,D3]\right)\Big) /$$
$$\left(D1\left(D1\,D2\,perm2\,perm3\,Cosh[(-b1+b2)\,D2]\,Cosh[(-b2+b3)\,D3]\,Sinh[b1\,D1] +\right.\right.$$
$$D2^2\,perm1\,perm3\,Cosh[b1\,D1]\,Cosh[(-b2+b3)\,D3]\,Sinh[(-b1+b2)\,D2] +$$
$$D2\,D3\,perm1\,perm2\,Cosh[b1\,D1]\,Cosh[(-b1+b2)\,D2]\,Sinh[(-b2+b3)\,D3] +$$
$$\left.\left.D1\,D3\,perm2^2\,Sinh[b1\,D1]\,Sinh[(-b1+b2)\,D2]\,Sinh[(-b2+b3)\,D3]\right)\right)$$

$$L2 \to \left(i\left(D2\,Hs3\,perm1\,perm2\,perm3\,w\,Cosh[b1\,D1] - D2\,Hs0\,perm1\,perm2\,perm3\,w\right.\right.$$
$$Cosh[b1\,D1]^2\,Cosh[(-b1+b2)\,D2]\,Cosh[(-b2+b3)\,D3] +$$
$$D2\,Hs0\,perm1\,perm2\,perm3\,w\,Cosh[(-b1+b2)\,D2]\,Cosh[(-b2+b3)\,D3]\,Sinh[b1\,D1]^2 -$$
$$D3\,Hs0\,perm1\,perm2^2\,w\,Cosh[b1\,D1]^2\,Sinh[(-b1+b2)\,D2]\,Sinh[(-b2+b3)\,D3] +$$
$$\left.\left.D3\,Hs0\,perm1\,perm2^2\,w\,Sinh[b1\,D1]^2\,Sinh[(-b1+b2)\,D2]\,Sinh[(-b2+b3)\,D3]\right)\right) /$$
$$\left(D1\,D2\,perm2\,perm3\,Cosh[(-b1+b2)\,D2]\,Cosh[(-b2+b3)\,D3]\,Sinh[b1\,D1] +\right.$$
$$D2^2\,perm1\,perm3\,Cosh[b1\,D1]\,Cosh[(-b2+b3)\,D3]\,Sinh[(-b1+b2)\,D2] +$$
$$D2\,D3\,perm1\,perm2\,Cosh[b1\,D1]\,Cosh[(-b1+b2)\,D2]\,Sinh[(-b2+b3)\,D3] +$$
$$\left.D1\,D3\,perm2^2\,Sinh[b1\,D1]\,Sinh[(-b1+b2)\,D2]\,Sinh[(-b2+b3)\,D3]\right)$$

$$L3 \to -\left(i\left(-D2\,Hs3\,perm1\,perm2\,perm3\,w\,Cosh[b1\,D1]\,Cosh[(-b1+b2)\,D2] +\right.\right.$$
$$D2\,Hs0\,perm1\,perm2\,perm3\,w\,Cosh[b1\,D1]^2\,Cosh[(-b1+b2)\,D2]^2\,Cosh[(-b2+b3)\,D3] -$$
$$D2\,Hs0\,perm1\,perm2\,perm3\,w\,Cosh[(-b1+b2)\,D2]^2\,Cosh[(-b2+b3)\,D3]\,Sinh[b1\,D1]^2 -$$
$$D1\,Hs3\,perm2^2\,perm3\,w\,Sinh[b1\,D1]\,Sinh[(-b1+b2)\,D2] -$$
$$D2\,Hs0\,perm1\,perm2\,perm3\,w\,Cosh[b1\,D1]^2\,Cosh[(-b2+b3)\,D3]\,Sinh[(-b1+b2)\,D2]^2 +$$
$$\left.\left.D2\,Hs0\,perm1\,perm2\,perm3\,w\,Cosh[(-b2+b3)\,D3]\,Sinh[b1\,D1]^2\,Sinh[(-b1+b2)\,D2]^2\right)\right) /$$
$$\left(D1\,D2\,perm2\,perm3\,Cosh[(-b1+b2)\,D2]\,Cosh[(-b2+b3)\,D3]\,Sinh[b1\,D1] +\right.$$
$$D2^2\,perm1\,perm3\,Cosh[b1\,D1]\,Cosh[(-b2+b3)\,D3]\,Sinh[(-b1+b2)\,D2] +$$
$$D2\,D3\,perm1\,perm2\,Cosh[b1\,D1]\,Cosh[(-b1+b2)\,D2]\,Sinh[(-b2+b3)\,D3] +$$
$$\left.D1\,D3\,perm2^2\,Sinh[b1\,D1]\,Sinh[(-b1+b2)\,D2]\,Sinh[(-b2+b3)\,D3]\right)$$

$$M1 \to \frac{i\, Hs0\, perm1\, w}{D1}$$

$$M2 \to \Big(i \Big(D1\, D2\, Hs3\, perm2^2\, perm3\, w\, \text{Sinh}[b1\, D1] + D2^2\, Hs0\, perm1\, perm2\, perm3\, w\, \text{Cosh}[b1\, D1]^2\, \text{Cosh}[(-b2+b3)\, D3]\, \text{Sinh}[(-b1+b2)\, D2] - D2^2\, Hs0\, perm1\, perm2\, perm3\, w\, \text{Cosh}[(-b2+b3)\, D3]\, \text{Sinh}[b1\, D1]^2\, \text{Sinh}[(-b1+b2)\, D2] + D2\, D3\, Hs0\, perm1\, perm2^2\, w\, \text{Cosh}[b1\, D1]^2\, \text{Cosh}[(-b1+b2)\, D2]\, \text{Sinh}[(-b2+b3)\, D3] - D2\, D3\, Hs0\, perm1\, perm2^2\, w\, \text{Cosh}[(-b1+b2)\, D2]\, \text{Sinh}[b1\, D1]^2\, \text{Sinh}[(-b2+b3)\, D3]\Big)\Big) \Big/ \Big(D2 \Big(D1\, D2\, perm2\, perm3\, \text{Cosh}[(-b1+b2)\, D2]\, \text{Cosh}[(-b2+b3)\, D3]\, \text{Sinh}[b1\, D1] + D2^2\, perm1\, perm3\, \text{Cosh}[b1\, D1]\, \text{Cosh}[(-b2+b3)\, D3]\, \text{Sinh}[(-b1+b2)\, D2] + D2\, D3\, perm1\, perm2\, \text{Cosh}[b1\, D1]\, \text{Cosh}[(-b1+b2)\, D2]\, \text{Sinh}[(-b2+b3)\, D3] + D1\, D3\, perm2^2\, \text{Sinh}[b1\, D1]\, \text{Sinh}[(-b1+b2)\, D2]\, \text{Sinh}[(-b2+b3)\, D3]\Big)\Big)$$

$$M3 \to \Big(i \Big(D1\, D2\, Hs3\, perm2\, perm3^2\, w\, \text{Cosh}[(-b1+b2)\, D2]\, \text{Sinh}[b1\, D1] + D2^2\, Hs3\, perm1\, perm3^2\, w\, \text{Cosh}[b1\, D1]\, \text{Sinh}[(-b1+b2)\, D2] + D2\, D3\, Hs0\, perm1\, perm2\, perm3\, w\, \text{Cosh}[b1\, D1]^2\, \text{Cosh}[(-b1+b2)\, D2]^2\, \text{Sinh}[(-b2+b3)\, D3] - D2\, D3\, Hs0\, perm1\, perm2\, perm3\, w\, \text{Cosh}[(-b1+b2)\, D2]^2\, \text{Sinh}[b1\, D1]^2\, \text{Sinh}[(-b2+b3)\, D3] - D2\, D3\, Hs0\, perm1\, perm2\, perm3\, w\, \text{Cosh}[b1\, D1]^2\, \text{Sinh}[(-b1+b2)\, D2]^2\, \text{Sinh}[(-b2+b3)\, D3] + D2\, D3\, Hs0\, perm1\, perm2\, perm3\, w\, \text{Sinh}[b1\, D1]^2\, \text{Sinh}[(-b1+b2)\, D2]^2\, \text{Sinh}[(-b2+b3)\, D3]\Big)\Big) \Big/ \Big(D3 \Big(D1\, D2\, perm2\, perm3\, \text{Cosh}[(-b1+b2)\, D2]\, \text{Cosh}[(-b2+b3)\, D3]\, \text{Sinh}[b1\, D1] + D2^2\, perm1\, perm3\, \text{Cosh}[b1\, D1]\, \text{Cosh}[(-b2+b3)\, D3]\, \text{Sinh}[(-b1+b2)\, D2] + D2\, D3\, perm1\, perm2\, \text{Cosh}[b1\, D1]\, \text{Cosh}[(-b1+b2)\, D2]\, \text{Sinh}[(-b2+b3)\, D3] + D1\, D3\, perm2^2\, \text{Sinh}[b1\, D1]\, \text{Sinh}[(-b1+b2)\, D2]\, \text{Sinh}[(-b2+b3)\, D3]\Big)\Big)$$

Figure 12: Resulting coefficient values for a three-layer structure. These are just values but it is more beneficial for simulations to implement them as parameterised functions.

The field equations, coefficients and higher level functions are then converted into a form that can be simulated in *Mathematica*.

```
$MaxExtraPrecision = 35;
$MaxPrecision = 1000;
$MinPrecision = 35;

w[f_] := 2 Pi f;
D1[f_, σ1_, μ1_] := (1 + I) Sqrt[w[f] σ1 μ1 / 2];
D2[f_, σ2_, μ2_] := (1 + I) Sqrt[w[f] σ2 μ2 / 2];
D3[f_, σ3_, μ3_] := (1 + I) Sqrt[w[f] σ3 μ3 / 2];
```

Coefficients

```
L1[f_, σ1_, σ2_, σ3_, μ1_, μ2_, μ3_, b1_, b2_, b3_] :=
 (i (D1[f, σ1, μ1] D2[f, σ2, μ2] Hs3 μ1 μ2 μ3 w[f] -
      D1[f, σ1, μ1] D2[f, σ2, μ2] Hs0 μ1 μ2 μ3 w[f] Cosh[b1 D1[f, σ1, μ1]]
       Cosh[(-b1 + b2) D2[f, σ2, μ2]] Cosh[(-b2 + b3) D3[f, σ3, μ3]] -
      D2[f, σ2, μ2]^2 Hs0 μ1^2 μ3 w[f] Cosh[(-b2 + b3) D3[f, σ3, μ3]]
       Sinh[b1 D1[f, σ1, μ1]] Sinh[(-b1 + b2) D2[f, σ2, μ2]] -
      D2[f, σ2, μ2] D3[f, σ3, μ3] Hs0 μ1^2 μ2 w[f] Cosh[(-b1 + b2) D2[f, σ2, μ2]]
       Sinh[b1 D1[f, σ1, μ1]] Sinh[(-b2 + b3) D3[f, σ3, μ3]] -
      D1[f, σ1, μ1] D3[f, σ3, μ3] Hs0 μ1 μ2^2 w[f] Cosh[b1 D1[f, σ1, μ1]]
       Sinh[(-b1 + b2) D2[f, σ2, μ2]] Sinh[(-b2 + b3) D3[f, σ3, μ3]])) /
  (D1[f, σ1, μ1]
    (D1[f, σ1, μ1] D2[f, σ2, μ2] μ2 μ3 Cosh[(-b1 + b2) D2[f, σ2, μ2]]
       Cosh[(-b2 + b3) D3[f, σ3, μ3]] Sinh[b1 D1[f, σ1, μ1]] +
      D2[f, σ2, μ2]^2 μ1 μ3 Cosh[b1 D1[f, σ1, μ1]] Cosh[(-b2 + b3) D3[f, σ3, μ3]]
       Sinh[(-b1 + b2) D2[f, σ2, μ2]] +
      D2[f, σ2, μ2] D3[f, σ3, μ3] μ1 μ2 Cosh[b1 D1[f, σ1, μ1]]
       Cosh[(-b1 + b2) D2[f, σ2, μ2]] Sinh[(-b2 + b3) D3[f, σ3, μ3]] +
      D1[f, σ1, μ1] D3[f, σ3, μ3] μ2^2 Sinh[b1 D1[f, σ1, μ1]]
       Sinh[(-b1 + b2) D2[f, σ2, μ2]] Sinh[(-b2 + b3) D3[f, σ3, μ3]]))
```

```
L2[f_, σ1_, σ2_, σ3_, μ1_, μ2_, μ3_, b1_, b2_, b3_] :=
 (i (D2[f, σ2, μ2] Hs3 μ1 μ2 μ3 w[f] Cosh[b1 D1[f, σ1, μ1]] -
      D2[f, σ2, μ2] Hs0 μ1 μ2 μ3 w[f] Cosh[b1 D1[f, σ1, μ1]]^2
       Cosh[(-b1 + b2) D2[f, σ2, μ2]] Cosh[(-b2 + b3) D3[f, σ3, μ3]] +
      D2[f, σ2, μ2] Hs0 μ1 μ2 μ3 w[f] Cosh[(-b1 + b2) D2[f, σ2, μ2]]
       Cosh[(-b2 + b3) D3[f, σ3, μ3]] Sinh[b1 D1[f, σ1, μ1]]^2 -
      D3[f, σ3, μ3] Hs0 μ1 μ2^2 w[f] Cosh[b1 D1[f, σ1, μ1]]^2
       Sinh[(-b1 + b2) D2[f, σ2, μ2]] Sinh[(-b2 + b3) D3[f, σ3, μ3]] +
      D3[f, σ3, μ3] Hs0 μ1 μ2^2 w[f] Sinh[b1 D1[f, σ1, μ1]]^2
       Sinh[(-b1 + b2) D2[f, σ2, μ2]] Sinh[(-b2 + b3) D3[f, σ3, μ3]])) /
  (D1[f, σ1, μ1] D2[f, σ2, μ2] μ2 μ3 Cosh[(-b1 + b2) D2[f, σ2, μ2]]
     Cosh[(-b2 + b3) D3[f, σ3, μ3]] Sinh[b1 D1[f, σ1, μ1]] +
    D2[f, σ2, μ2]^2 μ1 μ3 Cosh[b1 D1[f, σ1, μ1]] Cosh[(-b2 + b3) D3[f, σ3, μ3]]
     Sinh[(-b1 + b2) D2[f, σ2, μ2]] +
    D2[f, σ2, μ2] D3[f, σ3, μ3] μ1 μ2 Cosh[b1 D1[f, σ1, μ1]]
     Cosh[(-b1 + b2) D2[f, σ2, μ2]] Sinh[(-b2 + b3) D3[f, σ3, μ3]] +
    D1[f, σ1, μ1] D3[f, σ3, μ3] μ2^2 Sinh[b1 D1[f, σ1, μ1]]
     Sinh[(-b1 + b2) D2[f, σ2, μ2]] Sinh[(-b2 + b3) D3[f, σ3, μ3]])

L3[f_, σ1_, σ2_, σ3_, μ1_, μ2_, μ3_, b1_, b2_, b3_] :=
 -(i (-D2[f, σ2, μ2] Hs3 μ1 μ2 μ3 w[f] Cosh[b1 D1[f, σ1, μ1]]
       Cosh[(-b1 + b2) D2[f, σ2, μ2]] +
      D2[f, σ2, μ2] Hs0 μ1 μ2 μ3 w[f] Cosh[b1 D1[f, σ1, μ1]]^2
       Cosh[(-b1 + b2) D2[f, σ2, μ2]]^2 Cosh[(-b2 + b3) D3[f, σ3, μ3]] -
      D2[f, σ2, μ2] Hs0 μ1 μ2 μ3 w[f] Cosh[(-b1 + b2) D2[f, σ2, μ2]]^2
       Cosh[(-b2 + b3) D3[f, σ3, μ3]] Sinh[b1 D1[f, σ1, μ1]]^2 -
      D1[f, σ1, μ1] Hs3 μ2^2 μ3 w[f] Sinh[b1 D1[f, σ1, μ1]]
       Sinh[(-b1 + b2) D2[f, σ2, μ2]] -
      D2[f, σ2, μ2] Hs0 μ1 μ2 μ3 w[f] Cosh[b1 D1[f, σ1, μ1]]^2
       Cosh[(-b2 + b3) D3[f, σ3, μ3]] Sinh[(-b1 + b2) D2[f, σ2, μ2]]^2 +
      D2[f, σ2, μ2] Hs0 μ1 μ2 μ3 w[f] Cosh[(-b2 + b3) D3[f, σ3, μ3]]
       Sinh[b1 D1[f, σ1, μ1]]^2 Sinh[(-b1 + b2) D2[f, σ2, μ2]]^2)) /
  (D1[f, σ1, μ1] D2[f, σ2, μ2] μ2 μ3 Cosh[(-b1 + b2) D2[f, σ2, μ2]]
     Cosh[(-b2 + b3) D3[f, σ3, μ3]] Sinh[b1 D1[f, σ1, μ1]] +
    D2[f, σ2, μ2]^2 μ1 μ3 Cosh[b1 D1[f, σ1, μ1]] Cosh[(-b2 + b3) D3[f, σ3, μ3]]
     Sinh[(-b1 + b2) D2[f, σ2, μ2]] +
    D2[f, σ2, μ2] D3[f, σ3, μ3] μ1 μ2 Cosh[b1 D1[f, σ1, μ1]]
     Cosh[(-b1 + b2) D2[f, σ2, μ2]] Sinh[(-b2 + b3) D3[f, σ3, μ3]] +
    D1[f, σ1, μ1] D3[f, σ3, μ3] μ2^2 Sinh[b1 D1[f, σ1, μ1]]
     Sinh[(-b1 + b2) D2[f, σ2, μ2]] Sinh[(-b2 + b3) D3[f, σ3, μ3]])
```

```
M1[f_, σ1_, μ1_] := i Hs0 μ1 w[f] / D1[f, σ1, μ1]

M2[f_, σ1_, σ2_, σ3_, μ1_, μ2_, μ3_, b1_, b2_, b3_] :=
 (i (D1[f, σ1, μ1] D2[f, σ2, μ2] Hs3 μ2^2 μ3 w[f] Sinh[b1 D1[f, σ1, μ1]] +
      D2[f, σ2, μ2]^2 Hs0 μ1 μ2 μ3 w[f] Cosh[b1 D1[f, σ1, μ1]]^2
       Cosh[(-b2 + b3) D3[f, σ3, μ3]] Sinh[(-b1 + b2) D2[f, σ2, μ2]] -
      D2[f, σ2, μ2]^2 Hs0 μ1 μ2 μ3 w[f] Cosh[(-b2 + b3) D3[f, σ3, μ3]]
       Sinh[b1 D1[f, σ1, μ1]]^2 Sinh[(-b1 + b2) D2[f, σ2, μ2]] +
      D2[f, σ2, μ2] D3[f, σ3, μ3] Hs0 μ1 μ2^2 w[f] Cosh[b1 D1[f, σ1, μ1]]^2
       Cosh[(-b1 + b2) D2[f, σ2, μ2]] Sinh[(-b2 + b3) D3[f, σ3, μ3]] -
      D2[f, σ2, μ2] D3[f, σ3, μ3] Hs0 μ1 μ2^2 w[f] Cosh[(-b1 + b2) D2[f, σ2, μ2]]
       Sinh[b1 D1[f, σ1, μ1]]^2 Sinh[(-b2 + b3) D3[f, σ3, μ3]])) /
   (D2[f, σ2, μ2]
     (D1[f, σ1, μ1] D2[f, σ2, μ2] μ2 μ3 Cosh[(-b1 + b2) D2[f, σ2, μ2]]
        Cosh[(-b2 + b3) D3[f, σ3, μ3]] Sinh[b1 D1[f, σ1, μ1]] +
      D2[f, σ2, μ2]^2 μ1 μ3 Cosh[b1 D1[f, σ1, μ1]] Cosh[(-b2 + b3) D3[f, σ3, μ3]]
       Sinh[(-b1 + b2) D2[f, σ2, μ2]] +
      D2[f, σ2, μ2] D3[f, σ3, μ3] μ1 μ2 Cosh[b1 D1[f, σ1, μ1]]
       Cosh[(-b1 + b2) D2[f, σ2, μ2]] Sinh[(-b2 + b3) D3[f, σ3, μ3]] +
      D1[f, σ1, μ1] D3[f, σ3, μ3] μ2^2 Sinh[b1 D1[f, σ1, μ1]]
       Sinh[(-b1 + b2) D2[f, σ2, μ2]] Sinh[(-b2 + b3) D3[f, σ3, μ3]]))

M3[f_, σ1_, σ2_, σ3_, μ1_, μ2_, μ3_, b1_, b2_, b3_] :=
 (i (D1[f, σ1, μ1] D2[f, σ2, μ2] Hs3 μ2 μ3^2 w[f] Cosh[(-b1 + b2) D2[f, σ2, μ2]]
      Sinh[b1 D1[f, σ1, μ1]] + D2[f, σ2, μ2]^2 Hs3 μ1 μ3^2 w[f] Cosh[b1 D1[f, σ1, μ1]]
      Sinh[(-b1 + b2) D2[f, σ2, μ2]] +
     D2[f, σ2, μ2] D3[f, σ3, μ3] Hs0 μ1 μ2 μ3 w[f] Cosh[b1 D1[f, σ1, μ1]]^2
      Cosh[(-b1 + b2) D2[f, σ2, μ2]]^2 Sinh[(-b2 + b3) D3[f, σ3, μ3]] -
     D2[f, σ2, μ2] D3[f, σ3, μ3] Hs0 μ1 μ2 μ3 w[f] Cosh[(-b1 + b2) D2[f, σ2, μ2]]^2
      Sinh[b1 D1[f, σ1, μ1]]^2 Sinh[(-b2 + b3) D3[f, σ3, μ3]] -
     D2[f, σ2, μ2] D3[f, σ3, μ3] Hs0 μ1 μ2 μ3 w[f] Cosh[b1 D1[f, σ1, μ1]]^2
      Sinh[(-b1 + b2) D2[f, σ2, μ2]]^2 Sinh[(-b2 + b3) D3[f, σ3, μ3]] +
     D2[f, σ2, μ2] D3[f, σ3, μ3] Hs0 μ1 μ2 μ3 w[f] Sinh[b1 D1[f, σ1, μ1]]^2
      Sinh[(-b1 + b2) D2[f, σ2, μ2]]^2 Sinh[(-b2 + b3) D3[f, σ3, μ3]])) /
   (D3[f, σ3, μ3]
     (D1[f, σ1, μ1] D2[f, σ2, μ2] μ2 μ3 Cosh[(-b1 + b2) D2[f, σ2, μ2]]
        Cosh[(-b2 + b3) D3[f, σ3, μ3]] Sinh[b1 D1[f, σ1, μ1]] +
      D2[f, σ2, μ2]^2 μ1 μ3 Cosh[b1 D1[f, σ1, μ1]] Cosh[(-b2 + b3) D3[f, σ3, μ3]]
       Sinh[(-b1 + b2) D2[f, σ2, μ2]] +
      D2[f, σ2, μ2] D3[f, σ3, μ3] μ1 μ2 Cosh[b1 D1[f, σ1, μ1]]
       Cosh[(-b1 + b2) D2[f, σ2, μ2]] Sinh[(-b2 + b3) D3[f, σ3, μ3]] +
      D1[f, σ1, μ1] D3[f, σ3, μ3] μ2^2 Sinh[b1 D1[f, σ1, μ1]]
       Sinh[(-b1 + b2) D2[f, σ2, μ2]] Sinh[(-b2 + b3) D3[f, σ3, μ3]]))
```

Electric Fields

```
Ex1[y_, f_, σ1_, σ2_, σ3_, μ1_, μ2_, μ3_, b1_, b2_, b3_] :=
 L1[f, σ1, σ2, σ3, μ1, μ2, μ3, b1, b2,
b3] Cosh[D1[f, σ1, μ1] y] + M1[f, σ1, μ1] Sinh[D1[f, σ1, μ1] y]
Ex2[y_, f_, σ1_, σ2_, σ3_, μ1_, μ2_, μ3_, b1_, b2_, b3_] :=
 L2[f, σ1, σ2, σ3, μ1, μ2, μ3, b1, b2,
b3] Cosh[D2[f, σ2, μ2] (y - b1)] +
  M2[f, σ1, σ2, σ3, μ1, μ2, μ3, b1, b2, b3] Sinh[D2[f, σ2, μ2] (y - b1)]
Ex3[y_, f_, σ1_, σ2_, σ3_, μ1_, μ2_, μ3_, b1_, b2_, b3_] :=
 L3[f, σ1, σ2, σ3, μ1, μ2, μ3, b1, b2,
b3] Cosh[D3[f, σ3, μ3] (y - b2)] +
  M3[f, σ1, σ2, σ3, μ1, μ2, μ3, b1, b2, b3] Sinh[D3[f, σ3, μ3] (y - b2)]
```

Magnetic Fields

```
Hz1[y_, f_, σ1_, σ2_, σ3_, μ1_, μ2_, μ3_, b1_, b2_, b3_] :=
 L1[f, σ1, σ2, σ3, μ1, μ2, μ3, b1, b2,
 b3] D1[f, σ1, μ1]
-------------------- Sinh[D1[f, σ1, μ1] y] +
    I w[f] μ1
  M1[f, σ1, μ1] D1[f, σ1, μ1]
-------------------- Cosh[D1[f, σ1, μ1] y]
    I w[f] μ1
Hz2[y_, f_, σ1_, σ2_, σ3_, μ1_, μ2_, μ3_, b1_, b2_, b3_] :=
 L2[f, σ1, σ2, σ3, μ1, μ2, μ3, b1, b2,
 b3] D2[f, σ2, μ2]
-------------------- Sinh[D2[f, σ2, μ2] (y - b1)] +
    I w[f] μ2
    1
-------- M2[f, σ1, σ2, σ3, μ1, μ2, μ3, b1, b2, b3] D2[f, σ2, μ2]
I w[f] μ2
  Cosh[D2[f, σ2, μ2] (y - b1)]
Hz3[y_, f_, σ1_, σ2_, σ3_, μ1_, μ2_, μ3_, b1_, b2_, b3_] :=
 L3[f, σ1, σ2, σ3, μ1, μ2, μ3, b1, b2,
 b3] D3[f, σ3, μ3]
-------------------- Sinh[D3[f, σ3, μ3] (y - b2)] +
    I w[f] μ3
    1
-------- M3[f, σ1, σ2, σ3, μ1, μ2, μ3, b1, b2, b3] D3[f, σ3, μ3]
I w[f] μ3
  Cosh[D3[f, σ3, μ3] (y - b2)]
```

Current Densities

```
Jx1[y_, f_, σ1_, σ2_, σ3_, μ1_, μ2_, μ3_, b1_, b2_, b3_] :=
 σ1 Ex1[y, f, σ1, σ2, σ3, μ1, μ2, μ3, b1, b2, b3]
Jx2[y_, f_, σ1_, σ2_, σ3_, μ1_, μ2_, μ3_, b1_, b2_, b3_] :=
 σ2 Ex2[y, f, σ1, σ2, σ3, μ1, μ2, μ3, b1, b2, b3]
Jx3[y_, f_, σ1_, σ2_, σ3_, μ1_, μ2_, μ3_, b1_, b2_, b3_] :=
 σ3 Ex3[y, f, σ1, σ2, σ3, μ1, μ2, μ3, b1, b2, b3]
```

Power Equations for the layers

```
P1[f_, σ1_, σ2_, σ3_, μ1_, μ2_, μ3_, b1_, b2_, b3_] :=
 length width/(2 σ1) NIntegrate[Abs[Jx1[y, f, σ1, σ2, σ3, μ1, μ2, μ3, b1, b2, b3]^2],
   {y, 0, b1}, WorkingPrecision → $MinPrecision, AccuracyGoal → $MinPrecision]
(*average power*)
P2[f_, σ1_, σ2_, σ3_, μ1_, μ2_, μ3_, b1_, b2_, b3_] :=
 length width/(2 σ2) NIntegrate[Abs[Jx2[y, f, σ1, σ2, σ3, μ1, μ2, μ3, b1, b2, b3]^2],
   {y, b1, b2}, WorkingPrecision → $MinPrecision, AccuracyGoal → $MinPrecision]
P3[f_, σ1_, σ2_, σ3_, μ1_, μ2_, μ3_, b1_, b2_, b3_] :=
 length width/(2 σ3) NIntegrate[Abs[Jx3[y, f, σ1, σ2, σ3, μ1, μ2, μ3, b1, b2, b3]^2],
   {y, b2, b3}, WorkingPrecision → $MinPrecision, AccuracyGoal → $MinPrecision]
PTot[f_, σ1_, σ2_, σ3_, μ1_, μ2_, μ3_, b1_, b2_, b3_] :=
 P1[f, σ1, σ2, σ3, μ1, μ2, μ3, b1, b2, b3] + P2[f, σ1, σ2, σ3, μ1, μ2, μ3, b1, b2, b3] +
  P3[f, σ1, σ2, σ3, μ1, μ2, μ3, b1, b2, b3]
```

Resistance Equation

```
RDiff[f_, σ1_, σ2_, σ3_, μ1_, μ2_, μ3_, b1_, b2_, b3_] :=
 (2 PTot[f, σ1, σ2, σ3, μ1, μ2, μ3, b1, b2, b3]) / netCurrent^2
```

Figure 13: Parameterised functions for three-layer structures to simulate [1]'s method.

2.6 Four and Five Layer Structures

The power and impedance functions are developed in the same manner, just taking more inputs. There are three inputs for each layer of the structure, namely conductivity, permeability and thickness of that particular layer. For these purposes, only the initial Maxwell's equations are solved for coefficients are presented here. The method of generating these solutions is the same as that for the other structures of fewer layers, only that they are less complex and less computationally intense.

The implemented code for these layers can be found in the documents called: *"Four layer software model implementation.xps"* and *"Five layer software model implementation.xps"*. This is presented as part of the software contribution as the medium of print is inappropriate for such mathematical complexity. These equations are of considerable length as they become complex quickly with the increase in layer number. The complexity here is in generating a symbolic solution for the system of equations. Although this is desirable, the solution here becomes unmanageable and possibility more difficult to work with than a numerical solution. Though, will any number of layers however the symbolic solution presents an analytical tool that allows the user to gain insight into the workings of the system.

3. Conclusion

Presented in this document are the steps taken from [1]'s work in generating the necessary equations. This improves the repeatability of implementing the analytical method as software. The purpose here is to create valid software based on [1]'s analytical method and not to validate whether the analytical methodology is correct. This aspect is achieved by verifying the software results are the same as the [1]'s results calculated in another form. The equations are generated using *Mathematica* and their solution is implemented in code to a workable form that can be used to simulate the fields and derived values at various frequencies. This allows for more insight into the workings of multipath conductors. It is seen that the implemented code for five layers becomes unmanageable as a symbolic solution and may require and estimation method to be developed or a numerical solution.

Appendix B – Verification of Analytical Method Through Software

1. Introduction

The aim of this work is to establish whether the work of [1] is in fact true. The verification is achieved by a comparison of the analytical method of [1] through the use of the implemented software against a FEM analysis.

2. Translating [1]'s Method into Workable Software

[1]'s methodology for modelling multipath conductors along with the equations developed for certain structures is summarised here providing a basis for the development of the software solution. An explanation of how the model is implemented in software is given. Aspects regarding the choices made in implementing the software and the operation of the mathematical package used is shown to give insight into how the software is executing.

2.1 Summary of [1]'s method

[1] defined four steps to developing the necessary equations to model the structure. These are listed here:

1. The magnetic field intensity of the two exterior boundaries is determined since, regardless of the configuration, these values can always be determine although rely heavily on the configuration itself. This allows for *two* equations in terms of constants to be developed.
2. Continuity of the electric fields is enforced across layer boundaries. This is in accordance with Faraday's Law because neighbouring layers will be equated this gives rise to *n-1* equations.
3. Continuity of the magnetic fields is enforced across layer boundaries. This is in accordance with Ampere's Law and produces *n-1* equations.
4. The above steps develop *2n* equations and therefore allow for simultaneous equations to be developed and the unknown coefficients solved for.

The general solution of the above four steps is given by [1] is shown below, where i is the layer number ($i \geq 1$). This is for a flat, semi-infinite conductor.

$$E_{x_i}(y) = L_i cosh\big(D_i(y - b_{i-1})\big) + M_i sinh\big(D_i(y - b_{i-1})\big)$$

$$H_{z_i}(y) = \frac{L_i D_i}{j\omega\mu_i} cosh\big(D_i(y - b_{i-1})\big) + \frac{M_i D_i}{j\omega\mu_i} sinh\big(D_i(y - b_{i-1})\big)$$

$$J_{x_i}(y) = \sigma_i L_i cosh\big(D_i(y - b_{i-1})\big) + \sigma_i M_i sinh\big(D_i(y - b_{i-1})\big)$$

where, $D_i = (1+j)\sqrt{\frac{\omega \mu_i \sigma_i}{2}} = \frac{(1+j)}{\delta_i}$ and $b_{i-1} \leq y \leq b_i$

and μ represents permeability and σ represents conductivity.

This general solution is shown for simpler flat, semi-infinite conductive structures in the following sections.

3. Verification of Software Computation

FEM analysis using *Maxwell 2D Student Edition* (referred to as *Maxwell* in this document) is used as the correct standard against which the software, implemented in *Mathematica*, is verified. The software implementation is developed from [1] for developing the equations for multipath flat conductive structures. The equations are complex to implement and therefore are required to be verified. Verification occurs on a fundamental level where to the fields are confirmed to be correct. The derived functions for power and resistance are also required to be verified as they provide an abstraction from the fundamental field equations in order to better understand the behaviour of the conductors.

3.1 Verification of Derived Equations

Maxwell provides a numerical solution to the conductive structures. In order for the derived equations in this section to be verified, the resistance value from both the *Mathematica* simulation and the FEM analysis, using *Maxwell*, must agree. The resistance is chosen as it is the final calculated value in the derived equations implemented in *Mathematica* and is also used extensively in this work.

From the fundamental laws the power in a conductor at steady state using peak values is given by Equation (1).

$$Power\ loss\ per\ unit\ area = P_{average} = \frac{1}{2\sigma}\int_{l_{min}}^{l_{max}} |J^2| dl \tag{1}$$

The total power dissipated along the length of the conductor is given by (2).

$$Total\ Power\ loss\ in\ conductor = P_T = \frac{length \times width}{2\sigma}\int_{l_{min}}^{l_{max}} |J^2| dl \tag{2}$$

The total average power dissipated in the conductor is therefore:

$$P_T = \frac{1}{2}\left(I_{peak}\right)^2 R \tag{3}$$

$$\therefore Resistance\ of\ the\ conductor = R = \frac{2\ P_T}{I_{peak}^2} \tag{4}$$

Resistance at DC can also be found, apart from using (4), using (5).

$$R = \frac{length}{\sigma \times width \times height} \tag{5}$$

Using Equation (4) and Equation (5) the *Mathematica* calculator can be verified against the FEM analysis. In the following two subsections the implemented power and resistance equations that reflect Equation (2) and Equation (4) are presented. Equation (4) is used in the *Maxwell* calculations in order to shown how the two approaches calculate resistance. The results of the two methods are compared in Section 3.4.

3.2 Resistance Implemented in *Mathematica*

Equation (2) is implemented for each layer of the multipath conductor. This is the average power in each layer at steady state given the frequency and material properties of the conductor as a whole. The electric field of any given layer is affected by the material properties and electric fields of the other layers. Therefore the current density, J_x , of a given layer is a function of the other layer's material properties. Integrating this in the same manner as in Equation (2) is shown in Figure 1. The total average power loss, P_{Tot} , in the conductor is the linear sum of all the layer's average power.

```
P1[f_, σ1_, σ2_, σ3_, μ1_, μ2_, μ3_, b1_, b2_, b3_] :=
 length width/(2 σ1) NIntegrate[Abs[Jx1[y, f, σ1, σ2, σ3, μ1, μ2, μ3, b1, b2, b3]^2], {y, 0, b1},
   WorkingPrecision → $MinPrecision, AccuracyGoal → $MinPrecision] (*average power*)
P2[f_, σ1_, σ2_, σ3_, μ1_, μ2_, μ3_, b1_, b2_, b3_] :=
 length width/(2 σ2) NIntegrate[Abs[Jx2[y, f, σ1, σ2, σ3, μ1, μ2, μ3, b1, b2, b3]^2], {y, b1, b2},
   WorkingPrecision → $MinPrecision, AccuracyGoal → $MinPrecision]
P3[f_, σ1_, σ2_, σ3_, μ1_, μ2_, μ3_, b1_, b2_, b3_] :=
 length width/(2 σ3) NIntegrate[Abs[Jx3[y, f, σ1, σ2, σ3, μ1, μ2, μ3, b1, b2, b3]^2], {y, b2, b3},
   WorkingPrecision → $MinPrecision, AccuracyGoal → $MinPrecision]
PTot[f_, σ1_, σ2_, σ3_, μ1_, μ2_, μ3_, b1_, b2_, b3_] :=
 P1[f, σ1, σ2, σ3, μ1, μ2, μ3, b1, b2, b3] + P2[f, σ1, σ2, σ3, μ1, μ2, μ3, b1, b2, b3] +
  P3[f, σ1, σ2, σ3, μ1, μ2, μ3, b1, b2, b3]
```

Figure 1: Code snippet of the implemented Power equations in Mathematica for each layer of the conductor and for the total power loss.

Equation (4) specifies the resistance calculation using peak values. This is implemented in *Mathematica* by the code snippet below, Figure 2.

```
R[f_, σ1_, σ2_, σ3_, μ1_, μ2_, μ3_, b1_, b2_, b3_] :=
 (2 PTot[f, σ1, σ2, σ3, μ1, μ2, μ3, b1, b2, b3]) / netCurrent^2
```

Figure 2: Code snippet for the implemented resistance equation in Mathematica as the power is calculated using peak values.

3.3 Resistance in *Maxwell 2D Student Edition*

Maxwell calculates *EM Loss*, which is the numerical solution to Equation (1) when calculated along a vertical line through one half of the conductive layers. This is converted to implement Equation (2) by multiplying the power through the line by the width and length of the conductor. *Maxwell* uses peak values in calculating power and therefore the same Equation (4) is used to find the resistance of the conductor. Doing this calculated results in the resistance of the conductor at the given frequency that the FEM analysis was performed for.

3.4 Results of the two Approaches

Using the two approaches implemented in *Mathematica* and *Maxwell* the same value for resistance at different frequencies can be found. By finding the same value in the *Mathematica* simulation as found the FEM analysis, the complex calculations implemented in *Mathematica* can be verified to be correct and therefore act as a reliable foundation for performing further analyses with the new calculator.

The material properties and simulation variable values are captured in Table 1. Layers number increases as layers are added to the outer edges. Meaning Layer1 is the inner most layer on the one half – closest to the symmetrical axis.

Table 1: Material properties used in the simulations.

Simulation Constants	Property	Value
	Length	4 m
	Width	30 mm
	Peak Current	8 A
Properties for 1 Layer Simulation:		
Layer1 : Nickel	Conductivity	1103×10^4 S/m
	Relative Permeability	200
	Thickness	100 μm
Properties for 2 Layer Simulation:		
Layer1 : Brass	Conductivity	1307×10^4 S/m
	Relative Permeability	1
	Thickness	100 μm
Layer2 : Nickel	Conductivity	1103×10^4 S/m
	Relative Permeability	200

	Thickness	100 μm
Properties for 3 Layer Simulation:		
Layer1 : Brass	Conductivity	1500×10^4 S/m
	Relative Permeability	1
	Thickness	100 μm
Layer2 : Nickel	Conductivity	1450×10^4 S/m
	Relative Permeability	600
	Thickness	100 μm
Layer3 : Brass	Conductivity	1500×10^4 S/m
	Relative Permeability	1
	Thickness	300 μm

The simulation results are captured in Table 2 below using the two approaches.

Table 2: Results of the newly developed simulation tool in Mathematica compared to the established findings using FEM analysis.

Number Of Layers	Frequency (KHz)	FEM Resistance using *Maxwell*		Implemented Equations using *Mathematica*	% Error
		EM Loss	Resistance	Resistance	
1	DC	32.563688	0.12218	0.12218	0.0
	4	32.563688	0.12218	0.12218	0.0
	20	39.990358	0.149964	0.15012	-0.1
	100	95.135062	0.356756	0.35782	-0.3
	1000	300.83958	1.12815	1.12810	0.0
	6000	720.16893	2.70063	2.76326	-2.3
2	4	15.010787	0.0562905	0.056322	-0.1
	1000	27.106399	0.101649	0.101649	0.0
3	4	15.921573	0.0597059	0.059797	-0.2
	20	19.509435	0.0731604	0.073292	-0.2
	100	21.814685	0.0818051	0.081962	-0.2
	1000	24.045193	0.0901695	0.090388	-0.2
	6000	41.759672	0.156599	0.157782	-0.8

The results show that the implemented method in *Mathematica* agrees with the FEM analysis. A different number of layers and the properties of the layers are changed through the simulations. The agreement still holds therefore proving two points here:

1. The underlying physics is correct validating Brink's method of solving for the fields within the various layers.
2. The implementation of the field equations and derived functions such as power and resistance are implemented and simulated correctly

This agreement does breakdown as the frequency starts to increase which is due to the loss of precision in FEM analysis with higher frequencies. This is seen as a limitation of the tool used and that better agreement is achievable with more passes through the numerical analysis to a smaller percentage error.

4. Noteworthy Points for Proper Use of the Software

The true value must always be worked with in *Mathematica* since this tells *Mathematica* to use the given number to infinite precision. Working with infinite precision allows all calculations to proceed and evaluated to the default machine precision of 17 significant figures. If a number is entered that is fixed precision such as *2.0* then the outcome of operations is limited to this precision at best. The loss in precision causes the system to break as very large numbers start to be used as the frequency increases and the error becomes far greater than the resolution of the observable results. The implications of this are that at some point the default precision in *Mathematica* will limit the system's outcomes. At this point the precision will need to be specified accordingly. For most simulations under a reasonable frequency range, the precision limitations are not reached.

5. A Note on FEM implementation

The purpose of this document is to aid the user when reproducing numerical solutions to multilayer conductors using Maxwell 2D Student Edition. In this section a note on how the FEM analysis was achieved is presented. This section is not critical to the development of the verification but is supplementary in improving the repeatability of the procedures. This user guide is necessary as there is a lack of supporting material in this regard and in order to reproduce the same results it is important that the same steps be followed. This user guide explains how to set up a rectangular multilayer conductor and therefore uses rectangles for the shapes.

5.1 General Points

In order for functions to be available in Maxwell, an object may need to be selected first. This can be found in *Edit* where the *Select…* (or similar) is available. This allows the objects to be selected by clicking on them or by finding them by name etc.

Once the objects are selected the *select* function needs to end. Ending a function is done by right-clicking on the workspace. This allows all functions to be available again and will not be greyed out. Now the desired function can be applied to the selected items.

5.2 Set up of Drawings and Materials

The solver for this type of simulation must be set to an *Eddy Current* solution and the drawing will be in the *XY plane*. Select the *Define Model* option and select *Draw Model...* as shown in Figure 3.

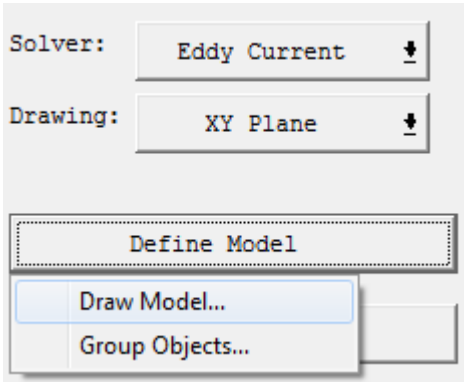

Figure 3: Defining a model

Draw a line to act as a reference A-Field for the simulations. This can be put in the centre on the diagram.

In drawing the actual conducting layers, the *rectangle* should be selected from the *Object* tab. In the bottom bar of the program a *U* and *V* coordinate appear. Enter the coordinates of one corner here, using the *tab* key to move to the next block and select the *Enter* option. It is important here to not move the mouse as any movement of the drawing space of the model will automatically place to mouse coordinates in the desired corner coordinates. Once *Enter* has been select using the *return* key, press *tab* until the *dU* is selected and enter the change in *U* from the previous corner entered and do the same for *dV*. Select *Enter* again and the rectangle will be drawn. Remember this is drawn from a starting corner, and then a change in height and width is entered essentially specifying the opposite corner of the rectangle.

5.3 Sources and Boundary Conditions

Select the vertical edges of the drawn model and assign using the boundary option even symmetry. Similarly assign a value to the centre line for the Vector Potential (A-Field). Assign sources to the upper and lower conductors that are 180 degrees out of phase. Note that the drawn model is scaled down and therefore the source current should undergo a proportional scaling to maintain the same current per conducting cross-sectional area. Also note that this current is defined as the peak value which effects how the total power is calculated. If there are multiple layers then each source should be assigned to the conductors in parallel.

5.4 Analysis of EM Loss and Plots

Define a *Line* in the postprocessor from the *Geometry -> Create* menu items. Make the line such that it covers the vertical aspects of the conducting structure that is desired to be measured.

5.4.1 EM Loss

In *Data -> Calculator* select from *Qty -> EM Loss* and from *Geom -> Line* (select the line with the same that was just drawn above). Then click the integral sign (∫) and then *Eval*. The equation developed will be drawn in the block above. In order to remove the line being evaluated, click the *Pop* option to remove the top line.

The figure that is calculated here is the power loss in Watts using the peak current value. This power value is the power loss along the defined vertical line and needs to be scaled to the correct width as the simulated structure. The value will then be per meter length and thus is required to be scaled by the length of the simulated conductor.

In order to find the resistance of the structure using Maxell the following progression of equations is used.

$$Power\ per\ unit\ area = P_{average} = \frac{1}{2\sigma}\int_{l_{min}}^{l_{max}} |J^2| dl$$

$$EM\ Loss\ [W] = \ P_{average} = I_{RMS}^2 R\ = \left(\frac{I_{peak}}{\sqrt{2}}\right)^2 R$$

$$also\ P_{average} = \ \frac{1}{2} I_{peak}^2\ R\ = EM\ Loss$$

$$this\ is\ only\ the\ power\ loss\ along\ the\ defined\ vertical\ line.$$

$$\therefore P_{Total\ average} = \frac{1}{2} I_{peak}^2 \times R \times width \times length$$

$$\therefore R_{conductor} = 2\ \frac{EM\ Loss}{I_{peak}^2 \times width \times length}$$

$$This\ is\ the\ total\ conductor\ resistance\ at\ steady\ state.$$

5.4.2 Plots

This process is more straight-forward. Select *Plot -> Field* and then the desired *Plot Quantity* the *Geometry* that makes sense or desired and the *Area* it is in.

5.5 Tips and Tricks

Use the copy feature on the projects page to make a working copy when solving the desired setup for different frequencies. Changing the frequency can cause the program to fail and in doing so, lose information in the setup such as the boundary conditions or the sources. This will need to be identified and re-added which can waste time and often lead to confusion. Rather make a new working copy and continue with the analysis.

5.6 Conclusion of FEM implementation

This is a basic and straight-forward guide to using Maxwell strictly to analyse multilayer flat conductors. The guide developed out of the lack of accessible and simple information explaining how to use Maxwell available on typical search engines and libraries. The guide describes how the software is used so that a user can get a feel for how to operate the software and get up and running using Maxwell so that more time can be spent on the interpretation of the analyses rather than be hindered by its difficult user interface. The setup of the drawing, materials, boundary conditions and sources are given. How to interpret the analyses performed in calculating resistance is also presented.

6. Conclusion - Implications of Working Software and Verified Approach

Finite Element Method has long been accepted as an established approach of simulating structures. The agreement between the software simulations and FEM suggest that the analytical approach of [1] is correct. A means of finding the values to compare is presented in this work too. The agreement also suggests that the implementation of the software itself is correct which allows for a reliable and enabling tool for further work to be based upon. A basic user guide is presented to improve the repeatability of the implemented FEM analysis.

7. References

[1] E. A. Brink and I. W. Hosajer, "Analytical Approach for Determining the Frequency-Dependent Characteristics of Multipath Conductive Structures," *Power Electronics, IEEE Transactions*, vol. 29, no. 11, pp. 5835-5845, Jan 2014.

Appendix C: Finding the Low Frequency Internal Inductance for Five Layer Multipath Conductors

```
ClearAll[length,width,netI,σ1,σ2,σ3,μ1,μ2,μ3,w1,w2,w3];
```

```
(*
    the magnetic engery stored in
  a material is represented using the following:

        1/2 L I^2 = W

    therefore,
    to calculate inductance we can use:
        L = 2/I^2 W                          (Equation 1)

    the energy per unit volume in a region of
   space of permeability μ containing magnetic field B is:

        ∪ = B^2/(2 μ)
        ∪ = (μ H)^2/(2 μ)
        ∪ = 1/2 μ H^2 per unit volume

    to get the total stored energy we need to integrate over the volume:

        W = 1/2 μ ∫ H^2 dV
        W = 1/2 length with μ ∫ H^2 dx     (Equation 2)

    In the one dimension DC case

        (path integral)∫ H • dl = I (the enclosed current)

        H 2 width = J width x
    where x is the thickness for of the enclosed path.

        H = 1/2 J x  for one half of the conductor and
        H = J x    for both halves of the conductor
        H = I/(width w) x                    (Equation 3)
    where w is the thickness of the conductor.

    With multipath conductors the total current, I,
splits at DC across the conducting layers proportionate
  to the conductance of each layer in the total conductance.
        I = i1 + i2 + i3 + …

        where:
```

$$i1 = \frac{w1\ \sigma 1}{\sum_{n=1}^{n} (wn\ \sigma n)} I$$

and σ is the conductivity material property of the layer, n.

from Equation 1, and Equation 2 and cosidering the Equation 3, and the fact the net current, I, has split within the conducting layers, we find the equation to be:

$$L = \frac{2}{I^2} \left(\frac{1}{2}\ length\ width \left(\mu 3 \int_0^{w3} \left(\frac{i3}{wid\ w3} x \right)^2 dx + \mu 2 \int_{w3}^{w3+w2} \left(\frac{i3}{wid\ w3} w3 + \frac{i2}{wid\ w2} (x - w3) \right)^2 dx + \mu 1 \int_{w3+w2}^{w3+w2+w1} \left(\frac{i3}{wid\ w3} w3 + \frac{i2}{wid\ w2} w2 + \frac{i1}{wid\ w1} (x - (w3+w2)) \right)^2 dx \right) \right)$$

*)

(*$L = \frac{2}{I^2} \left(\frac{1}{2}\ length\ with \left(\mu 3 \int_0^{w3} \left(\frac{i3}{wid\ w3} x \right)^2 dx + \mu 2 \int_{w3}^{w3+w2} \left(\frac{i3}{wid\ w3} w3 + \frac{i2}{wid\ w2} (x - w3) \right)^2 dx + \mu 1 \int_{w3+w2}^{w3+w2+w1} \left(\frac{i3}{wid\ w3} w3 + \frac{i2}{wid\ w2} w2 + \frac{i1}{wid\ w1} (x - (w3+w2)) \right)^2 dx \right) \right)$*)

General form of an *n-layered* mulitpath conductor:

- **where n is the total number of layers and j is the layer identifying number in the structure.**

$$L = \frac{2}{netI^2} \left(\sum_{j=n}^{1} \left(\frac{1}{2} \mu_j\ length\ width \int_{\sum_{z=n}^{j+1} w_z}^{\sum_{z=n}^{j} w_z} \left(\left(\frac{1}{width} \sum_{z=n}^{j+1} i_z \right) - \left(\frac{i_j}{width\ w_j} \left(\sum_{z=n}^{j+1} w_z \right) \right) + \frac{i_j}{width\ w_j} x \right)^2 dx \right) \right)$$

(*and*)

$$i_j = \frac{w_j\ \sigma_j}{\sum_{z=1}^{n} w_z\ \sigma_z}\ netI$$

Putting the definite integrals into *Mathematica* language, for 5 layers, is as follows:

$$InternalInductanceIntegrals = \frac{len\ wid}{netI^2} \left(\mu 5\ Integrate\left[\left(\frac{i5}{wid\ w5} x \right)^2, \{x, 0, w5\} \right] + \mu 4\ Integrate\left[\left(\frac{i5}{wid} - \frac{i4}{wid\ w4} w5 + \frac{i4}{wid\ w4} x \right)^2, \{x, w5, w5 + w4\} \right] + \mu 3\ Integrate\left[\left(\frac{i5}{wid} + \frac{i4}{wid} - \frac{i3}{wid\ w3} (w5 + w4) + \frac{i3}{wid\ w3} x \right)^2, \{x, w5 + w4, w5 + w4 + w3\} \right] + \mu 2\ Integrate\left[\left(\frac{i5}{wid} + \frac{i4}{wid} + \frac{i3}{wid} - \frac{i2}{wid\ w2} (w5 + w4 + w3) + \frac{i2}{wid\ w2} x \right)^2, \{x, w5 + w4 + w3, w5 + w4 + w3 + w2\} \right] + \mu 1\ Integrate\left[\left(\frac{i5}{wid} + \frac{i4}{wid} + \frac{i3}{wid} + \frac{i2}{wid} - \frac{i1}{wid\ w1} (w5 + w4 + w3 + w2) + \frac{i1}{wid\ w1} x \right)^2, \{x, w5 + w4 + w3 + w2, w5 + w4 + w3 + w2 + w1\} \right] \right)$$

$$InternalInductanceIntegrals = length \left(\mu 5 \frac{w5^3\ \sigma 5^2}{3\ width\ (w1\ \sigma 1 + w2\ \sigma 2 + w3\ \sigma 3 + w4\ \sigma 4 + w5\ \sigma 5)^2} + \right.$$

$$\mu 4\ \frac{\left(\frac{w4^3\ \sigma 4^2}{3} + w4^2\ w5\ \sigma 4\ \sigma 5 + w4\ w5^2\ \sigma 5^2\right)}{width\ (w1\ \sigma 1 + w2\ \sigma 2 + w3\ \sigma 3 + w4\ \sigma 4 + w5\ \sigma 5)^2} +$$
$$\mu 3\ \frac{w3\ \left(w3^2\ \sigma 3^2 + 3\ w3\ \sigma 3\ (w4\ \sigma 4 + w5\ \sigma 5) + 3\ (w4\ \sigma 4 + w5\ \sigma 5)^2\right)}{3\ width\ (w1\ \sigma 1 + w2\ \sigma 2 + w3\ \sigma 3 + w4\ \sigma 4 + w5\ \sigma 5)^2} +$$
$$\mu 2\ \left(w2\ \left(w2^2\ \sigma 2^2 + 3\ w2\ \sigma 2\ (w3\ \sigma 3 + w4\ \sigma 4 + w5\ \sigma 5) + 3\ (w3\ \sigma 3 + w4\ \sigma 4 + w5\ \sigma 5)^2\right)\right) /$$
$$\left(3\ width\ (w1\ \sigma 1 + w2\ \sigma 2 + w3\ \sigma 3 + w4\ \sigma 4 + w5\ \sigma 5)^2\right) + \mu 1\ w1\ \left(w1^2\ \sigma 1^2 +$$
$$3\ w1\ \sigma 1\ (w2\ \sigma 2 + w3\ \sigma 3 + w4\ \sigma 4 + w5\ \sigma 5) + 3\ (w2\ \sigma 2 + w3\ \sigma 3 + w4\ \sigma 4 + w5\ \sigma 5)^2\right) /$$
$$\left(3\ width\ (w1\ \sigma 1 + w2\ \sigma 2 + w3\ \sigma 3 + w4\ \sigma 4 + w5\ \sigma 5)^2\right)\Bigg)$$

Consider solving these integrals in their basic form and substituting in the parameters after finding their form.

```
Integrate[(a + b x)^2, x]
```

$$\frac{(a + b\ x)^3}{3\ b}$$

Now take into account the i1, i2 and i3 values that the net current has split into:

```
i5 = (w5 σ5 / (w1 σ1 + w2 σ2 + w3 σ3 + w4 σ4 + w5 σ5)) netI;
i4 = (w4 σ4 / (w1 σ1 + w2 σ2 + w3 σ3 + w4 σ4 + w5 σ5)) netI;
i3 = (w3 σ3 / (w1 σ1 + w2 σ2 + w3 σ3 + w4 σ4 + w5 σ5)) netI;
i2 = (w2 σ2 / (w1 σ1 + w2 σ2 + w3 σ3 + w4 σ4 + w5 σ5)) netI;
i1 = (w1 σ1 / (w1 σ1 + w2 σ2 + w3 σ3 + w4 σ4 + w5 σ5)) netI;
```

The first integral solved in the standard form

```
a = 0;
b = i5 / (wid w5);
Integrate[(a + b x)^2, {x, 0, w5}]
ClearAll[a, b]
```

$$\frac{w5^3\ \sigma 5^2}{3\ wid\ (w1\ \sigma 1 + w2\ \sigma 2 + w3\ \sigma 3 + w4\ \sigma 4 + w5\ \sigma 5)^2}$$

$$\frac{netI^2\ w5^3\ \sigma 5^2}{3\ wid^2\ (w1\ \sigma 1 + w2\ \sigma 2 + w3\ \sigma 3 + w4\ \sigma 4 + w5\ \sigma 5)^2}$$

The second integral solved in the standard form

```
a = i5 / wid - (i4 / (wid w4)) w5;
b = i4 / (wid w4);
Integrate[(a + b x)^2, {x, w5, w5 + w4}]
ClearAll[a, b]
```

$$\frac{\left(\frac{w4^3\,\sigma4^2}{3} + w4^2\,w5\,\sigma4\,\sigma5 + w4\,w5^2\,\sigma5^2\right)}{wid\,(w1\,\sigma1 + w2\,\sigma2 + w3\,\sigma3 + w4\,\sigma4 + w5\,\sigma5)^2}$$

$$\frac{netI^2\left(\frac{w4^3\,\sigma4^2}{3} + w4^2\,w5\,\sigma4\,\sigma5 + w4\,w5^2\,\sigma5^2\right)}{wid^2\,(w1\,\sigma1 + w2\,\sigma2 + w3\,\sigma3 + w4\,\sigma4 + w5\,\sigma5)^2}$$

The third integral solved in the standard form

```
a = i5/wid + i4/wid - i3/(wid w3) (w5 + w4);
b = i3/(wid w3);
Integrate[(a + b x)^2, {x, w5 + w4, w5 + w4 + w3}]
ClearAll[a, b]
```

$$\frac{w3\left(w3^2\,\sigma3^2 + 3\,w3\,\sigma3\,(w4\,\sigma4 + w5\,\sigma5) + 3\,(w4\,\sigma4 + w5\,\sigma5)^2\right)}{3\,wid\,(w1\,\sigma1 + w2\,\sigma2 + w3\,\sigma3 + w4\,\sigma4 + w5\,\sigma5)^2}$$

$$\frac{netI^2\,w3\left(w3^2\,\sigma3^2 + 3\,w3\,\sigma3\,(w4\,\sigma4 + w5\,\sigma5) + 3\,(w4\,\sigma4 + w5\,\sigma5)^2\right)}{3\,wid^2\,(w1\,\sigma1 + w2\,\sigma2 + w3\,\sigma3 + w4\,\sigma4 + w5\,\sigma5)^2}$$

The fourth integral solved in the standard form

```
a = i5/wid + i4/wid + i3/wid - i2/(wid w2) (w5 + w4 + w3);
b = i2/(wid w2);
Integrate[(a + b x)^2, {x, w5 + w4 + w3, w5 + w4 + w3 + w2}]
ClearAll[a, b]
```

$$\frac{w2\left(w2^2\,\sigma2^2 + 3\,w2\,\sigma2\,(w3\,\sigma3 + w4\,\sigma4 + w5\,\sigma5) + 3\,(w3\,\sigma3 + w4\,\sigma4 + w5\,\sigma5)^2\right)}{3\,wid\,(w1\,\sigma1 + w2\,\sigma2 + w3\,\sigma3 + w4\,\sigma4 + w5\,\sigma5)^2}$$

$$\frac{netI^2\,w2\left(w2^2\,\sigma2^2 + 3\,w2\,\sigma2\,(w3\,\sigma3 + w4\,\sigma4 + w5\,\sigma5) + 3\,(w3\,\sigma3 + w4\,\sigma4 + w5\,\sigma5)^2\right)}{3\,wid^2\,(w1\,\sigma1 + w2\,\sigma2 + w3\,\sigma3 + w4\,\sigma4 + w5\,\sigma5)^2}$$

The fifth integral solved in the standard form

```
a = i5/wid + i4/wid + i3/wid + i2/wid - i1/(wid w1) (w5 + w4 + w3 + w2);
b = i1/(wid w1);
Integrate[(a + b x)^2, {x, w5 + w4 + w3 + w2, w5 + w4 + w3 + w2 + w1}]
ClearAll[a, b]
```

$$\frac{w1\left(w1^2\,\sigma1^2 + 3\,w1\,\sigma1\,(w2\,\sigma2 + w3\,\sigma3 + w4\,\sigma4 + w5\,\sigma5) + 3\,(w2\,\sigma2 + w3\,\sigma3 + w4\,\sigma4 + w5\,\sigma5)^2\right)}{3\,wid\,(w1\,\sigma1 + w2\,\sigma2 + w3\,\sigma3 + w4\,\sigma4 + w5\,\sigma5)^2}$$

$$\frac{netI^2\,w1\left(w1^2\,\sigma1^2 + 3\,w1\,\sigma1\,(w2\,\sigma2 + w3\,\sigma3 + w4\,\sigma4 + w5\,\sigma5) + 3\,(w2\,\sigma2 + w3\,\sigma3 + w4\,\sigma4 + w5\,\sigma5)^2\right)}{3\,wid^2\,(w1\,\sigma1 + w2\,\sigma2 + w3\,\sigma3 + w4\,\sigma4 + w5\,\sigma5)^2}$$

These can now be simplified to eliminate the net current and we are left with the inductance in terms of the structure's material properties.

```
DCInternalInductance[σ1_, σ2_, σ3_, σ4_, σ5_, μ1_, μ2_, μ3_, μ4_, μ5_, w1_, w2_,
  w3_, w4_, w5_] := length (μ5 w5^3 σ5^2/(3 width (w1 σ1 + w2 σ2 + w3 σ3 + w4 σ4 + w5 σ5)^2) +
```

$$\mu 4\ \frac{\left(\frac{w4^3\,\sigma 4^2}{3} + w4^2\,w5\,\sigma 4\,\sigma 5 + w4\,w5^2\,\sigma 5^2\right)}{\text{width}\,(w1\,\sigma 1 + w2\,\sigma 2 + w3\,\sigma 3 + w4\,\sigma 4 + w5\,\sigma 5)^2} +$$

$$\mu 3\ \frac{w3\,\left(w3^2\,\sigma 3^2 + 3\,w3\,\sigma 3\,(w4\,\sigma 4 + w5\,\sigma 5) + 3\,(w4\,\sigma 4 + w5\,\sigma 5)^2\right)}{3\,\text{width}\,(w1\,\sigma 1 + w2\,\sigma 2 + w3\,\sigma 3 + w4\,\sigma 4 + w5\,\sigma 5)^2} +$$

$$\mu 2\ \frac{w2\,\left(w2^2\,\sigma 2^2 + 3\,w2\,\sigma 2\,(w3\,\sigma 3 + w4\,\sigma 4 + w5\,\sigma 5) + 3\,(w3\,\sigma 3 + w4\,\sigma 4 + w5\,\sigma 5)^2\right)}{3\,\text{width}\,(w1\,\sigma 1 + w2\,\sigma 2 + w3\,\sigma 3 + w4\,\sigma 4 + w5\,\sigma 5)^2} +$$

$$\mu 1\ w1\,\left(w1^2\,\sigma 1^2 + 3\,w1\,\sigma 1\,(w2\,\sigma 2 + w3\,\sigma 3 + w4\,\sigma 4 + w5\,\sigma 5) + 3\,(w2\,\sigma 2 + w3\,\sigma 3 + w4\,\sigma 4 + w5\,\sigma 5)^2\right) \Big/$$

$$\left(3\,\text{width}\,(w1\,\sigma 1 + w2\,\sigma 2 + w3\,\sigma 3 + w4\,\sigma 4 + w5\,\sigma 5)^2\right)$$

Furthermore, once the outer layer no longer conducts current the original integral can and modelling can be done in several ways:

- **Remodel the structure with one less layer from scratch and resolve the intergrals using the same parameters, integrating over an outer meaningless layer. This requires equally complex integrals and new functions being made for the set.**
- **Remodel, not considering the outer layer. This allows for simpler integrals yet still the need for new functions to be made.**
- **Set the size of the outer layer to zero and use the same model and equation.**

This final approach follows here as an example to show the simplified final equations rather than the simplied model resulting in a new set of equations each time.

```
ClearAll[w1, w2, w3, w4, w5]
```

$$\text{length}\left(\mu 5\ \frac{w5^3\,\sigma 5^2}{3\,\text{width}\,(w1\,\sigma 1 + w2\,\sigma 2 + w3\,\sigma 3 + w4\,\sigma 4 + w5\,\sigma 5)^2} +\right.$$

$$\mu 4\ \frac{\left(\frac{w4^3\,\sigma 4^2}{3} + w4^2\,w5\,\sigma 4\,\sigma 5 + w4\,w5^2\,\sigma 5^2\right)}{\text{width}\,(w1\,\sigma 1 + w2\,\sigma 2 + w3\,\sigma 3 + w4\,\sigma 4 + w5\,\sigma 5)^2} +$$

$$\mu 3\ \frac{w3\,\left(w3^2\,\sigma 3^2 + 3\,w3\,\sigma 3\,(w4\,\sigma 4 + w5\,\sigma 5) + 3\,(w4\,\sigma 4 + w5\,\sigma 5)^2\right)}{3\,\text{width}\,(w1\,\sigma 1 + w2\,\sigma 2 + w3\,\sigma 3 + w4\,\sigma 4 + w5\,\sigma 5)^2} +$$

$$\mu 2\ \frac{w2\,\left(w2^2\,\sigma 2^2 + 3\,w2\,\sigma 2\,(w3\,\sigma 3 + w4\,\sigma 4 + w5\,\sigma 5) + 3\,(w3\,\sigma 3 + w4\,\sigma 4 + w5\,\sigma 5)^2\right)}{3\,\text{width}\,(w1\,\sigma 1 + w2\,\sigma 2 + w3\,\sigma 3 + w4\,\sigma 4 + w5\,\sigma 5)^2} +$$

$$\mu 1\ w1\,\left(w1^2\,\sigma 1^2 + 3\,w1\,\sigma 1\,(w2\,\sigma 2 + w3\,\sigma 3 + w4\,\sigma 4 + w5\,\sigma 5) + 3\,(w2\,\sigma 2 + w3\,\sigma 3 + w4\,\sigma 4 + w5\,\sigma 5)^2\right) \Big/$$

$$\left.\left(3\,\text{width}\,(w1\,\sigma 1 + w2\,\sigma 2 + w3\,\sigma 3 + w4\,\sigma 4 + w5\,\sigma 5)^2\right)\right)$$

```
(*
    all thicknesses are present
*)
DCInternalInductanceFiveActive[σ1_, σ2_, σ3_,
  σ4_, σ5_, μ1_, μ2_, μ3_, μ4_, μ5_, w1_, w2_, w3_, w4_, w5_] :=
```

```
 length ( w5^3 μ5 σ5^2 / (3 width (w1 σ1 + w2 σ2 + w3 σ3 + w4 σ4 + w5 σ5)^2) +
     (μ4 ((w4^3 σ4^2)/3 + w4^2 w5 σ4 σ5 + w4 w5^2 σ5^2)) /
      (width (w1 σ1 + w2 σ2 + w3 σ3 + w4 σ4 + w5 σ5)^2) +
     (w3 μ3 (w3^2 σ3^2 + 3 w3 σ3 (w4 σ4 + w5 σ5) + 3 (w4 σ4 + w5 σ5)^2)) /
      (3 width (w1 σ1 + w2 σ2 + w3 σ3 + w4 σ4 + w5 σ5)^2) +
     (w2 μ2 (w2^2 σ2^2 + 3 w2 σ2 (w3 σ3 + w4 σ4 + w5 σ5) + 3 (w3 σ3 + w4 σ4 + w5 σ5)^2)) /
      (3 width (w1 σ1 + w2 σ2 + w3 σ3 + w4 σ4 + w5 σ5)^2) + (w1 μ1 (w1^2 σ1^2 +
           3 w1 σ1 (w2 σ2 + w3 σ3 + w4 σ4 + w5 σ5) + 3 (w2 σ2 + w3 σ3 + w4 σ4 + w5 σ5)^2)) /
      (3 width (w1 σ1 + w2 σ2 + w3 σ3 + w4 σ4 + w5 σ5)^2) )

(*
    w5 = 0
*)
DCInternalInductanceFourActive[σ1_, σ2_, σ3_, σ4_,
  σ5_, μ1_, μ2_, μ3_, μ4_, μ5_, w1_, w2_, w3_, w4_, w5_] := length
  ( w4^3 μ4 σ4^2 / (3 width (w1 σ1 + w2 σ2 + w3 σ3 + w4 σ4)^2) + (w3 μ3 (w3^2 σ3^2 + 3 w3 w4 σ3 σ4 + 3 w4^2 σ4^2)) /
     (3 width (w1 σ1 + w2 σ2 + w3 σ3 + w4 σ4)^2) +
    (w2 μ2 (w2^2 σ2^2 + 3 w2 σ2 (w3 σ3 + w4 σ4) + 3 (w3 σ3 + w4 σ4)^2)) /
     (3 width (w1 σ1 + w2 σ2 + w3 σ3 + w4 σ4)^2) +
    (w1 μ1 (w1^2 σ1^2 + 3 w1 σ1 (w2 σ2 + w3 σ3 + w4 σ4) + 3 (w2 σ2 + w3 σ3 + w4 σ4)^2)) /
     (3 width (w1 σ1 + w2 σ2 + w3 σ3 + w4 σ4)^2) )

(*
    w4 = 0
*)
DCInternalInductanceThreeActive[σ1_, σ2_, σ3_,
  σ4_, σ5_, μ1_, μ2_, μ3_, μ4_, μ5_, w1_, w2_, w3_, w4_, w5_] :=
 length ( w3^3 μ3 σ3^2 / (3 width (w1 σ1 + w2 σ2 + w3 σ3)^2) + (w2 μ2 (w2^2 σ2^2 + 3 w2 w3 σ2 σ3 + 3 w3^2 σ3^2)) /
     (3 width (w1 σ1 + w2 σ2 + w3 σ3)^2) +
    (w1 μ1 (w1^2 σ1^2 + 3 w1 σ1 (w2 σ2 + w3 σ3) + 3 (w2 σ2 + w3 σ3)^2)) /
     (3 width (w1 σ1 + w2 σ2 + w3 σ3)^2) )

(*
    w3 = 0
*)
DCInternalInductanceTwoActive[σ1_, σ2_, σ3_, σ4_,
  σ5_, μ1_, μ2_, μ3_, μ4_, μ5_, w1_, w2_, w3_, w4_, w5_] :=
 length ( w2^3 μ2 σ2^2 / (3 width (w1 σ1 + w2 σ2)^2) + (w1 μ1 (w1^2 σ1^2 + 3 w1 w2 σ1 σ2 + 3 w2^2 σ2^2)) /
     (3 width (w1 σ1 + w2 σ2)^2) )

(*
```

```
    w2 = 0
*)
DCInternalInductanceOneActive[σ1_, σ2_, σ3_, σ4_, σ5_,
  μ1_, μ2_, μ3_, μ4_, μ5_, w1_, w2_, w3_, w4_, w5_] := length w1 μ1 / (3 width)
```

Appendix D: Development of Design-Oriented Equations for Multipath Conductors

1. Introduction

The aim of this appendix is to show the mathematical progression or simplification from initial concepts to the final form of the equations. The final forms of the equations are used in designing multipath conductors based on a desired resistance profile with frequency. The desired resistance profile is specified in terms of resistance-frequency pairs that represent characteristic points in the curve on a log-log scale plot. Each pair of values requires another material layer in solution. Using the final form of the design equations, each pair provides enough information to allow the designer to make trade-off decisions in terms of one variable per layer to arrive at a potential solution. The solution is in terms of material properties that when simulated, produces the desired response. The initial equations stem from the *n*-structure method and structural averaging. The error margin that originates with these approximation techniques is carried through to the design equations and thus the final design solution carries with it a similar error. Quantification of the error margin within these techniques is yet to be established and is recommended as future work.

2. Development of Design Equations

This section contains equations developed up to three layers that are solved for each material property present in a given conductor. The same progression through the equations can be followed in order to determine the design equations for structures comprised of more layers. Structural averaging is a technique developed that allows for a multipath structure to be represented, at low frequency, by an effective single layer. The material properties of the effective single layer arise by finding the weighted average of conductivity (and permeability) based on its layer thickness to the total thickness of the structure. The design equations arise from two primary concepts. These are based on an effective single layer reduction of the multipath structure. The equations used and the material properties for each layer solved for is shown in Table 1.

Table 1: Equations used and the material properties solved for from them for design purposes.

Equation	**Material Property Solved For**
Low Frequency Single Layer Resistance	Conductivity; Layer Thickness
Low Frequency Single Layer Skin Depth	Permeability; Layer Thickness

The designed points focus only on the resistance profile. This is an incomplete view of the total impedance, however, beneficial from the designer's perspective as specifying the exact value of internal inductance is not a common practice. The complex component of impedance also does not produce real losses. Real losses are required for dissipative

filters and the goal of multipath conductor design in this context. By not specifying the required internal inductance component of behaviour, the skin depth equation is used and the system of equations is under-defined. This is done purposefully to consider the designer's perspective. The layer thickness can therefore be found from both the resistance and skin depth equations, as it is common to both.

The design of the conductor relies on the ability to solve for each layer's material properties for a given desired resistance profile. The equations to demonstrate this capability are presented in this section.

2.1 Layer Conductivity and Thickness From Resistance Specification

The resistance equation in its standard form for effective single layers is given by Equation (1). This standard form is expanded upon for each of the layers present in the structural scenario under investigation. In the case of a three-layer structure, there are three structural scenarios: a three-layer scenario (Equation (8)), a two-layer scenario (Equation (4)) and a one-layer scenario (Equation (1)). The progression starts with the simplest case, a single layer and continues to increase in layers. The parameterised summation terms are first expanded to be in the same format as the resistance equation for many layers, E.g. Equation (2) and Equation (5). The conductivity or thickness is then solved for, Equation (3).

$$r_1 = \frac{l}{wid\ w_{e_1}\sigma_{e_1}} \tag{1}$$

$$r_1 = \frac{l}{wid\ w_1\sigma_1} \tag{2}$$

$$\sigma_1 = \frac{l}{wid\ w_1\ r_1} = \frac{l}{wid\ w_1}\left(\frac{1}{r_1}\right) \tag{3}$$

When dealing with two layers the resistance specification of the first layer is also defined. Therefore the conductivity of the first layer, Equation (3) can be substituted back into Equation (6) in order to solve for the conductivity of the second layer in terms of the resistance values specified. This method is carried out for the three-layer structural scenario by Equations (8)-(12). An interesting observation here is that the three-layer conductivity is only in terms of the second and third resistance values and not the first. This same relationship continues with increasing number of layers. This generalisation is captured by Equation (13) for *n*-layered conductivity and Equation (14) for *n*-layered thickness.

$$r_2 = \frac{l}{width\ w_{e_2}\sigma_{e_2}} \tag{4}$$

$$r_2 = \frac{l}{width\ (w_1\sigma_1 + w_2\sigma_2)} \tag{5}$$

$$\sigma_2 = \frac{1}{w_2}\left(\frac{l}{width\, r_2} - w_1\sigma_1\right) \tag{6}$$

$$\sigma_2 = \frac{l}{width\, w_2}\left(\frac{1}{r_2} - \frac{1}{r_1}\right) \tag{7}$$

$$r_3 = \frac{l}{width\, w_{e_3}\sigma_{e_3}} \tag{8}$$

$$r_3 = \frac{l}{width\, (w_1\sigma_1 + w_2\sigma_2 + w_3\sigma_3)} \tag{9}$$

$$\sigma_3 = \frac{1}{w_3}\left(\frac{l}{width\, r_3} - w_1\sigma_1 - w_2\sigma_2\right) \tag{10}$$

$$\sigma_3 = \frac{l}{width\ \mathrm{r_3 w_3}} - \frac{l}{width\ \mathrm{r_2\, w_3}} \tag{11}$$

$$\sigma_3 = \frac{l}{width\ \mathrm{w_3}}\left(\frac{1}{\mathrm{r_3}} - \frac{1}{\mathrm{r_2}}\right) \tag{12}$$

$$\sigma_n = \frac{l}{width\ \mathrm{w_n}}\left(\frac{1}{\mathrm{r_n}} - \frac{1}{\mathrm{r_{n-1}}}\right) \tag{13}$$

$$w_n = \frac{l}{width\ \sigma_n}\left(\frac{1}{\mathrm{r_n}} - \frac{1}{\mathrm{r_{n-1}}}\right) \tag{14}$$

When *n-1* is equal to zero then whole term is evaluated as zero. The relationship between the specified resistance points and the conductivity has been established. The same relationship is true for the layer thickness. The permeability is required in order to solve for the full set of parameters in the multipath system.

2.1 Layer Permeability and Thickness Based on Resistance and Frequency Specification

A similar method to finding conductivity is followed in order to find the permeability from the skin depth equation. The skin depth equation, Equation (15), is used to find the characteristic knee point frequency – the skin depth frequency. The frequency component of the designer specified points encompass the underlying modelling of the approach. This is such that the skin depth of the structure is equal to the total effective thickness of the appropriate underlying structural scenario, Equation (16)-(17). This equation relates conductivity, permeability and thickness together at a given frequency. The conductivity and thickness has been solved for and the permeability remains. Permeability is solved for using this approach. Layer thickness is solved for here too. This indicates an under-defined system and is commented on later.

The effective permeability is shown in Equation (17). Equations (18) and (19) show the progression to solve for the permeability of the first layer. Equation (20) solves this for layer thickness.

$$\delta = \sqrt{\frac{1}{\pi f \sigma \mu_0 \mu_r}} \tag{15}$$

$$\mu = \frac{1}{\pi f \sigma \delta^2} \tag{16}$$

$$\mu_e = \frac{1}{\pi f \sigma_e w_e^2} \tag{17}$$

$$\mu_1 = \mu_{e_1} = \frac{1}{\pi f_1 \sigma_{e_1} w_{e_1}^2} = \frac{1}{\pi f_1 \sigma_1 w_1^2} \tag{18}$$

$$\mu_1 = \frac{1}{\pi f_1 \frac{l}{wid\ w_1 r_1} w_1^2} = \frac{wid\ r_1}{\pi f_1 l\ w_1} = \frac{wid}{\pi l\ w_1}\left(\frac{r_1}{f_1}\right) \tag{19}$$

$$w_1 = \frac{wid\ r_1}{\pi f_1 l\ \mu_1} \tag{20}$$

The progression in solving for the second layer's permeability (and/or thickness) is shown by Equations (21)-(29). A similar observation from the resistance method is found here, Equation (28) shows the second layer's permeability in terms of the first and second design points. The third layer is related to the second and third design points by a similar progression found in Equations (30)-(36).

$$\mu_{e_2} = \frac{w_1}{w_1 + w_2}\mu_1 + \frac{w_2}{w_1 + w_2}\mu_2 = \frac{1}{\pi f_2 \sigma_{e_2} w_{e_2}^2} \tag{21}$$

$$\mu_2 = \frac{w_1 + w_2}{w_2}\left(\frac{1}{\pi f_2 \sigma_{e_2} w_{e_2}^2} - \frac{w_1}{w_1 + w_2}\mu_1\right) \tag{22}$$

$$r_i = \frac{l}{wid\ w_{e_i}\ \sigma_{e_i}} \tag{23}$$

$$\mu_2 = \frac{w_1 + w_2}{w_2}\left(\frac{1}{\pi f_2 \left(\frac{w_1}{w_1 + w_2}\sigma_1 + \frac{w_2}{w_1 + w_2}\sigma_2\right)(w_1 + w_2)^2} - \frac{w_1}{w_1 + w_2}\mu_1\right) \tag{24}$$

$$\mu_2 = \frac{1}{w_2}\left(\frac{1}{\pi f_2 (w_1\sigma_1 + w_2\sigma_2)} - w_1\frac{1}{\pi f_1 \sigma_1 w_1^2}\right) \tag{25}$$

$$\mu_2 = \frac{1}{w_2}\left(\frac{1}{\pi f_2\left(w_1\left(\frac{l}{wid\, w_1 r_1}\right) + w_2\left(\frac{l}{wid\, w_2 r_2} - \frac{1}{w_2}\frac{l}{wid\, r_1}\right)\right)} - w_1\frac{1}{\pi f_1 w_1^2\left(\frac{l}{wid\, w_1 r_1}\right)}\right) \tag{26}$$

$$\mu_2 = \frac{wid\, r_2}{w_2 \pi f_2 l} - \frac{1}{w_2}\frac{1}{\pi f_1 \frac{l}{wid\, r_1}} \tag{27}$$

$$\mu_2 = \frac{wid}{w_2 \pi l}\left(\frac{r_2}{f_2} - \frac{r_1}{f_1}\right) \tag{28}$$

$$w_2 = \frac{wid}{\mu_2 \pi l}\left(\frac{r_2}{f_2} - \frac{r_1}{f_1}\right) \tag{29}$$

$$\mu_{e_3} = \frac{w_1}{w_1 + w_2 + w_3}\mu_1 + \frac{w_2}{w_1 + w_2 + w_3}\mu_2 + \frac{w_3}{w_1 + w_2 + w_3}\mu_3 = \frac{1}{\pi f_3 \sigma_{e_3} w_{e_3}^2} \tag{30}$$

$$\mu_3 = \frac{w_1 + w_2 + w_3}{w_3}\left(\frac{1}{\pi f_3 \sigma_{e_3} w_{e_3}^2} - \frac{w_2}{w_1 + w_2 + w_3}\mu_2 - \frac{w_1}{w_1 + w_2 + w_3}\mu_1\right) \tag{31}$$

$$\mu_3 = \frac{1}{w_3}\left(\frac{1}{\pi f_3 (w_1\sigma_1 + w_2\sigma_2 + w_3\sigma_3)} - w_2\mu_2 - w_1\mu_1\right) \tag{32}$$

$$\mu_3 = \frac{wid\ \mathrm{r_3}}{\pi\, \mathrm{f_3} l\, \mathrm{w_3}} - \frac{\mathrm{w_1}}{\mathrm{w_3}}\frac{1}{\mathrm{f_1}\pi\, w_1^2 \frac{l}{wid\ \mathrm{w_1\, r_1}}} - \frac{\mathrm{w_2}}{\mathrm{w_3}}\left(\frac{wid\ \mathrm{r_2}}{\pi\, \mathrm{f_2}\, l \mathrm{w_2}} - \frac{\mathrm{w_1}}{\mathrm{w_2}}\frac{1}{\mathrm{f_1}\pi\, w_1^2 \frac{l}{wid\, \mathrm{w_1\, r_1}}}\right) \tag{33}$$

$$\mu_3 = \frac{wid\ \mathrm{r_3}}{\pi\, \mathrm{f_3}\, l\, \mathrm{w_3}} - \frac{1}{\mathrm{w_3}}\frac{wid\, \mathrm{r_1}}{\mathrm{f_1}\pi\, l} - \frac{1}{\mathrm{w_3}}\left(\frac{wid\ \mathrm{r_2}}{\pi\, \mathrm{f_2}\, l} - \frac{wid\, \mathrm{r_1}}{\mathrm{f_1}\pi\, l}\right) \tag{34}$$

$$\mu_3 = \frac{wid}{\pi\, l\, \mathrm{w_3}}\left(\frac{\mathrm{r_3}}{\mathrm{f_3}} - \frac{\mathrm{r_2}}{\mathrm{f_2}}\right) \tag{35}$$

$$w_3 = \frac{wid}{\pi\, l\, \mu_3}\left(\frac{\mathrm{r_3}}{\mathrm{f_3}} - \frac{\mathrm{r_2}}{\mathrm{f_2}}\right) \tag{36}$$

$$\mu_n = \frac{wid}{\pi\, l\, \mathrm{w_n}}\left(\frac{\mathrm{r_n}}{\mathrm{f_n}} - \frac{\mathrm{r_{n-1}}}{\mathrm{f_{n-1}}}\right) \tag{37}$$

$$w_n = \frac{wid}{\pi\, l\, \mu_n}\left(\frac{\mathrm{r_n}}{\mathrm{f_n}} - \frac{\mathrm{r_{n-1}}}{\mathrm{f_{n-1}}}\right) \tag{38}$$

Equations (37) and (38) show a generalised solution following the same approach for *n*-layers. When *n-1* is equal to zero then whole term is evaluated as zero.

There are three variables present with only two equations to solve for them, making this system under-defined. An exact design can only be achieved through trade-off decisions made by the designer. This allows for a flexible design methodology. The designer is required to choose a value for one of the variables in each layer and solve

Equations (13)(14)(37) and (38) appropriately. A practical example of this is to set the permeability and solve for the conductivity and layer thickness using the equations in the case that a specific permeability value is more difficult to manufacture than specific conductivity and thickness. The resistance profile, when simulated, will follow the desired profile. An internal inductance profile can be found as a consequence of the material property values chosen.

3. Conclusion

The design equations and the progression to determining them, using the resistance equation and the skin depth equation for effective single layers, are presented in this appendix. The methodology can be generalised to n layers to solve for more complex multipath structures. The methodology is based on the n-structure method and thus any error margin and limitations are inherent to this approach. The design methodology only allows the designer to specify the desired resistance profile focussing on the desired real losses. This does not account the reactive component of the impedance behaviour and as a result the system is under-defined. The designer is required to make trade-off decisions, as a result, in order to solve for the material properties of each layer that will produce the desired resistance profile.